

See discussions, stats, and author profiles for this publication at: <https://www.researchgate.net/publication/264272865>

Controlled Synthesis and Energy Applications of One-Dimensional Conducting Polymer Nanostructures: An Overview

ARTICLE in ADVANCED ENERGY MATERIALS · FEBRUARY 2012

Impact Factor: 16.15 · DOI: 10.1002/aenm.201100560

CITATIONS

101

READS

56

2 AUTHORS:



Zhigang Yin

Chinese Academy of Sciences

23 PUBLICATIONS 372 CITATIONS

[SEE PROFILE](#)



Qingdong Zheng

Chinese Academy of Sciences

82 PUBLICATIONS 2,845 CITATIONS

[SEE PROFILE](#)

Controlled Synthesis and Energy Applications of One-Dimensional Conducting Polymer Nanostructures: An Overview

Zhigang Yin and Qingdong Zheng*

The past decade has witnessed increasing attention in the synthesis, properties, and applications of one-dimensional (1D) conducting polymer nanostructures. This overview first summarizes the synthetic strategies for various 1D nanostructures of conjugated polypyrrole (PPy), polyaniline (PANI), polythiophene (PTh), poly(*p*-phenylenevinylene) (PPV) and derivatives thereof. By using template-directed or template-free methods, nanoscale rods, wires/fibers, belts/ribbons, tubes, arrays, or composites have been successfully synthesized. With their unique structures and advantageous characteristics (e.g., high conductivity, high carrier mobility, good electrochemical activity, large specific surface area, short and direct path for charge/ion transportation, good mechanical properties), 1D conducting polymer nanostructures are demonstrated to be very useful for energy applications. Next, their applications in solar cells, fuel cells, rechargeable lithium batteries, and electrochemical supercapacitors are highlighted, with a strong emphasis on recent literature examples. Finally, this review ends with a summary and some perspectives on the challenges and opportunities in this emerging area of research.

1. Introduction

The growing demand for renewable and sustainable resources has recently triggered research in advanced energy materials for various applications. Nanomaterials with different morphologies and compositions have been extensively investigated, and they display various kinds of functionalities towards energy related applications over the past ten years.^[1–3] Among the nanomaterials, one-dimensional (1D) nanostructures are emerging as a representative family of new energy materials because they represent the smallest dimensional structures for efficient transport of excitons and charges in energy conversion and storage devices.^[4–7] On this account, a great number of efforts have been made to promote their application in different energy-related fields. The various functional materials at 1D nanoscale with high performance are of significant importance for slowing down the world's ever-growing demand for conventional fossil fuel resources.

Recently, several approaches including vapor growth, liquid growth and self-assembly have been developed for the fabrication of 1D metallic, inorganic, and organometallic nanomaterials to achieve the desired structures and high performances in various energy conversion and storage devices.^[8–11] At the same time, controlled synthesis of 1D nanostructured organic materials, such as (semi-)conducting polymers and small molecular semiconductors for energy applications have also attracted increasing interests, owing to their advantages of light weight, low cost, facile synthesis, excellent electrical and electrochemical activity, good flexibility and processability.^[12] Regarding conducting polymers, the pioneering one is conducting polyacetylene (PA) doped

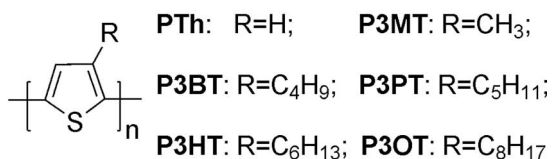
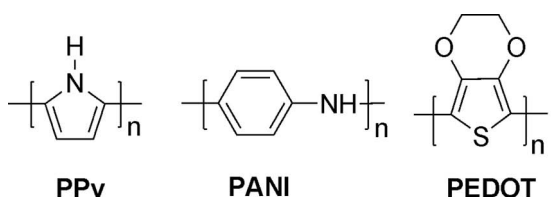
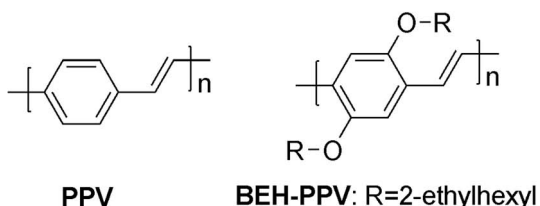
with iodine discovered by MacDiarmid, Heeger, and Shirakawa and co-workers in 1977. Since then, conducting polymers are rapidly gaining attraction in various applications due to the availability of more materials with good electrical, physical, and mechanical properties, as well as excellent solution processability. As shown in Figure 1, intrinsically conducting polymers include polypyrrole (PPy), polyaniline (PANI), polythiophene (PTh) and its derivatives (i.e., poly(3-methylthiophene) (P3MT), poly(3-butylthiophene) (P3BT), poly(3-hexylthiophene) (P3HT), poly(3-octylthiophene) (P3OT), poly(3-pentylthiophene) (P3PT), poly(3,4-ethylenedioxythiophene) (PEDOT)), poly(*p*-phenylenevinylene) (PPV) and its derivatives, etc. In order to make PTh and PPV soluble and processable, soluble alkyl or alkoxy side chains are introduced (Figure 1). All these conjugated polymers have controllable conductivity ranging from insulator to semiconductors or conductors depending on the dopants and doping levels.

It should be noted that the semiconducting forms of PPy and PANI are of little importance in the development of semiconducting polymers probably due to their easy protonation-induced transition from insulators to conductors. On the contrary, the salt forms of PANI and PPy have been regarded as important conducting polymers for electronic applications where high conductivity of the materials is required. Similarly, the conducting form of PEDOT (known as PEDOT:PSS), which

Z. Yin, Prof. Q. D. Zheng
State Key Laboratory of Structural Chemistry
Fujian Institute of Research on the Structure of Matter
Chinese Academy of Sciences
155 Yangqiao West Road, Fuzhou, Fujian 350002,
People's Republic of China
E-mail: qingdongzheng@fjirsm.ac.cn

DOI: 10.1002/aenm.201100560



**PTh and its derivatives****Figure 1.** Molecular structures of some representative conducting polymers (undoped form).

can be acquired by doping the semiconducting PEDOT with sulfonated polystyrene, is also more important compared to its parent pristine semiconductor. Therefore, in this review PPy, PANI and PEDOT are mostly discussed as their conducting forms for the applications in fuel cells, batteries, and supercapacitors. As is well known, PTh, PPV and derivatives thereof are regarded as second-generation polymeric semiconductors. They exhibit excellent optical and electrical characteristics while retain good mechanical properties and processing advantages of polymers. Since PTh, PPV and derivatives thereof are mostly used in their semiconducting forms for the applications in solar



Qingdong Zheng received his B. S. degree in fine chemicals from East China University of Science and Technology, China in 1998. He obtained his Ph.D. degree in chemistry from the State University of New York at Buffalo in 2005. After carrying out his postdoctoral research at the Johns Hopkins University, he joined the Fujian Institute of

Research on the Structure of Matter, Chinese Academy of Sciences, and became a Full Professor in 2010. His main interests focus on multifunctional molecular materials and in particular on the fields of polymeric semiconducting materials for energy related applications.

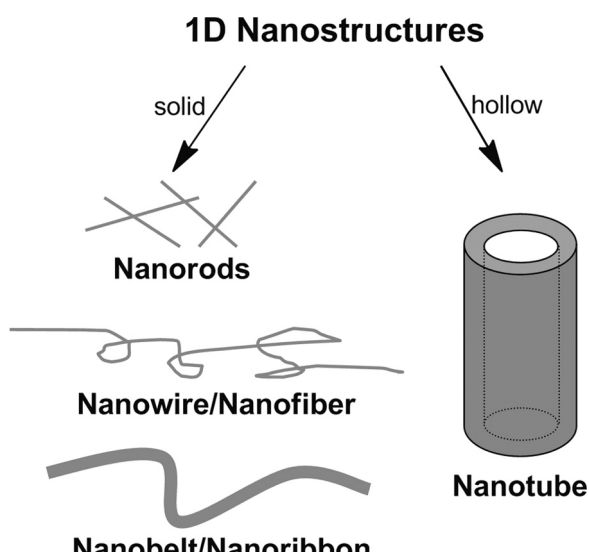


Zhigang Yin is now a research assistant in Professor Qingdong Zheng's group at the Fujian Institute of Research on the Structure of Matter, Chinese Academy of Sciences. He received his B.S. degree in polymer materials and engineering from Xi'an Technological University in 2008 and a M.Sc. degree in materials physics and chem-

istry from Fuzhou University in 2011. His current research focuses on the design and synthesis of one-dimensional nanostructured conducting polymers for applications in solar cells, lithium batteries, and other optoelectronic devices.

cells, they should be called as semiconductors under a strict definition. However, for simplicity they are also called as conducting polymers in this review and others.^[6] When conducting polymers are designed and fabricated into their 1D nanostructured materials, they can display more attractive characteristics and better device performances compared to their bulk solids, such as better electrical conductivities, larger specific surface areas, shorter and more direct pathways for charge transportation and ion diffusion, as well as better electrochemical activities.^[6,12]

So far, several synthetic strategies have been developed for the fabrication of various 1D conducting polymer nanomaterials. As shown in **Figure 2**, 1D conducting polymer nanostructures include solid-type structures (e.g., nanorods (NRs), nanowires (NWs)/nanofibers (NFs), nanobelts (NBs)/nanoribbons, etc.) and hollow-type structures (nanotubes (NTs)). With a rational synthetic design, nanostructures with different diameters/widths, thicknesses, and lengths can be fabricated under control. For the “morphology control” and “size control” of 1D conducting polymer nanomaterials, template-based synthesis and

**Figure 2.** Solid and hollow 1D nanostructures of conducting polymers.

template-free synthesis are two main strategies. The template-based synthesis can be classified into three kinds according to the type of template used, namely, conventional hard-template method, soft-template method and novel wire-template method. However, for the template-free strategy, 1D nanostructured conducting polymers are fabricated without any templates. Up to now, the mostly used template-free methods include self-assembly, electrospinning, and nanoscale patterning, etc. Amongst them, the patterning technique is an effective and attractive template-free method to engineer 1D conducting polymer nanostructures, which has already been covered in other reviews.^[13,14] Thus, in section 2 of this review, we will elaborate on the template-based strategies for the controllable synthesis of 1D nanostructured conducting polymer materials, while only briefly introduce the template-free strategies. Specifically, we will systematically discuss fundamental concepts, mechanisms, merits, shortcomings, and latest achievements in the template-directed methods.

The 1D conducting polymer nanostructures exhibit improved electrical and charge transport properties, and enhanced electrochemical and optical properties, compared to their bulk polymer materials. Based on these characters, in Section 3, we will highlight their energy conversion and storage applications in solar cells, fuel cells, supercapacitors and rechargeable lithium batteries. We note that π -conjugated conducting polymers for applications in information and biomedical areas, which are also of growing interest, have been discussed in other reviews,^[15–17] and thus are not in the scope of this review. Although, the function of conducting polymers in the energy conversion application may be different from that in the energy storage and release application, a synergistic understanding of both will help to tackle the energy challenges facing us now as well as in the future. For example, current photovoltaic arrays rely on advanced energy storage devices such as batteries or supercapacitors to store the energy that is harvested from the sun. Therefore, a comprehensive overview on energy-related applications of conducting polymers may provide us with an all around knowledge regarding the unique features associated with them, especially when they are fabricated into various 1D nanostructures. At the same time, it would be of great importance for exploring advanced devices of future with multiple functionalities integrated. Finally, in section 4, we will give personal concluding comments on the advances discussed in this review as well as some challenges and opportunities for research in the field of 1D conducting polymer nanostructures.

2. Methodologies for Controlled Synthesis of 1D Conducting Polymer Nanostructures

This section covers two main strategies for controlled synthesis of 1D conducting polymer nanostructures, which are template-based synthesis and template-free synthesis. The former methodology is specially discussed and concluded as one of the efficient strategies for synthesizing various 1D conducting polymer nanostructures with controllable morphology and size. Template-free synthetic strategies such as self-assembly, and electrospinning are only briefly discussed.

2.1. Template-Based Synthesis

As is well known, template-based synthesis represents one of most popular strategies for fabricating different kinds of 1D nanomaterials such as metals, inorganic semiconductors, structural ceramics, and functional composites.^[5,18] Similarly, it is also an important and effective methodology for the synthesis of 1D conducting polymer nanostructures with controlled shapes and tunable dimensions/sizes. Herein, the template synthesis means a process employing nanostructured matters as templates, which provide the spatial confinement function to promote 1D growth of conducting polymers on their inner pores and/or outer surfaces assisted by some physical, chemical, or multiple measures.^[5] Eventually, 1D conducting polymer nanostructures with controllable morphology and size are obtained after removal (or not) of the as-used templates.

In this part, three kinds of template-based synthesis, specifically, the conventional hard-template method, the soft-template method, and the wire-template method, are introduced according to the difference in the employed templates. And several issues related to the mechanisms, the advantages and defects, as well as the latest advancements of these template-directed approaches are systematically analyzed.

2.1.1. Conventional Hard-Template Method

The conventional hard-template method pioneered by Martin's group,^[19–21] is a powerful, feasible, and controllable technique to engineer 1D nanostructures. Porous membrane materials such as anodic aluminum oxide (AAO) and particle track-etched membranes (PTM) containing massive micro/nanopores are the most commonly employed templates in such synthesis. When the templates are used, a monomer solution is loaded into their pores and subsequently the polymerization of the monomer takes place in the channels through chemical and/or electrochemical reactions. It is observed that, the uniform width and depth ranging from several nanometers to micrometers within the pre-formed pores of hard-templates offers an efficient way to control over the size, shape and orientation of the polymerized products. On the other side, due to the good stability of the hard-templates, the morphology and size of 1D conducting polymer nanostructures can also be easily controlled by tailoring the synthetic conditions (i.e., reaction rate, reaction time and temperature, as well as feeding amounts and concentrations of monomers, oxidants, and dopants, etc.) during the polymerization process, so as to realize the desired diameter and aspect ratio of the resulting products.

A variety of controllable nanorods, nanofibers/wires, nanotubes from pure conducting polymers such as PPy,^[22–24] PANI,^[20,25] PTh,^[26,27] P3HT,^[28,29] P3MT,^[30] PEDOT,^[31–33] PPV and its derivatives,^[34–36] and poly(9,9-diethylfluorene-co-bithiophene) (F8T2)^[37] have been successfully synthesized by chemical/electrochemical polymerization with the use of AAO and/or polycarbonate-PTM (PC-PTM) templates. For example, Foulger et al. first reported on the synthesis of 1D PEDOT nanostructures in various forms using an AAO template (pore size ~ 250 nm, thickness ~ 60 μm).^[31] They found that, the uniform PEDOT nanotubes with an average diameter of ~ 250 nm and a length of over 5 μm could be obtained by fast polymerization of the

diluted monomer solution. And the wall thickness of the tubules could be controlled in the range of 20–80 nm, which increased with elevated concentrations of FeCl_3 and the reaction temperatures. By carefully controlling the synthetic conditions, nanobelts, nanorods, and nanothimbles of PEDOTs were further synthesized. Using electrochemical synthesis in an AAO template, Mallouk et al. found that the growth of highly electrocapacitive PANI nanowires was strongly influenced by the electrolyte concentration and the applied potential. At a high anodic potential, a transition from solid PANI wires with tubular ends to open wires was found with the increase in H_2SO_4 electrolyte concentration.^[25] Whereas, at a lower anodic potential, the obtained PANI products have dense morphology, and appear to consist of interconnected nanofibers. By direct electrochemical oxidation of thiophene in AAO membranes, aligned PTh tubes with ~ 20 nm diameters were prepared by Shi et al., which showed strong and broad redox responses and nearly 30 times larger capacity of charge/discharge than that of the common PTh film, suggesting a promising perspective in energy applications.^[26] Additionally, employing the flexible PC-PTM templates, the synthesis of 1D hollow or solid conducting polymer nanostructures has also been intensively studied by Lee's group, where the controllable processes, mechanisms, as well as the factors determining the

morphology and size, properties and application prospects have been described in their account article.^[38]

Besides the AAO and PC-PTM templates, porous diblock copolymer films^[24] and nanotubular TiO_2 porous membranes^[39,40] have also been used as porous membrane hard templates to fabricate 1D nanostructures of pure conducting polymers. One of most attractive examples is that, a very dense array of vertically aligned PPy nanorods ($\sim 10^{11}/\text{cm}^2$) was electrochemically generated in a porous polystyrene-*b*-polymethyl methacrylate (PS-*b*-PMMA) membrane template (pore diameter of ca. 25 nm) (Figure 3A–B).^[24] The height of the nanorods was controlled by the time used in the electro-polymerization under a constant voltage. It was also observed that, the self-supporting PPy nanorods were oriented normally to the substrate after removal of the template by washing with toluene (Figure 3B). They exhibited a higher conductivity than a homogeneous PPy thin-film, as characterized by a technique of current-sensing atomic force microscopy (CS-AFM) (Figure 3C). This study demonstrates a useful hard-template method to construct ultrahigh density arrays of conducting polymer nanorods with good electric conductivity and current-voltage characteristic. It can be extended to other conducting polymers (e.g., P3HT and PPV) for developing high density nanorod arrays on flexible

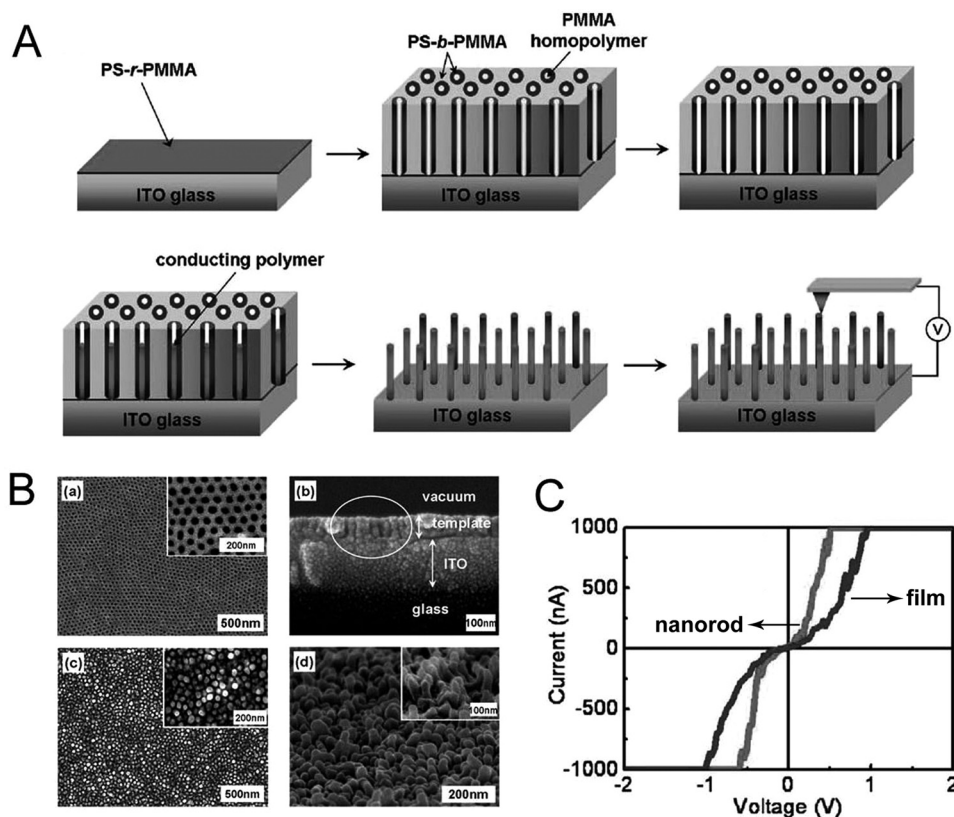


Figure 3. A) Illustrated synthesis of ultrahigh density arrays of PPy nanorods by a nanoporous block copolymer membrane template. B) Field-emission scanning electron microscopy (FE-SEM) images of the nanoporous template fabricated by PS-*b*-PMMA/PMMA mixture film on the indium tin oxide (ITO) glass and PPy nanorods: (a) top and (b) cross-sectional images of the nanoporous template, (c) top and (d) cross-sectional images of the PPy nanorods. C) Current-voltage (*I*-*V*) curves of PPy nanorods and homogeneous PPy thin-film template. Reproduced with permission.^[24] Copyright 2008, American Chemical Society.

substrates, which suggests a great potential in organic photovoltaic applications.

Furthermore, 1D hybrid or composite nanostructures of conducting polymers with spatially controllable compositions have also been effectively synthesized based on the hard-template method. For example, the light-emitting color barcode nanowires with optically distinct compartments were produced in AAO templates by sequential polymerization of P3MT, P3BT, and PEDOT.^[41] Moreover, core-shell nanowires such as MnO₂/PEDOT,^[42] PPY/ZnS,^[43] PTh/CdS,^[44] PANI/Au,^[45] as well as metal-coated PTh nanotubules (i.e., PTh/Cu, PTh/Ni, PTh/Co),^[46] etc., were also prepared through the hard-template routes. In addition, by controlling the spatial composition of nanowires, the hard-template approach can be applied to the controlled synthesis of segmented nanowires along their axis. Two-segmented Ni-PPY, Au-PANI, CdS-PPY and CdS-PTh nanowires,^[44,45,47,48] trisegmented Ni-PPY-Pd, Au-PPY-Au, Ni-Au-PANI, Ni-PEDOT-Au, Au-PEDOT-Au nanowires,^[45,47,49,50], and tetra-segmented Au-PEDOT-PPY-Au nanowires^[50] were all successfully realized, which showed multi-functional properties including good conductivities, good charge-transport abilities, and attractive optoelectronic characteristics. All of these highly refined, unusual, anisotropic structures of conducting polymer hybrids or composites with improved performance demonstrate a powerful compositional control at 1D nanoscale level using the hard-template strategy.

Apparently, the hard-template method has the advantages of good reproducibility and broad applicability. Its capacity to synthesize 1D conducting polymers-based nanomaterials with regular shapes and controllable sizes, especially for those with the structures of nanoarrays and spatially composition-graded nanowires, offers a powerful way for the device engineering in various applications. Nevertheless, it should be noted that, this methodology still suffers from the complicated template-prefabrication procedure and the harsh post-treatment process of the template removal, which result in an increase in the processing cost as well as the possible damage of products. Thus, large-scale production at low cost will be a big challenge for this hard-template method considering the industrial applications of 1D nanostructured conducting polymers. To solve this, the future method of choice for the hard-template synthesis of 1D conducting polymer nanostructures will probably be combined with other advanced methods such as sol-gel deposition, atomic layer deposition (ALD), surface patterning and nanolithography, etc., aiming to generate more feasible, effective, and inexpensive routes to various electronic and optoelectronic devices.

2.1.2. Soft-Template Method

Another effective template approach to prepare 1D conducting polymer nanostructures is the soft-template method, which has been extensively investigated during the past decade. Generally, the soft templates used in this method are ordered aggregates (also called mesophase structures) self-assembled from amphiphilic molecules through hydrophilic-hydrophobic interactions, hydrogen bonds, and Van der Waals forces, etc., when the concentration of the molecules is above the critical micelle concentration.^[51] A series of soft materials such as surfactants,^[52–54] liquid crystals,^[55] copolymers,^[56] and other

amphiphilic molecules,^[57–59] are used to form micelles or reversed micelles in solutions for guiding the *in situ* anisotropic growth of conducting polymers along the cylindrical soft-templates. After removing the templates, solid nanorods/nanowires/nanofibers or hollow nanotubules of conducting polymers are facilely produced in large scale. The morphology, diameter, and length of the products are mainly determined by the pre-assembled micelles depending on the types and concentrations of amphiphilic matters, therefore providing controllable routes to synthesize 1D conducting polymer nanostructures in the micro/nanoreactors of micelles.

Surfactant directed soft-templates are usually employed to synthesize 1D conducting polymer nanostructures. The nature of the surfactants as well as their concentrations has a big impact on the morphology and size of the 1D nanostructured products. Cationic surfactants such as cetyltrimethylammonium bromide (CTAB), dodeyltrimethylammonium bromide (DTAB) are always added into a mixed solution of pyrrole and an oxidant of ammonium persulfate (APS) to establish insoluble lamellar mesostructures as soft-templates, which promote the anisotropic growth of PPY.^[60,61] The use of cationic surfactants of CTAB and DTAB with long alkyl chains produced PPY nanowires/ribbons in widths of 25–85 nm and in lengths exceeding several micrometers, whereas the employment of cationic surfactant octyltrimethylammonium bromide (OTAB) with shorter chains, or nonionic surfactant poly(ethylene glycol) mono-*p*-nonylphenyl ether resulted in non-1D nanostructures. Meanwhile, the morphology of the resulting PPY nanostructures was strongly dependent on both the surfactant and the monomer concentrations (Figure 4A). The nanowire-like PPY products showed a typical nonmetallic behavior,^[62] and their temperature-dependent conductivity profile, was found to be well consistent with Mott's law for quasi-1D variable-range hopping (Figure 4B).^[63] However, the relatively poor conductivity of the PPY products (e.g. room temperature conductivity $\sim 7.3 \times 10^{-3}$ S cm⁻¹) arising from the low doping level, is still the bottleneck for this soft template method assisted by surfactants.

In addition, cationic surfactant of hexadecyltrimethylammonium bromide (HTAB),^[65,66] anionic surfactants of sodium dodecyl sulfate (SDS) and 5,10,15,20-tetrakis(4-sulfonatophenyl) porphyrin (TPPS),^[52,67] as well as surfactant gels of hexadecyltrimethylammonium chloride^[68] and cholic acid-polyethylene glycol 400^[53] have also been employed to produce the soft-templates for the synthesis of uniform nanowires/nanofibers/nanorods of PPY, PANI, and PEDOT. In these soft-template processes, the morphology and size control of the conducting polymers can be achieved by controlling the synthetic conditions to some extent.

The ability to produce hollow tubular nanostructures by the above surfactant templates is still unavailable, although it is feasible to synthesize solid nanostructures with rod-like, wire-like/fiber-like, or ribbon-like/belt-like morphology. Reverse microemulsion polymerization is commonly used to solve this problem, where the reversed micelles containing a nanoscale aqueous pool (water-in-oil) are usually formed by a surfactant, sodium bis(2-ethylhexyl) sulfosuccinate (AOT), in an apolar solvent. Early investigations by Jang's group reported that PPY nanotubes could be controllably synthesized in an AOT reverse emulsion through an oxidative polymerization.^[69,70] As illustrated in

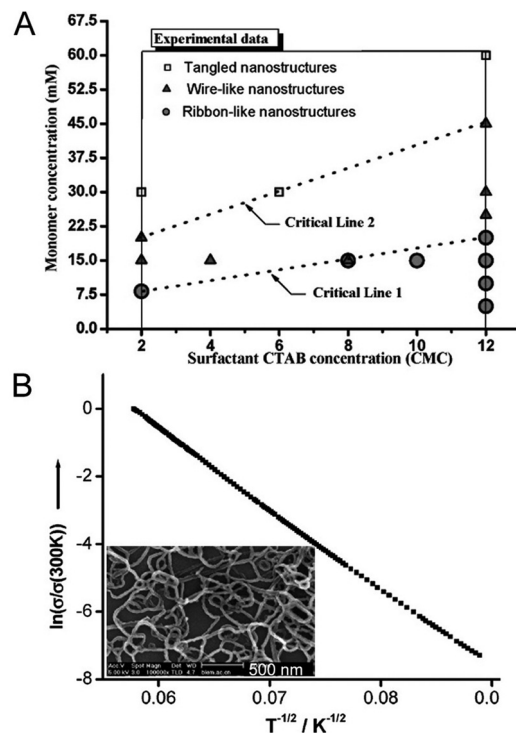


Figure 4. A) Threshold pyrrole concentrations for the PPy nanostructures versus the surfactant concentration in the pyrrole/CTAB/APS system. In the area below Critical Line 1, nanoribbons would be synthesized, and in the area between Critical Line 1 and 2, nanowires would be formed. Above Critical Line 2, highly entangled nanowires and irregular structure of PPy would appear. B) Conductivity–temperature curve of the resulting PPy nanowires synthesized in the system of pyrrole/CTAB/APS (inset: SEM image of nanowire-like PPy). Reproduced with permission.^[64] Copyright 2006, American Chemical Society.

Figure 5A, the AOT reversed cylindrical micelles were generated via a cooperative interaction between an aqueous FeCl_3 solution and AOT in an apolar solvent, and the formed micelles serve as the soft-templates to promote a rapid polymerization of pyrrole monomer catalyzed by Fe^{3+} ions along the outer surface of the templates. After removal of the AOT residue by washing with excessive ethanol, the hollow PPy nanotubes with ~95 nm in diameter and >5 μm in length were synthesized (Figure 5B). Notably, a series of parameters such as the weight ratio of aqueous FeCl_3 solution (9.0 M) to AOT, the type of solvents, and the reaction temperature have significant effects on the AOT reverse cylindrical micelle phase and the subsequent nanotube preparation, providing a promising route to tailor the structures of products. The diameter of PPy nanotubes increased with the increments of the weight ratio of aqueous FeCl_3 solution to AOT, the hydrocarbon chain length of apolar solvents, and the polymerization temperature.^[69] By using a similar method, uniform PEDOT nanotubes (Figure 5C) and PEDOT nanorods were also controllably prepared in Jang's group and Monohar's group.^[54,71,72] These results suggest the availability of the soft-template method based on AOT reversed micelles for the fabrication of 1D hollow- or solid-type conducting polymer nanostructures. Recently, it was also demonstrated by Wang et al., that

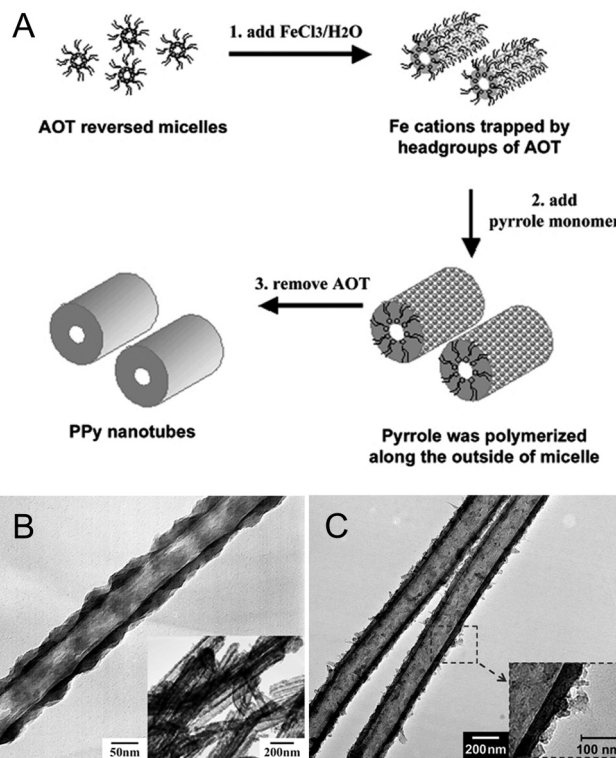


Figure 5. A) Schematic illustration of PPy nanotubes fabrication using AOT reversed microemulsion polymerization, B) Transmission electron microscopy (TEM) image of the resulting PPy nanotubes. Reproduced with permission.^[69] Copyright 2003, The Royal Society of Chemistry. C) TEM image of the resultant PEDOT nanotubes. Reproduced with permission.^[54]

the regular and well-dispersed PEDOT nanorods with widths of 40–60 nm and lengths of 370–460 nm can be synthesized by using AOT as a surfactant and $\text{Ce}(\text{SO}_4)_2 \cdot 4\text{H}_2\text{O}$ as an oxidant.^[73]

Clearly, the soft-template method is an important strategy for the design, synthesis, and regulation of 1D conducting polymer nanomaterials comparable to the hard-template method because of their salient advantages such as simplicity, versatility, low-cost production, easy operation, and ambient liquid conditions, etc. However, poor stability of the soft templates and the difficulty in a refined control over size and morphology of the obtained products, limit the application of the soft-template method. Therefore, more efforts are needed to solve these problems by in-depth understanding the mechanisms associated with this method.

2.1.3. Novel Wire-Template Method

As a significant progress, novel wire-template method has emerged as one of powerful and rising-star strategies for the controlled synthesis of 1D conducting polymer nanostructures because it combines the merits of both the hard-templates (good stability) and the soft-templates (easy for pre-formation and post-removal). In principle, this wire-template method employs pre-existing 1D nanomaterials as the templates to form 1D nanocomposites by growing conducting polymers on their surfaces. For this method, the used templates act as the roles of physical scaffolds and/or

reactive reagents.^[18] Thus, hollow tubular nanostructures of conducting polymers can be obtained and the templates can be easily removed (i.e., post-treatment of mild etching, washing by water, or self-degradation etc.). The main advantage of this wire-template method lies in the fact that, large quantities of nanotubes can be obtained at low cost and the size (e.g., inner/outer diameter, length, and aspect ratio) of the obtained materials can be effectively controlled at the same time. In addition, this method can also be used to selectively produce various conducting polymer based 1D nanocomposites with refined structures, such as core-shell nanowires, coaxial nanocables, and hybrid nanotubes.

In this method, the wire-templates can be derived from many ordinary materials such as metals, oxides and inorganic salts, organic molecules and polymers, organometallic complexes, as well as biomaterials, etc. According to the characteristics of the wire-templates, we will summarize and discuss some recent achievements as below. It should be pointed out that some articles have covered the controllable synthesis of a variety of 1D conducting polymer nanostructures and their composites using some conventional wire-templates, such as TiO₂ nanowires,^[74,75] Bi₂S₃ nanorods,^[76] carbon nanotubes (CNTs),^[77–79] PANI nanorods,^[80] electrospun polymer nanofibers,^[81] thin glass tubes,^[82] nitrocellulose fibers,^[83] etc. However, their synthetic details will not be discussed in this review because the involved mechanisms in the wire-template method are similar to those in the conventional hard-template method.

Water-Soluble Wire Templates. With good water-dissolvability, some of 1D nanostructured materials have unique merits to be used as the wire-templates to synthesize new 1D nanostructures, because they can be easily removed by simple water washing without any hazardous or toxic solvents. Some water-soluble wire-templates such as Na₂SO₄ nanowires, Na₃Au(SO₃)₂ nanobelts, and KCdCl₃ nanowires have recently been developed, and served as versatile wire-templates for the large-scale synthesis of organic polyelectrolyte nanotubes, metallic Au nanotubes, as well as inorganic CdS and CdSe semiconductor nanotubes.^[84–86] By contrast, fewer studies have focused on the use of water-soluble wire-templates to produce 1D conducting polymer nanostructures. As a typical case, Dai and Lu employed the water-soluble but acid-solution stable methyl orange (MO) fibrils as a general wire-template to fabricate tubular conducting polymer nanostructures, where the uniform PPy, PANI and PEDOT micro-/nanotubes were obtained after washing the collected precipitates with neutral water.^[87] This finding offers a novel, facile, versatile, and inexpensive approach to synthesize hollow conducting polymer micro-/nanotubules in mass production though their electric conductivities are not high (<0.1 S cm⁻¹) due to the low doping level.^[87] This method circumvents the shortcomings of both “hard” and “soft” templates to a certain extent, and can be extended to other systems for the fabrication of functional nanostructures. However, the toxicity of MO hinders its practical usages. So, developing 1D water-soluble template materials with nontoxicity (or low toxicity) such as water-dissolvable inorganic salts, amino acid complexes, polymers, etc., is particularly important for future research in this field. This water-soluble template method implies a promising and important “green” synthetic strategy for nano-fabrication and nano-engineering, not only of 1D nanotubular structures but also of other advanced composite hollow nanoarchitectures.

Reactive Self-Degraded Wire Templates. In recent years, the template synthesis based on reactive self-degraded nanowires/nanofibers has drawn increasing attention for the controlled preparation of 1D conducting polymer nanostructures. A fibrillar complex of FeCl₃ and MO (FeCl₃-MO) has acted as a reactive self-degraded template as well as an effective dopant to synthesize PPy on its surface and subsequently to promote the formation of hollow azo-functionalized PPy nanotubes.^[88] During this synthetic process, the FeCl₃-MO complex oxidized the pyrrole monomer to initiate a polymerization while itself reduced to soluble Fe²⁺ ions, thus caused the continuous consumption and degradation of the reactive wire-template, finally formed highly conductive PPy nanotubes (~ 96 S cm⁻¹) without any additional template removal steps. In this system, the morphology and size control can be realized by introducing a cationic CTAB surfactant with different concentrations to modify the reactive FeCl₃-MO template (Figure 6).^[89] When the CTAB concentration increased to a value higher than its critical micelle concentration, the hollow PPy nanotubes got thinner and eventually became solid

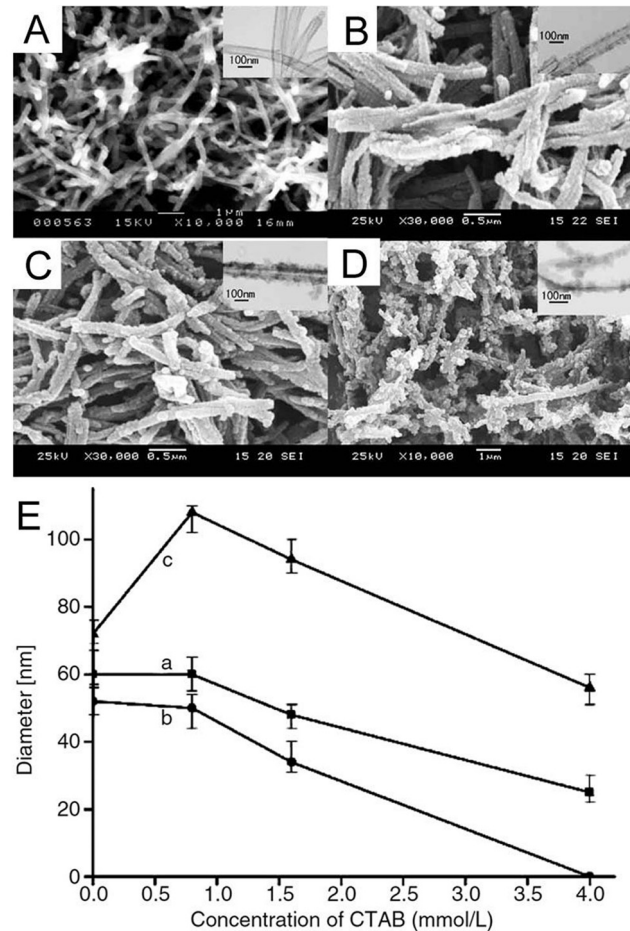


Figure 6. SEM and TEM (insets) images of PPy nanotubes/wires synthesized by a FeCl₃-MO reactive self-degraded wire-template under different CTAB concentrations: (A) 0, (B) 0.8 mM, (C) 1.6 mM, and (D) 4.0 mM. E) Plots of (a) template diameter, (b) inner and (c) outer diameters of 1D nanostructured PPy, as a function of CTAB concentration. Reproduced with permission.^[89] Copyright 2006, The Institute of Physics Publishing Ltd.

PPy nanowires (Figure 6). The good versatility of the $\text{FeCl}_3\text{-MO}$ fibrils also renders them to act as a reactive wire-template for the synthesis of nanotubular PANI and PANI/Au composite nanotubes.^[90] During the reaction, the template itself self-degraded automatically. Similarly, another fibrillar complex of $\text{AgNO}_3\text{-MO}$ was also developed as the active self-degraded wire-template to generate MO-doped PPy/Ag composite micro-/nanotubes with high conductivity (10 S cm^{-1}) and good electrochemical activity.^[91] The reactive self-degraded wire-template based on MO complex family suggests a simple and effective synthetic strategy to 1D conducting polymer nanostructures with controllable shapes, sizes and compositions. Thus this wire-template synthesis has the virtues of no trivial process for template removal and easy production in large scale, which are very helpful to obtain 1D conducting polymer nanostructures for various applications.

1D nanostructured metal oxides, as another important class of reactive self-degraded templates, have also been intensively used to produce 1D conducting polymer nanostructures. In the case of MnO_2 nanowires, they served as both the wire-template and the oxidant for the synthesis of PANI nanotubes.^[92] The oxidation potential of MnO_2 was able to initiate the aniline polymerization, and as the polymerization proceeded, the PANI layers generated along the surfaces of the MnO_2 nanowires while the MnO_2 core was consumed at the same time (Figure 7A). As a result, the morphology of the MnO_2 nanowires was finally

transferred to that of PANI nanotubes, whose external size and shape were similar in dimensions to that of the MnO_2 nanowire template (Figure 7C–D). By simply varying the morphologies and sizes of the MnO_2 templates, the structural parameters of PANI products (i.e., diameter, length, and morphology) could be accurately controlled. When MnO_2 nanotubes were used as the alternative to MnO_2 nanowires, the double-shell PANI nanotubules (one round and closed, and the other opened end) were obtained by this self-degraded wire-template method (Figure 7B and 7E–F). Because the reactive MnO_2 wire-template was converted to soluble Mn^{2+} ions during the polymerization process, no additional purification steps were needed to obtain the pure conducting polymers. Besides the MnO_2 wire-templates, nanobelts/nanoribbons of MoO_3 , VO_2 , and SnO_2 have also been used as reactive wire-templates because of their anisotropic nanostructures and oxidizing characters.^[93] As a consequence, several hybrid types of metal oxide semiconductor-PPy/PANI core-shell nanobelts were synthesized by this kind of in situ polymerization. And it is possible to control the composition, morphology and size of the products by selecting suitable hydrothermal parameters (e.g., pH value, reaction temperature and time). All of these results demonstrate that the reactive self-degraded wire-template method is a simple, convenient, and effective strategy to refinedly controlled synthesis of 1D nanostructured conducting polymers and some complicated hollow structures, as well as some organic/inorganic/metallic hybrid nanocomposites.

Seeding Wire Templates. By introducing a small amount of 1D nanostructures such as PANI nanofibers (~50 nm diameter), or SWNTs bundles (~20 nm diameter), or hexapeptide nanofibers (~12 nm diameter), or nanofibrous V_2O_5 (~15 nm diameter) into the polymerized system of aniline solutions, Monohar et al. firstly proposed a “seeding template” approach for the controlled synthesis of PANI nanofibers.^[94] Notably, only 1–4 mg of the nanowire seeds was enough for the synthesis of about 200 mg of PANI nanofibers with an average diameter of 20–60 nm and a conductivity of 2–10 S cm^{-1} . These seeding wire-templates were also used to synthesize doped-PPy nanofibers (60–90 nm in diameter, ~50 S cm^{-1} in conductivity) and doped-PEDOT nanofibers (100–180 nm in diameter, ~16 S cm^{-1} in conductivity), whereas only granular products were obtained without using any seeding templates.^[95,96] The nanofibrillar morphology of the seeds is crucial for nanofiber synthesis because the granular seeds only produce granular, agglomerated polymer nanostructures. It was also found that, different reaction conditions play an essential role in determining the morphology and diameter of nanofiber precipitates. For example, PPy nanofibers synthesized in the system of ethanol solvent were smoother, more regular and free of any granules compared to PPy products obtained under aqueous solutions. In the ethanol system, by using V_2O_5 nanofibrils as seed wire-templates and FeCl_3 as an oxidant, the PPy nanofibers with smallest diameter (around 30 nm) were achieved by stirring the V_2O_5 seeds in ethanol for 30 min, and the increased diameter of PPy nanofibers up to 100 nm was obtained upon stirring for 12 h.^[95] A recent “green” nanofabrication reported by Liu and Zhang et al. further suggested that 2 mg of V_2O_5 nanofibers could be served as a catalytic seeding template to synthesize ~100 mg of PPy nanofibers (diameters: 80–100 nm) in a H_2O_2 oxidant condition.^[97]

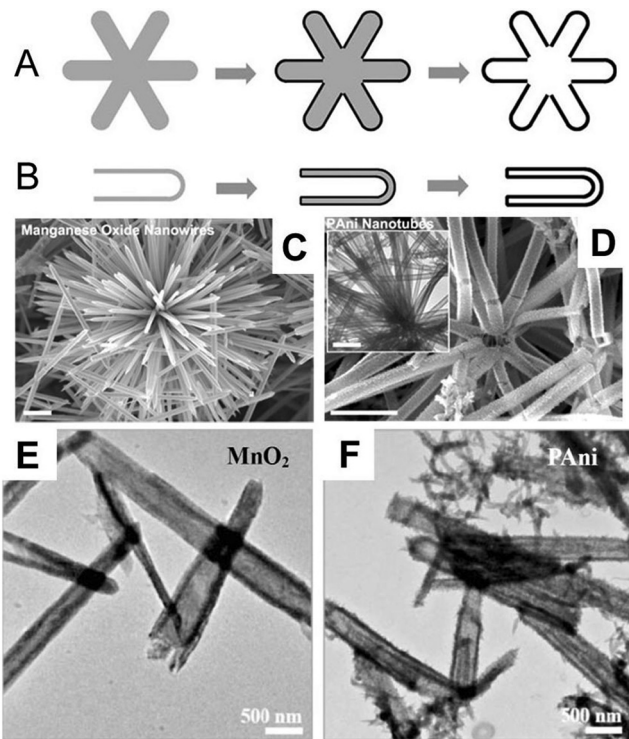


Figure 7. Schematic illustration of the formation mechanism of the PANI nanotubes fabricated from (A) MnO_2 nanowires and (B) MnO_2 nanotubes, respectively. SEM images of (C) the MnO_2 nanowire templates, and (D) the resulting PANI nanotubes (inset: a TEM image of the PANI nanotubes). The scale bar is 1 μm . TEM images of (E) the MnO_2 nanotube templates, and (F) the resultant double-shell PANI nanotubes. The scale bar is 500 nm. Reproduced with permission.^[92] Copyright 2007, Wiley VCH.

Afterwards, it should be mentioned that, when the V₂O₅ nanofibers were used in large amounts, they would not act as the seeding wire-templates but just as the typically metal oxide wire-templates.^[98] In this case, the doped-PPy nanotubes with an electrical conductivity of ~2 S cm⁻¹ and the pore diameters as small as 4–8 nm were obtained. These nanotubes could be fabricated into 1D hybrid nanostructures of nanotubular PPY supported nanoparticles of Ag, Au, and Pd, etc.

Obviously, using the novel seeding wire-template method, bulk quantities of various conducting polymer nanowires/fibers can be rapidly synthesized in one-step. The fibrillar nano-seeds always play a dual role as both the wire-templates and the reactive oxidants, hence guiding the anisotropic growth of products while omitting a post-treatment of template removal. Consequently, this method indicates a more facile and effective strategy compared with the conventional hard- or soft-template methods. However, there is still difficulty in fabricating hollow nanotubular structures of conducting polymers as well as some advanced 1D nanostructures, and the precise mechanism of how such a small amount of seeds can generate bulk quantities of conducting polymer nanofibers is still not clear. Furthermore, its broader utilizing range is restricted in fewer members of the seed families. Therefore, all of these need further investigations.

Biological Wire-templates. As one of the representative bio-templates, tobacco mosaic virus (TMV) has served as a useful scaffold to grow 1D conducting polymer nanostructures by Niu and Koley et al.^[99–101] Because TMV particles possessed uniform nanotubular structures (~18 nm in diameter, and 300 nm in length with a 4 nm cylindrical cavity along the central core) and the negatively charged surface residues, these biological wire-templates thus could “bind” monomers of pyrrole/aniline through electrostatic interactions or hydrogen bonding, and then effectively directed the *in situ* generation of conducting polymer nanowires with controllable narrow size distributions. Besides TMV, a series of other biological molecules such as DNAs,^[102,103] peptides,^[104] and proteins^[105] have also been employed as the novel wire-templates to synthesize 1D nanostructured conducting polymers and composites, such as PANI nanowires, PPY nanowires, core-shell peptide/PANI nanowires and PANI nanotubes, as well as conducting PEDOT nanowire networks. Although the utilization of these biological wire-templates for the synthesis of 1D conducting polymer nanostructures is still in its infancy, and some issues on the controlled synthesis of 1D nanostructures remain not resolved, there is no doubt that, they will have good potentials in the future due to their good biocompatibility and wide applications in the field of biomedicines.

2.2. Template-Free Synthesis

In template-free synthesis, 1D nanostructured conducting polymers are fabricated without any hard or soft templates. Mostly used template-free methods include self-assembly, electrospinning, and nanoscale patterning, etc. Amongst them, the self-assembly belongs to a native chemical method to synthesize 1D conducting polymer nanostructures, whereas the electrospinning is one of important physical methods to produce

conducting polymers at 1D nanoscale level. As to the patterning technique, it is an effective and attractive template-free method to engineer 1D conjugated polymer nanostructures, particularly for the direct and efficient process on various organic opto-electronic devices. However, discussions of the nanoscale patterning will not be covered in this overview because they have been discussed in other comprehensive reviews.^[13,14]

2.2.1. Self Assembly

Self-assembly is widely adopted in mass production of 1D conducting polymer nanostructures. Ordinarily, it is accomplished by non-covalent forces such as π-π stacking, dipole-dipole, hydrophobic, Van der Waals, hydrogen bonding, electrostatic, and ion-dipole interactions of the building blocks to spontaneously form anisotropic aggregates or oriented structures under suitable conditions. By using the self-assembly, several explorations have been made to obtain 1D nanostructured conducting polymers in abundance.^[6,12,106]

The solution self-assembly developed by Wan et al. is a simple and fully effective template-free strategy based on a dopant induced micelle self-assembly route to various 1D conducting polymer nanostructures without any external templates.^[106] Solid nanofibers/nanowires and hollow nanotubes of conducting PPY, PANI, PEDOT, and their functionalized composites or hybrids have all been successfully synthesized by this *in situ* doping polymerization in the presence of an organic acid such as β-naphthalene sulfuric acid (β-NSA) or enantiomeric camphor sulfonic acid (CSA) as the dopant. Control over the morphology and size of the products can be achieved by manipulating the synthetic conditions such as different kinds of dopants and oxidants, varied molar ratios of monomer to dopant and monomer to oxidant, as well as polymerization time and temperature. The formation mechanisms, affecting parameters, physical and chemical properties of these self-assembled 1D conducting polymer nanostructures have been systematically summarized in some review papers^[17,106,107] and a book,^[108] thus we will not further discuss them here.

Some other template-free polymerizations have also been developed to prepare nanofibers or nanotubes of conducting polymers without using any structural directing agents.^[6] For example, Kaner's group proposed an aqueous/organic interfacial polymerization to synthesize high-quality PANI nanofibers under ambient conditions, where the products generated at the interface and then self-dispersed into the water phase.^[109,110] These entangled polymer nanofibers showed excellent electrochemical and sensing properties, and had a controllable diameter between 30 and 120 nm depending on the type of acid used for the polymerization. With this interfacial polymerization, conducting PEDOT nanorods and Au-PEDOT nanocables were fabricated in a similar way.^[111,112] Besides, rapid-mixing reaction,^[113] dilute polymerization,^[114] ultrasonic synthesis,^[115] radiolytic synthesis,^[116] and microwave-assisted synthesis^[117,118] have also been used to produce 1D conducting polymer nanostructures. Additionally, a template-free electrochemical strategy to the direct synthesis of PANI, PPY, and PEDOT nanorods/nanofibers/nanowires/nanobelts has been realized in solutions^[119–121] or in channels between two electrodes^[122–124] by controlling the electrochemical synthesis conditions (pH,

oxidation potential, electrode geometry). Despite many differences existed in these template-free approaches, it stands to reason that the anisotropic products can be obtained by a careful control of the synthetic conditions. In fact, the essence of all these methods is the self-assembly process because the inherently anisotropic growth of the products from molecules or particles to nanostructured conducting polymers does not need the assistance of any templates or structure directing agents during the chemical or electrochemical polymerization process.

Apart from above mentioned self-assembly associated with the polymerizations, the synthesized conducting polymers themselves can self-assemble into 1D nanostructures by controlling suitable surroundings for their nucleation and anisotropic growth. Among most of π -conjugated polymers, the non-covalent forces are dominated by the π - π stacking due to their planar molecular frameworks and highly delocalized π -systems.^[12] Such a determined anisotropy in non-covalent intermolecular interactions leads to preferential self-assembly or self-organization in one direction. Thus π -conjugated polymers appear to have a strong tendency to grow orientedly fibrillar nanostructures during crystallization processes of the common precipitation in bulk solution systems or of the solvent evaporation/drying on thin films. Recent investigations on the self-assembled nanowires, nanofibers and nanoarrays from conducting polymers have demonstrated its promise and versatility among diverse types of π -conjugated molecular structures, such as PANI,^[125,126] P3HT,^[127,128] P3BT,^[129] and P3OT,^[130] etc. Self-assembly to these 1D nanostructures is commonly generated in bulk solution or surface/interface, which has been discussed in depth in some excellent reviews,^[6,12,131] so it will not be discussed in this section again.

Indeed, the simplicity and versatility of these template-free chemical routes make the self-assembly strategy a fascinating methodology for the synthesis of 1D conducting polymer nanostructures. The synthetic method of self-assembled 1D nanostructured conducting polymers and composites is very useful for processing low-cost, light-weight and flexible thin-film devices such as field-effect transistors (FETs), solar cells, and light-emitting diodes (LEDs) at micro/nanoscale level.^[13,14,132] However, the mechanisms of the self-assembly involved in these template-free methods are complicated and not clearly understood. Besides, it still lacks a precise control in the morphologies, dimensions, and properties of the self-assembled conducting polymer nanostructures. All of these are important areas of future research.

2.2.2. Electrospinning

Electrospinning is an easy and effective physical method to prepare micro-/nanoscale fibers without any templates.^[133] Commonly, the basic set up for electrospinning consists of three major components: a high-voltage power supply, a spinneret,

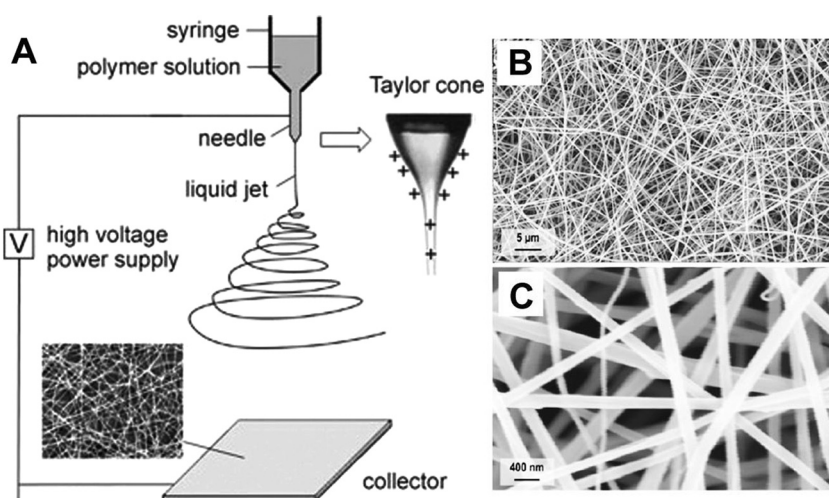


Figure 8. A) Schematic diagram of the basic setup for electrospinning. Reproduced with permission.^[134] Copyright 2004, Wiley VCH. B-C) SEM images with different magnifications of the electrospun composite BEH-PPV/methanofullerene heterojunction nanofibers with a weight ratio of 1:10. Reproduced with permission.^[137] Copyright 2009, American Chemical Society.

and an electrical conductive collector (Figure 8A).^[134] When using electrospinning to fabricate nanofibers, a high electrical field is applied between a polymer fluid contained in a syringe with a capillary tip and a conductive collection screen. Once the applied electric field reaches a high enough value to allow the electrostatic forces to overcome the surface tension of the polymer solution, a liquid jet forms and moves towards the counter electrode. During the movement and stretching of the liquid jet, the solvent evaporates (or the melt solidifies), and the solid fibers with certain diameters ranging from nanometer to micrometer are accumulated on the collector surface. The morphology and size of the fibers are controlled by the processing parameters,^[108,135] such as the applied voltage, the viscosity/conductivity of solution, the solution surface tension, the humidity of the environment, as well as the distance between the nozzle and the collector, etc. In contrast to the template-based synthesis and self-assembly, electrospinning is advantageous for synthesizing long nanofibers with high aspect ratios and good surface quality. Thus, it has been widely employed to produce nanofibers or coaxial nanocables of conducting polymers and their composites.^[12,136]

PANI is one of the first conducting polymers studied in the generation of 1D electrospun nanostructures, where the electrospinning process has been carried out from a solution of PANI in sulfuric acid,^[138,139] or a blend of PANI and poly(ethylene oxide) (PEO) (or PC, PS, PMMA) in chloroform,^[140,141] or a coaxial fluid of PANI and poly(vinyl alcohol) (PVA) in water.^[142] Controllable diameters of these PANI and PANI-based composite nanofibers varied from 5 nm to 2 μ m, relying mainly on the preparation conditions. The increased conductivity of the nanofibers up to 0.1 S cm⁻¹ could be obtained by using CSA as a dopant in the electrospun solution.^[139,143] Conducting PPy nanofibers with diameters of 70–300 nm and composite PPy/PEO nanofibers have also been fabricated by electrospinning.^[144] It was found that, both the average diameter and electrical conductivity of the electrospun PPy nanofibers could be adjusted

by the content ratio of PPy/PEO. Using the electrospinning method, the nanofibrous blends of a conducting donor polymer, poly[2,5-(2'-ethylhexyloxy)]-1,4-phenylenevinylene (BEH-PPV) with a soluble electron acceptor of methanofullerene was developed, and the diameters of the electrospun fibers were uniform throughout and ranged from ~100 to 250 nm (Figure 8B–C).^[137] The obtained electrospun nanofibers showed a complete quenching of photoluminescence (PL) emission because of the ultrafast charge transfer from BEH-PPV to methanofullerene, indicating a promising application of electrospinning for the construction of nanostructured heterojunctions in solar cells. Nanofibers based on other conducting polymers such as PPV and its derivatives, P3HT and its derivatives, and other conjugated polymers/inorganic semiconductors can be also produced by electrospinning. The researches related to their morphology and size control, electrical/optical properties investigation, as well as the device applications in FETs, LEDs, solar cells and sensors have been systematically documented in recent reviews.^[12,145]

Although the electrospinning is a powerful physical strategy for large-scale synthesis of continuous long nanofibers of polymers and their composites, it still seems not easy to obtain pure nanofibers or nanotubes of all conducting polymers without the assistance of a flexible-chain insulating polymers. These challenges mainly originate from the small molecular weight, high chains rigidity, and limited solubility of most conjugated polymers. On the other hand, the conductivity of the electrospun nanofibers of conducting polymers is usually low (<0.1 S cm⁻¹), which limits their practical applications.

3. Energy Applications of 1D Conducting Polymer Nanostructures

As discussed in previous sections, various 1D conducting polymer nanomaterials with desired morphology and size can be controllably synthesized by using an efficient template methodology, or a template-free methodology. The unique electrical properties, charge transport properties, optical properties, and redox electrochemical properties of these functional materials are related with their anisotropic nanostructures. These advantages make them promising candidates for applications in high performance energy devices. Therefore, this kind of advanced nanostructured materials can act as important active materials, or electrodes, or buffer materials, or catalysts, or electrode/catalyst supports, which play critical roles in energy conversion and storage applications such as various solar cells, fuel cells, rechargeable lithium batteries, and electrochemical supercapacitors. Significant advances in the energy applications of 1D conducting polymer nanostructures are reviewed in this section, where the relationships between the material structures and device performances are discussed in depth as below.

3.1. Solar Cells

Solar cells, which can convert sun light energy to electrical energy, are considered as the most promising devices to utilize the renewable and clean solar energy resource in a sustainable

way. Although silicon solar cells (i.e., crystalline silicon, and polysilicon systems) dominate the market now, the cost of these cells limits their popularization. In contrast, organic or hybrid photovoltaic devices including polymer solar cells (PSCs), hybrid solar cells (HSCs), and dye-sensitized solar cells (DSSCs) have attracted considerable attention over the past decade due to their advantages such as light weight, flexibility and low cost.^[146–149] The focus on solar cell devices is to improve the energy conversion efficiency and the device stability while decreasing the processing cost. It has been known that the performance of solar cells depends not only on the employed materials (active materials, electrode materials, and buffer materials), but also on their morphologies and the interfacial contact properties. So, the scientific issues in materials design and device engineering are of critical importance in order to bring various solar cells to full commercialization. From the view of pursuing solar cell devices with low cost, thin, light, and flexible architectures, conducting polymers are more competitive candidates for photovoltaic cells than conventional inorganic counterparts.^[150,151] Currently, the progress on the synthesis of new π -conjugated polymers as well as the fabrication of novel 1D semiconducting polymers with controllable nanostructures and improved performance,^[12] has paved a new way for next generation high performance solar cells at low cost.

3.1.1. Polymer Solar Cells (PSCs)

Polymer solar cells (PSCs), also known as OSCs, have drawn increasing attention in recent years.^[152–155] For most of PSCs, the device structure is composed of an active layer, electrodes and interfacial buffer layers. **Figure 9** depicts the schematic device structure and the current density-voltage (*J*-*V*) characteristic of a typical solar cell device. As shown in Figure 9A, a photoactive layer of about 100–200 nm, is sandwiched between the anode and cathode (one of the electrodes must be transparent for light transmittance), while additional thin films of electron or hole transporting materials as buffer layers are selectively inserted (or not) between electrodes and active materials layers in a solar cell device. A series of parameters including open-circuit voltage (V_{oc}), short-circuit current density (J_{sc}), and maximum output power (P_{max}) extracted from the *J*-*V* curve, are generally used to calculate the photovoltaic performance of solar cells (Figure 9B). A higher V_{oc} , a larger fill factor (FF) and a higher power conversion efficiency (PCE) indicate the better performance of a solar cell device, where the FF and PCE are defined as the ratio of $(P_{max})/(V_{oc} \times J_{sc})$ and the ratio of $P_{max}/P_{in} = (FF \times V_{oc} \times J_{sc})/P_{in}$, respectively, and P_{in} is the input irradiation power. The external quantum efficiency (EQE), also known as the incident photon to current efficiency (IPCE), represents the ratio of the number of electrons collected under short circuit conditions to the number of incident photons. This basic parameter is also introduced to estimate the cell performance, which can give a direct description of the light utilization efficiency for a solar cell device.

In PSCs, one of the most fundamental issues is the selection of suitable materials to serve as donors (p-type) and acceptors (n-type) to form an efficient heterojunction structure, which can generate excitons and help the dissociated charge carriers (free electrons or holes) to transport to the corresponding

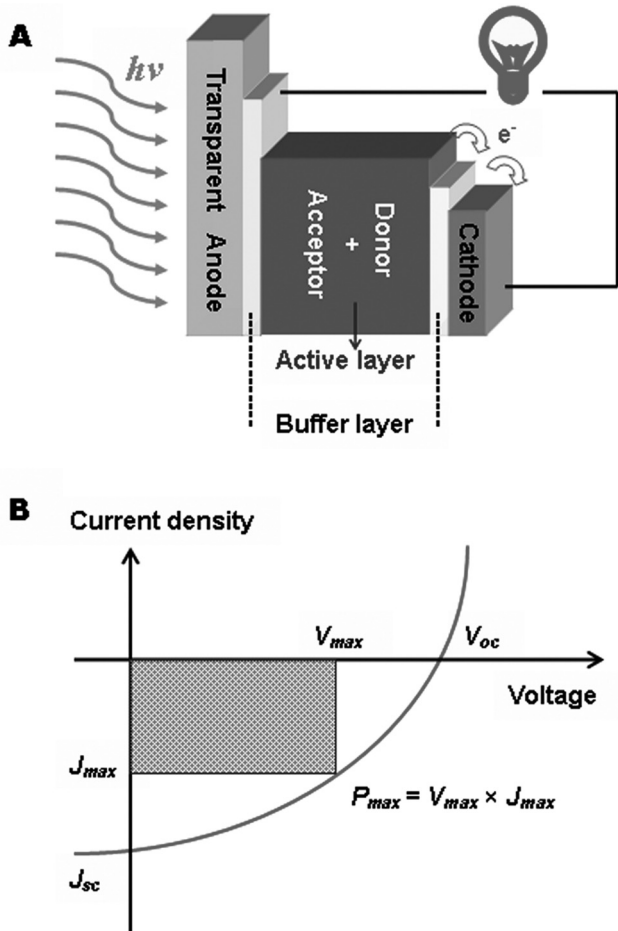


Figure 9. A) Schematic representation of one-single solar cell with a device configuration of transparent anode/anode buffer layer/active layer/cathode buffer layer/cathode, and B) Current density-voltage (J - V) characteristic of a solar cell under sunlight illumination.

electrodes under light illumination. PTh derivatives (i.e., P3HT, P3BT, P3OT, and so on), are the most used p-type conjugated polymers (donors), and fullerene (C_{60}) and its soluble derivatives ([6,6]-phenyl- C_{61} -butyric acid methyl ester (PCBM) and [6,6]-phenyl- C_{71} -butyric acid methyl ester ($PC_{70}BM$)), are the most important n-type materials (acceptors). Due to their salient light harvesting and charge transport properties, the PCEs achieved in most P3HT/PCBM based PSCs are in the range of 2–6% with the conventional or inverted device configurations.^[156–160] By contrast, another important PSC system based on poly[2-methoxy-5-(3',7'-dimethyloctyloxy)-1,4-phenylenevinylene] (MDMO-PPV) and C_{60} (or PCBM and $PC_{70}BM$) generally showed lower PCE values (<3%).^[161,162] Therefore, the photo-active layer based on P3HT/PCBM is frequently used because of its attractive advantages,^[12,151] and numerous studies have focused on the fabrication and optimization of P3HT/PCBM based PSC devices.^[163] Certainly some other newly designed materials such as low band-gap polymers with thieno[3,4-*b*]-thiophene and benzodithiophene alternating units^[164a], and ladder-type oligo-*p*-phenylene-containing copolymers^[165] have also been developed for PSCs due to the high efficiency (PCE ~ 8%),

and/or the large open circuit voltage ($V_{oc} > 1.0$ V). It should be noted that, PSC efficiencies as high as 9.2% have been achieved according to media reports, and the highest confirmed PSC efficiency to date is 8.3%.^[164b–d]

To achieve highly efficient PSCs, it is critical to control over the morphology of donor/acceptor (D/A) active layer to get the desired nanoscale phase separation. Especially for the donor polymer semiconductors, after being fabricated into 1D nanostructures, they can enhance their molecular orientation and crystallization, improve the percolation of acceptor materials, enlarge contact area between D/A interface, and provide short and continuous pathway for charge isolation and transportation.^[166–169] These benefits led to an improved light-harvesting, enhanced charge generation and dissociation, and a reduced recombination of electrons and holes, ultimately a high performance of PSCs.^[169–171] So far, tremendous efforts have been made to the design and synthesis of new low band-gap polymers, to the fabrication of 1D polymer nanostructures, as well as to the engineering of the D/A heterojunction blends used in PSCs. Subsequently, there have been a great deal of reports on photovoltaic properties of these 1D π -conjugated polymer nanostructures for solar cells applications.^[12,172,173] **Table 1** summarizes the device characteristics of some representative PSCs based on 1D conducting polymer nanostructures.

Studies by many groups in the past years demonstrated that various 1D PTh derived polymers can be prepared by the in situ growth on the bulk heterojunction (BHJ) blend.^[195] Thermal annealing^[167,177,178,196] and solvent assisted annealing^[178,179,183] are frequently used for the in situ growth of the active BHJ blend containing 1D semiconducting nanostructures due to the easy processing. Initially, both thermal and solvent annealing can lead to the formation of a highly concentrated phase of the donor polymer, which contains a small amount of polymer crystals. Then, with the annealing process going on, the crystal nucleation and the anisotropic growth of the polymer take place, and finally resulting in a continuous donor polymer phase surrounded by an acceptor material phase. Using this method, a nanoscale phase separation in the active layer can be achieved to induce large D/A interface area, high charge transport ability and good substantial durability.^[177,197] On the other hand, novel strategies of self-assembly to 1D PTh derivative nanowires, nanofibers, nanorods, and others have been developed in solution systems,^[182,190,192,194] where these pre-fabricated 1D nanostructures are extensively employed as a solid active donor to blend with the acceptor component for attaining the nanoscale phase separation of the active layer in PSCs.^[180,184] The merit of this method lies in the fact that a high efficiency can be controllably actualized without post-treatment while similar benefits from the 1D nanostructured donor polymers are retained.

As one of the most important PTh derivatives, regioregular P3HT with the morphology of nanowires or nanofibers has been mostly explored as a donor in PSCs because it combines the advantages of an ideal size (ca. 10–50 nm diameters, which are within the exciton diffusion length range), a good crystallinity, a high carrier mobility, an excellent dispersibility in organic solvents, and a favorable optical absorption spectrum.^[163,177] In the P3HT nanofibers/nanowires based PSC system, BHJ solar cells are the mostly designed device structure because of their high performance (usually in the range of 3–5% PCE, see Table 1),

Table 1. Device characteristics of some representative PSCs based on 1D conducting polymer nanostructures.

Active donor-acceptor layer	Cathode configuration ^{a)}	V_{oc} [V]	J_{sc} [mA cm ⁻²]	FF [%]	PCE [%]	Refs.
P3HT-NWs:PCBM	LiF/Al	0.61	10.42	64	4.09	[174]
P3HT-NWs:PCBM	Ca/Al	0.59	9.51	58	3.23	[175]
P3HT/P3HT-NWs:PCBM	Ca/Al	0.59	10.27	65	3.94	[175]
P3HT-NWs:PCBM	Ca/Al	0.60	10.9	62.1	4.04	[176]
P3HT-NWs:PCBM	LiF/Al	0.58	10.9	61	3.8	[177]
P3HT-NFs:PCBM	Ca/Al	0.60	11.09	63	4.14	[178]
P3HT-NFs:PCBM	Ca/Al	0.60	10.64	68.4	4.29	[179]
P3HT-NFs:PCBM	LiF/Al	0.589	10.51	58.2	3.6	[180]
P3HT-NFs:PCBM	LiF/Al	0.60	9.4	62	3.5	[167]
P3HT-NFs:PCBM	Al	0.53	10.13	42	2.29	[181]
P3HT-NFs:PCBM	PF-EP/Al	0.62	9.58	61	3.6	[182]
P3HT-NFs:PCBM	LiF/Al	0.57	10.72	54	3.29	[183]
P3HT-NFs:F8BT	Al	0.93	0.291	20	0.055	[184]
P3HT:PCBM nanoarrays	LiF/Al	0.658	10.54	64	4.43	[185]
P3HT-NRs:C ₆₀	LiF/Al	0.51	4.75	46	1.12	[186]
Core-shell P3HT:PCBM NR arrays	Al	0.46	8.7	50	2.00	[187a]
Core-shell P3HT:PCBM NR arrays	ITO/TiO _x ^{b)}	0.59	10.70	56.8	3.60	[187b]
P3HT-NR arrays:F8TBT	Al	1.14	3.3	49	1.85	[188]
P3BT-NWs:PCBM	LiF/Al	0.60	9.01	47	2.52	[189]
P3BT-NWs:PC ₇₀ BM	LiF/Al	0.60	8.43	59	3.0	[190]
P3BT-NWs:PC ₇₀ BM	LiF/Al	0.66	8.12	63	3.35	[191]
P3PT-NWs:PCBM	LiF/Al	0.56	7.19	65	2.62	[192]
P3PT-NWs:PC ₇₀ BM	LiF/Al	0.54	9.81	63	3.33	[192]
P3MBT-NWs:PC ₇₀ BM	Ca/Al	0.72	9.15	63	4.15	[193]
P3BT-block-P3OT NWs:PC ₇₀ BM	LiF/Al	0.53	9.85	0.65	3.38	[194]

^{a)}The anode configuration was fixed as: ITO/PEDOT:PSS; ^{b)}An inverted structure with the anode configuration of MoO₃/Ag.

while the PSCs based on planar heterojunction (PHJ) have also been developed in spite of their low efficiencies.^[186]

Using the *in situ* growth of 1D nanostructured P3HT as the donor in BHJ blend by post annealing treatment, a series of PSCs were fabricated and their photovoltaic properties were investigated considering several influencing factors on the device performances.^[167,177–179,183] After thermal or solvent assisted annealing, the morphology of the initial P3HT/PCBM blend turned into well oriented P3HT nanowires surrounded by crystalline PCBM in the active layer, which led to an enhanced light absorption, a better exciton separation, and a more efficient and balanced transportation of free carriers to the electrodes within the BHJ PSCs, subsequently resulting in the increased values of FF, J_{sc} , and PCEs of the corresponding solar cell devices.^[177] Furthermore, annealing conditions have a large impact on the morphology of blend films and the resulting solar cell performance. Jo and Kim et al. demonstrated that a mild solvent annealing led to an improved performance of solar cells ($V_{oc} = 0.60$ V, $J_{sc} = 11.09$ mA cm⁻², FF = 63%, and PCE = 4.14%) due to the well-ordered and stable morphology of P3HT nanofibers/PCBM BHJ. On the contrary, a

directly strong thermal annealing condition (150 °C) resulted in poor BHJ morphology and an apparently lower efficiency ($V_{oc} = 0.63$ V, $J_{sc} = 9.95$ mA cm⁻², FF = 49%, and PCE = 3.1%) due to the prevention of forming more elongated P3HT crystals.^[178] Using the solvent annealing strategy, the same group investigated the effect of different vertical component distributions (**Figure 10A–C**) on the performance of P3HT nanofibrils/PCBM PSCs. An optimized solvent annealing for 120 min, drove the PCBM molecules to migrate or diffuse towards the top surface of the BHJ active layer, thus induced a new vertical component distribution favorable for improving the performance of the solar cells, especially for the PCE and internal quantum efficiency (η_{IQE}).^[179] The J–V characteristics under dark and AM 1.5G illumination conditions, as shown in **Figure 10D**, describe that the optimized solar cells exhibit very low series resistance (R_s) of 1.6 Ω cm² and good device performance with a PCE = 4.29%, a $V_{oc} = 0.60$ V, a $J_{sc} = 10.64$ mA cm⁻², an FF = 68.4%. Considering that the active layer of these optimized devices has a thickness of around 290 nm (cross-sectional TEM image in **Figure 10D**), the average η_{IQE} value of ~78% was reasonably high for this type of BHJ PSCs (**Figure 10E**). Despite the devices

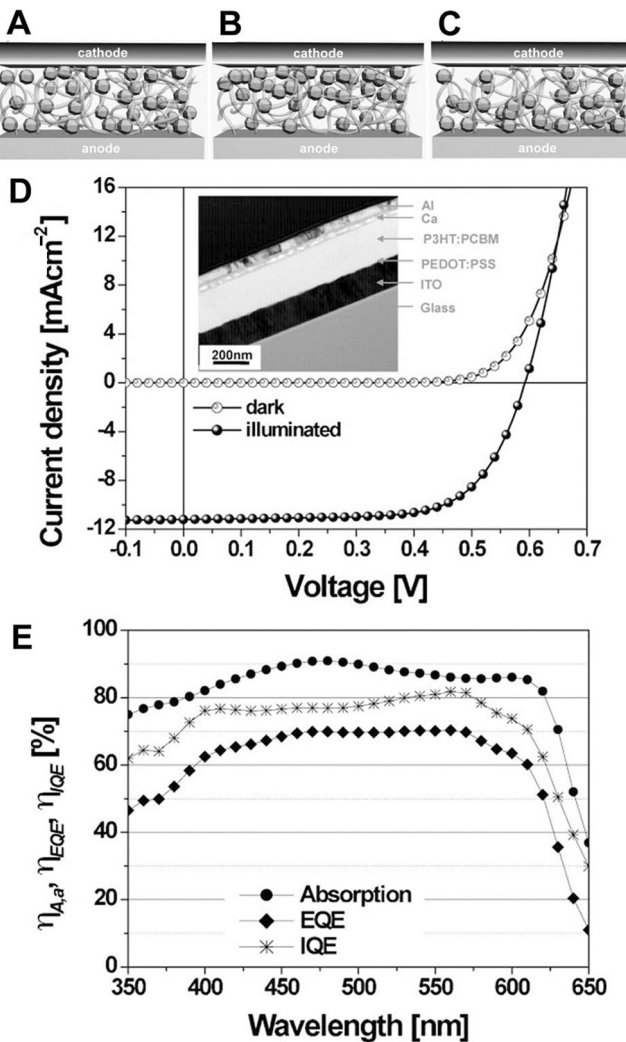


Figure 10. Schematic illustration of different vertical component distributions in a cross-sectional P3HT/PCBM blend: (A) a homogeneous distribution, (B) a PCBM-rich, and (C) a PCBM-poor distribution near the top electrode, as predicted from the distribution of PCBM crystals in the nanofibrillar P3HT matrix, (D) J-V characteristics under dark and AM 1.5G illuminated conditions of a high-performance P3HT:PCBM solar cell fabricated by controlled solvent annealing for 120 min (inset: cross-sectional TEM image of the device), and (E) The spectra of absorption efficiency ($\eta_{A,a}$), IPCE (η_{EQE}), and η_{IQE} of the device. Reproduced with permission.^[179] Copyright 2009, Wiley VCH.

based on P3HT/PCBM BHJ show quite high efficiencies owing to superior nanoscale phase separation of the BHJ blend after the annealing treatments,^[196] devices with better performances would be realized via further optimizations. Thus, other variables affecting the device performance, such as the composition and mass ratio of BHJ components, the thickness of BHJ layer, the selection of buffer layers, the morphology and thickness of buffer layers, and new device configurations with inverted or tandem structures should be considered.^[198,199]

With regard to the preformed P3HT nanowires employed in PSCs, BHJ solar cells based on solution crystallization processed P3HT nanowires and PCBM were demonstrated to have a PCE

of 3.23% by spin-coating a 60 h aged P3HT nanowires/PCBM blend solution as an active layer (Figure 11A–B).^[175] AFM and TEM studies suggested that the optimized photovoltaic properties arose from the formation of an interconnected network of highly oriented P3HT nanowires self-assembled together with PCBM (Figure 11D–G), which enhanced both the light absorption and the balanced charge transport. Photovoltaic cells with a compositionally graded architecture were further constructed by inserting a pure P3HT buffer layer between this P3HT nanowires/PCBM active layer and the hole-collecting electrode (Figure 11C). Thus an improved PCE approaching 4% was achieved after applying optimized annealing conditions to the P3HT buffer layer. The graded thin-film device structure by involving a P3HT-only region, reduced the charge recombination and the electron injection to the ITO electrode and improved the cell performance. BHJ PSCs fabricated from ultrasonic-assisted self-assembly of a P3HT nanowires/PCBM blend showed higher

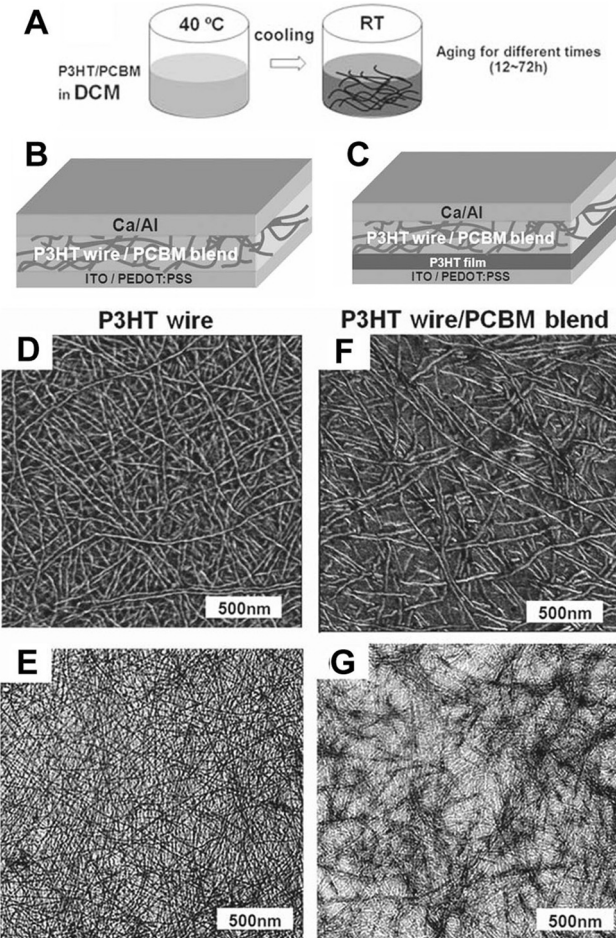


Figure 11. A) Scheme illustrating fabrication route to blend solutions of P3HT nanowires and PCBM via a solution crystallization method, B) A schematic solar cell device with the configuration of ITO/PEDOT:PSS/ P3HT nanowires/PCBM/Ca/Al, and C) A schematic solar cell device with the configuration of ITO/PEDOT:PSS/P3HT film/P3HT nanowires/ PCBM/Ca/Al. AFM and TEM images, respectively, of (D, E) homo-P3HT nanowires and (F, G) P3HT nanowires/PCBM blend film. Reproduced with permission.^[175] Copyright 2011, Wiley VCH.

values in J_{sc} , FF and PCE than those made from a homogeneous P3HT/PCBM solution.^[174] As expected, a 4.09% PCE was realized by the thermally annealed treatment of the BHJ layer containing the self-assembled 98% P3HT nanowires. Other self-organized P3HT nanowires or nanofibers have similarly been developed for high performance BHJ PSCs. Many efforts were devoted to the materials selection, device configurations, and morphology control for achieving high efficiency PSC devices at low cost.^[176,180–182,184] It was found that the pre-synthesis of wire-like (fiber-like, or rod-like) P3HT nanostructures is a more controllable approach to nanowire-based BHJ with desired morphology and good photovoltaic properties than that based on in situ processing P3HT nanofibers/nanowires in a BHJ blend.

Alternatively, a significant trend to obtain high performance PSCs is to build ordered BHJ solar cells with better nanoscale phase-separation and charge transport ability. This is mainly due to the facts that the ordered BHJ blends hold rational size of the donor or the acceptor within the exciton diffusion length range, and can balance the exciton dissociation and charge transport requirements, whereas inherently disordered structure of conventional BHJ blends can cause both the reduction of carrier mobilities and the increase of recombination between charges of opposite polarity.^[169] By using a commercially available AAO membrane filter to tailor the surface morphology of a P3HT/PCBM active layer, ordered BHJ PSCs based on the orderly nanostructured blend showed a 25% improvement in PCE (from 3.52% to 4.43%).^[185] In this case, morphological control of the BHJ surface led to the increased light utilization, the enhancement of electron transfer arising from the decreased numbers of dead ends in the PCBM phases, and the improvement of hole transport because of an improved crystalline ordering of the P3HT domain, all of which eventually resulted in a better device performance. Indeed, by controlling over the morphology and dimension of nanostructured donor polymers, PSCs with ordered BHJ can be formed, which exhibited an improved device performance. Cho and coworkers reported that the PCE of ordered BHJ PSCs made by the blend of hexagonal P3HT nanorod arrays and C₆₀ remarkably increased from 0.17% to 1.12% (a factor of 6.6) when comparing to devices based on planar P3HT/C₆₀ bilayer films, due to a larger D/A interfacial contact area, more efficient charge separation, and nearly 10 times improvement in carrier motility afforded by the crystalline P3HT nanorods with aligned chain orientation.^[186]

Unlike the above ordered BHJ PSCs, an ordered BHJ solar cell fabricated from the active layer of P3HT-shell/PCBM-core nanorod arrays (ca. 67 nm in core diameter and 110 nm in rod length) has been recently reported by Wang and Wei et al. using a melt-assisted wetting of porous AAO template (**Figure 12A–B**).^[187a] It was found that, the PSCs based on the arrays of these vertically aligned P3HT/PCBM core-shell nanorods exhibited an initial PCE of 1.3%, and improved PCE values of 1.43% and 2.0% after the thermal annealing at 100 °C and 120 °C for 10 min, respectively (Figure 12C). Furthermore, the same group fabricated inverted BHJ solar cell devices incorporating PCBM/P3HT core/shell nanorod arrays using an AAO membrane.^[187b] In the work, the more efficient carrier transport of the device incorporating the core/shell nanorod arrays provided it with both a higher short-circuit current density of 10.70 mA cm⁻² and a higher power conversion efficiency of

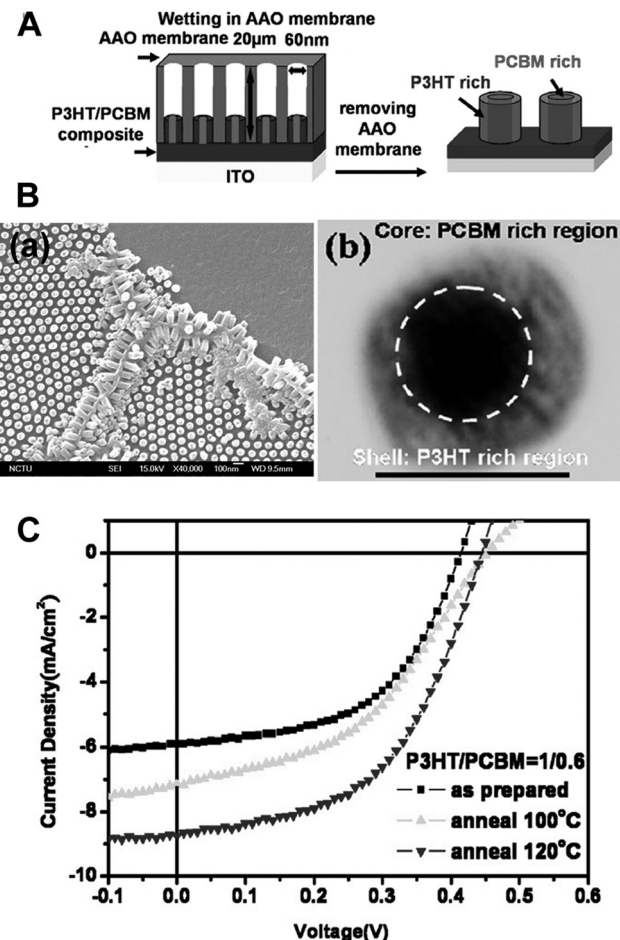


Figure 12. A) Cartoon representation of the well-ordered P3HT/PCBM core-shell nanorods by an AAO template method, B) SEM image (a) of the P3HT/PCBM nanorod arrays and top-view TEM image (b) of one-single P3HT/PCBM nanorod (scale bar: 50 nm), and C) J-V characteristics of P3HT/PCBM nanorod arrays devices prepared after annealing at various temperatures, measured under AM1.5G illumination at an intensity of 100 mW cm⁻². Reproduced with permission.^[187a] Copyright 2009, The Institute of Physics Publishing Ltd.

3.6%, relative to those of the conventional device. Although the performance of this type of ordered BHJ PSCs (with a conventional or inverted structure) is still inferior to most traditional BHJ blend film PSCs, these studies can be considered as pioneering works for the controlled fabrication of PSCs with refined and complicated BHJ structure at the nanoscale level. This novel strategy for achieving better phase-separated blends is of great importance for the design and engineering of novel materials (or structures) for high performance PSCs.

Besides the P3HT/PCBM system, very recently, ordered BHJ all-polymer solar cells based on P3HT nanocolumns and poly((9,9-diethylfluorene)-2,7-diyl-alt-[4,7-bis(3-hexylthien-5-yl)-2,1,3-benzothiadiazole]-2',2''-diyl) (F8TBT) have been developed by Greenham et al.^[188] They demonstrated that a double nanoimprinting process allowed the formation of nanostructured polymer heterojunctions of composition and morphology be selected independently. For these polymer solar cells, the

25 nm column heterojunction space is close to the exciton diffusion length, and a large, short, continuous electron/hole transport path to each electrode can be generated, leading to a record high PCE of 1.9% and a V_{oc} of 1.14 V. The high V_{oc} of 1.14 V for these devices is larger than that of their corresponding PHJ or conventional BHJ devices, as well as most of other all-polymer solar cells. This study paves a new way to obtain phase-separated donor and acceptor materials for all-polymer solar cells, and also indicates the possibility to find a broader range of acceptor candidates beyond the fullerene family for building highly efficient PSCs. Nevertheless, the light intensity absorption of these ordered PSCs is not efficient owing to the limited height (80 nm) of the patterned structures. And there is considerable room for further improvement.

Other PTh derivative semiconductors, such as P3BT, P3PT and poly(3-2-methylbutylthiophene) (P3MBT), whose 1D nanostructures have also been successfully incorporated into the active layer to develop high performance PSCs comparable to P3HT based PSCs (see Table 1). As to P3BT, Jenekhe's group first found that highly efficient BHJ PSCs can be fabricated by using pre-assembled nanowires of P3BT as the donor along with PCBM or PC₇₀BM acceptor (Figure 13).^[190] As shown by TEM and AFM images (Figure 13D–E), the P3BT nanowires of 8–10 nm in diameter and 5–10 μ m in length form an interconnected 3D network surrounded by a continuous PCBM phase, forming quasi-bicontinuous nanoscale morphology (Figure 13B). Moreover, the hole mobility of P3BT nanowires/PCBM BHJ layer ($\sim 8.0 \times 10^{-3} \text{ cm}^2/\text{V s}$) measured from FET devices was found to be 2 orders of magnitude larger than that of a conventional P3BT/PCBM thin film ($3.8 \times 10^{-5} \text{ cm}^2/\text{Vs}$). Thus, with similar light absorbing abilities (Figure 13C), the improved device performance (PCE: from 1.0% to 2.2%, V_{oc} : from 0.42 V to 0.50 V, J_{sc} : from 4.90 mA cm^{-2} to 7.68 mA cm^{-2} , FF: from 48% to 57%) in air under AM1.5 illumination was observed (Figure 13F). By replacing PCBM with PC₇₀BM, the PCE of the corresponding cells was further increased to 3.0%, which is comparable to that of a P3HT:PC₇₀BM BHJ device (Figure 13G). On the other hand, the same group has similarly fabricated the interconnected network BHJs based on the blends of in situ self-assembled P3BT nanowires (ca. 11–15 nm in width and 5–10 μ m in length) and an amorphous continuous PCBM phase.^[189] The photovoltaic properties of P3BT nanowires/PCBM solar cells, including the J_{sc} , FF, and PCE were found to be strongly relied on the blend composition. By controlling the mass ratio of P3BT nanowires to PCBM as 2:1 in BHJ, a maximum PCE of 2.52% was obtained under ambient conditions. Certainly, these two studies suggest that 1D P3BT nanostructures are promising donor materials for efficient PSCs similar to P3HT. However, whatever pre-assembled or in situ self-assembled P3BT nanowires, their structures still have a great potential for optimization, and the efficiency of PSCs based on them can be further improved. When a combination of thermal and solvent annealing was used to tailor the P3BT nanowires/fullerene blends, a high average PCE of 3.35% was achieved in a BHJ structure, which maintains the interpenetrating network of nanowires and fullerene phase, but avoids the device bridging and reduces the recombination and shunt loss associated with it.^[191] In the case of another PTh derivative, the pre-synthesized, highly dense and crystalline nanowires of P3MBT were used to blend with PC₇₀BM to achieve short and

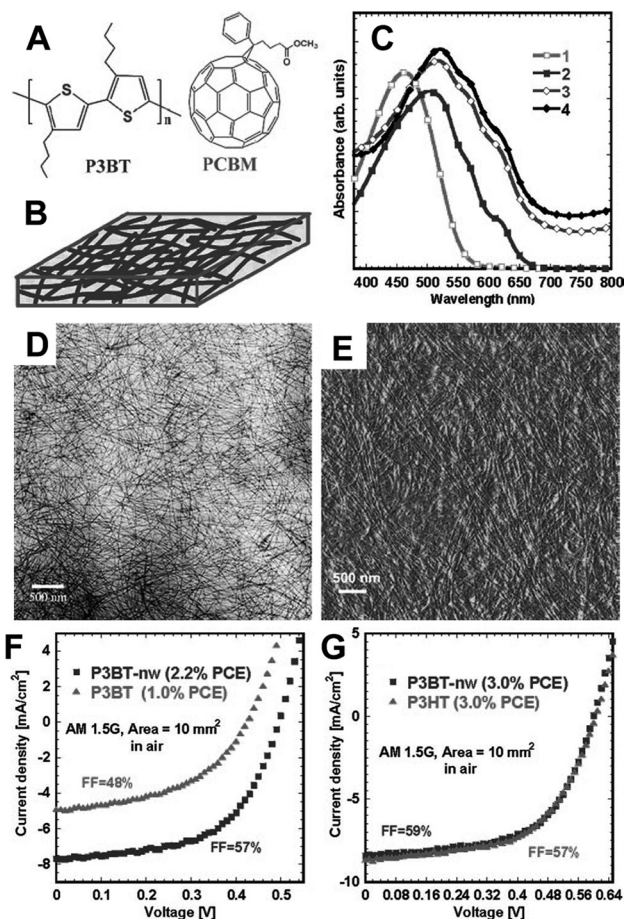


Figure 13. (A) Chemical structures of P3BT and PCBM, (B) Schematic illustration of P3BT-NWs/PCBM nanocomposite, and (C) UV-Vis absorption spectra: (1) P3BT solution in 1,2-dichlorobenzene (ODCB); (2) P3BT NWs suspension in ODCB; (3) P3BT:PCBM blend on ITO/PEDOT substrate; and (4) P3BT-NWs:PCBM nanocomposites on ITO/PEDOT substrate. (D) TEM and (E) AFM images of P3BT-NWs:PCBM (1:1 wt ratio) nanocomposites. J-V characteristics of PSCs under AM1.5 illumination with different active layers: (F) P3BT-NWs:PCBM (1:1 wt ratio, 70 nm, ■) and P3BT:PCBM (1:1 wt ratio, 80 nm, ▲); (G) P3BT-NWs:PC₇₀BM (1:0.75 wt ratio, 90 nm, ■) and P3HT:PC₇₀BM (1:1 wt ratio, 120 nm, ▲). The films in panel (F) were dried in a vacuum oven at 60 °C overnight and films in panel (G) were annealed in a glovebox at 110 °C for 10 min. Reproduced with permission.^[190] Copyright 2008, American Chemical Society.

continuous pathways in the photoactive BHJ layer for realizing high efficiency PSCs.^[193] Subsequently, an optimized cell with an active layer containing 66.7 wt% P3MBT nanowires and 33.3 wt% PC₇₀BM showed a V_{oc} of 0.72 V, a J_{sc} of 9.15 mA cm^{-2} , an FF of 63%, and a remarkable PCE of 4.15%. Unambiguously, this study proves that conjugated polymers with branched alkyl side chains are thermodynamically in favor of forming nanowires over the polymers with linear alkyl side chains. It opens a useful route to the solution processable 1D nanostructures of polymers with branched or dendritic chains for high performance photovoltaic devices.

Solution self-assembled P3PT nanowires with high crystallinity and hole mobility, have similarly been used to fabricate nanostructured BHJ PSCs. The fabricated solar cell device

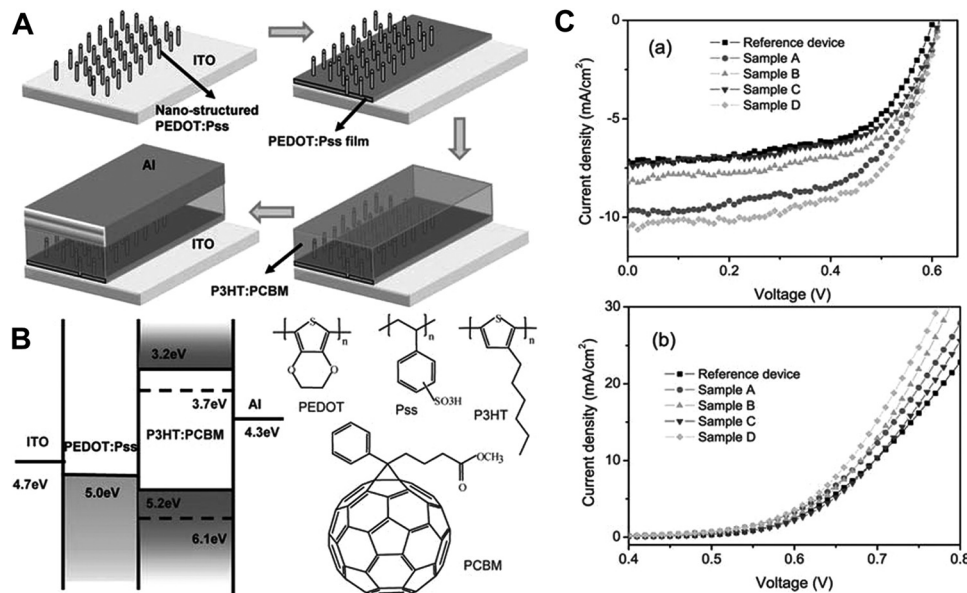


Figure 14. A) Schematic device fabrication and (B) energy level diagram of the PSCs with the configuration of ITO/PEDOT:PSS/P3HT:PCBM/Al, and (C) J - V characteristics of as-prepared PSCs under conditions of (a) AM 1.5 illumination and (b) in the dark. Reproduced with permission.^[202] Copyright 2010, The Royal Society of Chemistry.

exhibited a high PCE of 3.3%, which was comparable to that of the traditional P3BT/PC₇₀BM based solar cells (3.7% PCE).^[192] These results are analogous to those found in P3HT nanowires based BHJ devices, indicating a good potential of P3PT and its anisotropic nanostructures for PSCs and other organic device applications. With a similar solution phase self-assembly method, copolymer nanowires of P3BT-block-P3OT have recently been studied as the donor component to fabricate the nanostructured BHJ active layer.^[194] The PSCs based on the composites of these diblock copolymer nanowires and PC₇₀BM displayed a dependence of device efficiency on the length/width aspect ratio of the nanowires, where 3.38% PCE was achieved at the highest aspect ratio of 260. The observed improvement of photovoltaic efficiency with increasing aspect ratio of the NWs was attributed to the enhanced exciton and charge photogeneration, transportation, and collection in the BHJ PSCs. Significantly, this discovery provides a tunable way to control over the photovoltaic properties of PSCs by tailoring the morphology and size (such as aspect ratio) of the corresponding active materials, which will be extended to other PSC systems and may provide some new inspiration.

Additionally, a novel thermally reactive PTh derivative poly[3-(2-(2-tetrahydropyranoyloxy)ethyl)thiophene] (PTHPET) has been recently designed into 1D nanoarray architecture for PSCs via a simple solution route assisted by a PMMA template, where the nano-patterned PTHPET/PCBM solar cells exhibited higher values in PCE and EQE than the corresponding PHJ and BHJ devices.^[200] The main reason is that the ordered 1D nanostructure obtained in the patterned BHJs, enlarges the D/A interface, reduces the charge trapping, and facilitates a pathway for electrons and holes to reach their electrodes. Nonetheless, the relatively low efficiency arising from the nature of PTHPET hinders its practical usages compared to P3HT-based PSCs. Hence, further attempts to improve the inherent charge mobility, decrease

the domain size, and enhance the overlap with solar spectrum of 1D nanopatterned conducting polymers will be a potential strategy for realizing high performance PSCs.

As one of important 1D conducting polymers, PEDOT and its derivative nanofibers can be used as a buffer layer for charge collection and transport in PSCs, which show an improved device performance compared to those with the planar buffer layers (i.e., PEDOT:PSS, LiF, and Cs₂CO₃, etc.).^[201] A vertically aligned nanostructured buffer layer can provide large and direct conducting area between active layer and electrode layer for transporting electrons and holes, reduce interfacial resistances, and thus result in an improved cell efficiency. By employing electrochemically synthesized columnar-like PEDOT:PSS nanostructures on ITO substrate as the buffer layer to fabricate P3HT/PCBM PSCs, Yang et al. demonstrated a 50% higher PCE (an increase from 2.56 to 3.86%) than that of the spin-coated PEDOT:PSS planar structures (Figure 14).^[202] Besides, an improved performance in MDMO-PPV:PCBM solar cells using 1D PANI nano-islands as the anode buffer layer material has also been reported.^[203] The performance of these devices was comparable to that of the devices using PEDOT:PSS as a buffer layer, indicating their good potential in solar cell applications.

3.1.2. Hybrid Solar Cells (HSCs)

In addition to serving as active materials or interfacial buffer materials in PSCs, 1D conducting polymer nanostructures also play an important role in the construction of HSC devices. As p-type donors, they have been utilized to fabricate HSCs by being combined with n-type acceptor inorganic semiconductors such as ZnO,^[160,204] TiO₂,^[205–208] CdS,^[209] CdSe,^[210] Si,^[211,212] and CNTs.^[213] According to the structural difference in their active materials, polymeric/inorganic HSC devices can be divided into three categories: (1) conventional BHJ HSCs, (2) ordered BHJ

Table 2. Device characteristics of some representative HSCs based on 1D conducting polymer nanostructures.

Device type of HSCs	Configuration of active donor/acceptor layer	V_{oc} [V]	J_{sc} [mA cm^{-2}]	FF [%]	PCE [%]	Refs.
Conventional BHJ HSCs	CdSe NRs/P3HT NFs (BHJ film)	0.62	8.79	50	2.9 ^{a)}	[210]
Ordered BHJ HSCs	TiO ₂ NRs/P3HT arrays (ordered BHJ) ^{b)}	0.67	7.47	48	2.41	[205]
	TiO ₂ NTs/P3HT (ordered BHJ)	0.41	1.8	46	0.34 ^{c)}	[208]
	TiO ₂ NTs/dye/P3HT (ordered BHJ)	0.55	10.75	55	3.8 ^{c)}	[208]
	Si/PEDOT:PSS core-shell NW arrays	0.47	19.28	61	5.09	[211]
	Si/PEDOT:PSS core-shell NW arrays	0.46	21.6	64	6.35	[212]
Single nanowire HSCs	ZnO/P3HT core-shell NW <i>p-n</i> junction	0.40	0.32	28	0.036	[204]
	CdS-PPy coaxial NW <i>p-n</i> junction	0.094	0.043	26.5	0.018 ^{d)}	[209]

^{a)}Measured at an illumination intensity of 92 mW cm⁻²; ^{b)}With an inverted configuration of ITO/TiO_x/TiO₂ NR:P3HT/MoO₃/Ag; ^{c)}Measured at an illumination intensity of 90 mW cm⁻²; ^{d)}Measured at an illumination intensity of 6.05 mW cm⁻².

HSCs, and (3) single nanowire HSCs. A summary of some representative device examples and their performance is listed in **Table 2**. It should be noted that, conducting polymers-based 1D *p-n* heterojunctions without solar cell device investigations are excluded in this review, because they have been covered in some reviews.^[214,215]

Similar to PSCs, most HSCs are built on active materials with the conventional BHJ structure. For HSCs, it is of critical importance to get a beneficial morphology and size control in the BHJ active layer, in order to get a large D/A interface area for effective excitons production and dissociation, as well as an interpenetrating bicontinuous pathway for the efficient transport of free charges to their corresponding electrodes.^[147,216,217] Processing HSCs with different solvents is found to strongly affect the BHJ morphology and efficiencies of the resulting devices. Sun and Greenham demonstrated HSCs fabricated from a BHJ blend of P3HT and CdSe nanorods, where three solvents with different boiling points (chloroform 61 °C, thiophene 84 °C and 1,2,4-trichlorobenzene 219 °C) were used to improve the cell performance through an optimization of the BHJ film morphology.^[210] The solvent with a higher boiling point caused a longer drying time during the film deposition, which contributed to form large-scale self-assembled P3HT nanofibers in favor of holes transport in the devices. As a consequence, an improved PCE of 2.9% for 1,2,4-trichlorobenzene-processed P3HT NFs/CdSe NRs HSCs was obtained under AM 1.5G with 92 mW cm⁻² illumination intensity, which is higher than those from chloroform-processed HSCs (PCE = 1.8%) and thiophene-processed HSCs (PCE = 2.4%).

Recently, development of BHJ HSCs with ordered conducting polymer nanostructures has attracted increasing attention because the highly oriented blends created on them can enlarge D/A interfacial area, facilitate charge transport and reduce contact resistances similar to the ordered BHJ PSCs.^[218,219] Wei et al.^[215] fabricated inverted BHJ HSCs in the same way as one of their previous PSC work,^[187b] by replacing the PCBM/P3HT NR array active layer with the TiO₂ NR/P3HT array active layer. Under an optimized composite rod array structure, a higher

hole mobility of the HSC device was found compared to that of a device with the conventional TiO₂ NR/P3HT blend film. Due to the more efficient carrier transport of the device incorporating the nanorod arrays, it exhibited a better device performance ($V_{oc} = 0.67$ V, $J_{sc} = 7.47$ mA cm⁻², FF = 48%, PCE = 2.41%) in comparison with the device incorporating the conventional TiO₂ NR/P3HT blend film ($V_{oc} = 0.54$ V, $J_{sc} = 3.91$ mA cm⁻², FF = 62%, PCE = 1.31%).^[205] However, the relatively low FF of the inverted device indicated that there still is room to improve its performance with a more balanced charge transport in the device. Ravirajan and coworkers reported that conjugated polymer F8T2 could be successfully infiltrated into a nanoporous TiO₂ film as deep as 100 nm via a dip coating route.^[206] The developed HSCs showed a peak EQE of 13% and a monochromatic PCE of 1.4%. Alternatively, by using *in situ* polymerization of P3HT in tubular TiO₂ nanoarrays, Tepavcevic and Darling et al. found that the ordered BHJ HSCs exhibited a 1000 times larger photocurrent density (under an illumination of 620 nm light at 38 mW cm⁻² incident intensity) than those of HSCs fabricated by penetrating pre-synthesized P3HT into TiO₂ nanotubes.^[207] Furthermore, the photovoltaic performance of ordered BHJ HSCs can be enhanced by surface modification of semiconductors in the BHJ blend. Grimes et al. reported on ordered BHJ HSC devices generated on an n-type TiO₂ nanotube array, which was modified by a near-infrared (NIR) absorbing organic dye in combination with penetrated p-type P3HT. This was an exciting design for ordered BHJ HSCs since it combined higher photons absorption with enhanced charge mobility.^[208] Subsequently, the cell displayed a broad spectral response (from near-UV to NIR) with an EQE up to 65%, and a PCE of 3.8% ($V_{oc} = 0.55$ V, $J_{sc} = 10.75$ mA cm⁻², FF = 55%) under UV filtered AM 1.5G of 90 mW cm⁻² intensity. The PCE is much higher than that of a typical HSC with the TiO₂ nanotube array/P3HT (no organic dye) BHJ (PCE = 0.34%, $V_{oc} = 0.41$ V, $J_{sc} = 1.8$ mA cm⁻², FF = 46%). The novel device architecture in this study has paved an important way to achieve an improved light harvesting and an increased V_{oc} by modifying inorganic semiconductor (i.e., TiO₂, ZnO, etc.) surface to raise

the conduction band position or by developing other p-type polymers where the HOMO level positions are more negative with respect to that of P3HT.

Recently, an ordered BHJ HSC with a record high efficiency exceeding 5% has been realized based on well-aligned Si/PEDOT:PSS coaxial nanowires reported by Shiu and Lin et al.^[211] Using a solution procedure, the hole-conducting PEDOT (p-type) was coated on the hydrophilic n-type Si nanowire surface to produce a highly oriented core-shell heterojunction (the thickness of PEDOT:PSS sheath is around 20 nm) (Figure 15A–B), which increased the D/A contact area, shortened the carrier diffusion distance and subsequently enhanced the efficiency

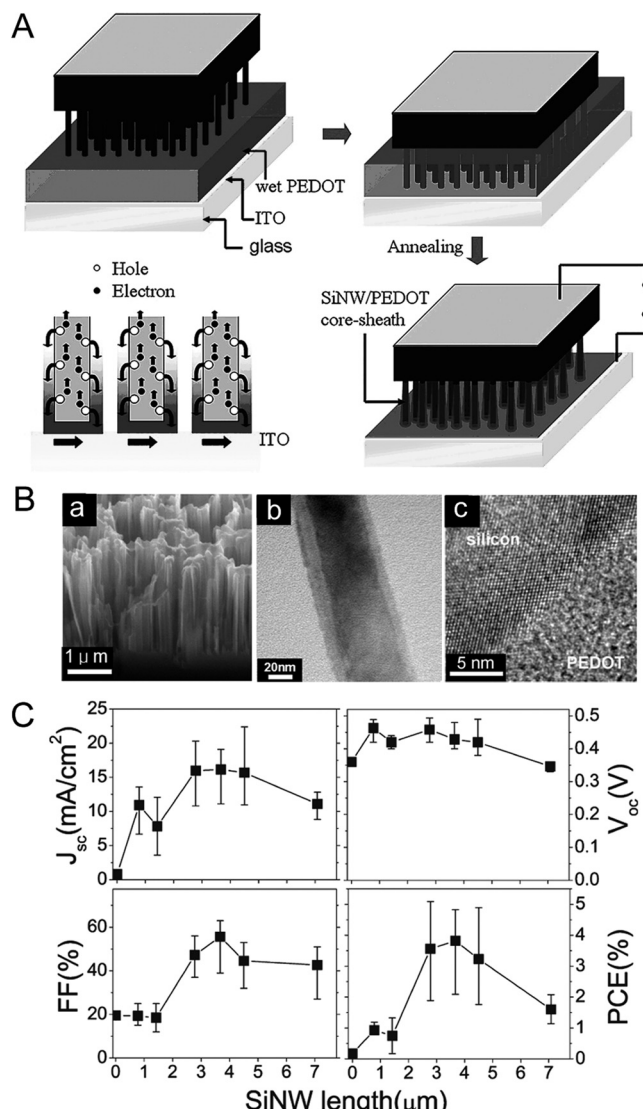


Figure 15. A) Schematic diagrams presenting the fabricating procedures and cell configuration for the Si/PEDOT:PSS core-shell nanowire ordered BHJ HSC, B) SEM image (a) of the PEDOT coated-Si nanowire arrays, TEM image (b) of one single Si/PEDOT core-shell nanowire, and HR-TEM image (c) of the Si nanowire/PEDOT interface. C) J_{sc} , V_{oc} , FF, and PCE of the Si/PEDOT ordered HSCs are plotted as function of the length of Si nanowires. Reproduced with permission.^[211] Copyright 2010, American Chemical Society.

of charge transport and collection. In contrast to the planar Si/PEDOT HSCs, the series resistance of the Si/PEDOT-based ordered BHJ HSCs decreased from $60.42 \Omega \text{ cm}^2$ to $1.47 \Omega \text{ cm}^2$, while the V_{oc} increased from 0.34 V to 0.47 V, J_{sc} from 1.27 mA cm^{-2} to 19.28 mA cm^{-2} , and FF from 18% to 61%, generating a dramatic improvement in PCE from 0.08% to 5.09%. Meanwhile, the HSC device could harvest photons from 400 to 1100 nm and produce a maximum EQE value of ~32% at 700 nm, which was much higher than the 1.94% EQE of the planar HSC. Additionally, there was an obvious size-dependence on the photovoltaic performance of the ordered BHJ HSCs (Figure 15C), because the length of Si nanowires had a large influence on the light absorption and light-trapping between Si nanowires. More recently, this type of ordered BHJ HSCs based on Si/PEDOT:PSS core-shell nanowire arrays were also fabricated by Lu and Chen et al., and found to have a better photovoltaic performance (PCE = 6.35%).^[212] Evidently, all of these results prove an excellent way to regulate the morphology and size of 1D organic/inorganic heterojunction for high performance HSCs, and it can be extended to other photovoltaic devices.

On the other hand, single nanowire HSCs have also been investigated by combining conducting polymer donors with inorganic semiconductor acceptors. As an interesting example, Fréchet, Yang, and co-workers described that a single ZnO/P3HT nanowire HSC exhibited well-resolved photovoltaic characteristics with a PCE of 0.036%, a V_{oc} of 0.4 V, a J_{sc} of 0.32 mA cm^{-2} , and an FF of 28% under AM 1.5 illumination (100 mW cm^{-2} light intensity), where the hybrid ZnO/P3HT core-shell nanostructures were made from ZnO nanowires and P3HT shells (a phosphonic ester ended P3HT) with thicknesses of ~5 to 20 nm.^[204] Recently, Guo and Li et al. carried out a similar investigation on a single organic/inorganic *p-n* junction nanowire HSC.^[209] A coaxial hybrid nanowire composed of two segments, hole-conductive PPy and electron-conductive CdS, was successfully fabricated through an AAO template and then used to develop a single *p-n* heterojunction HSC to convert light energy into electricity. The nanowire cell device produced a PCE of 0.018% ($V_{oc} = 0.094 \text{ V}$, $J_{sc} = 0.043 \text{ mA cm}^{-2}$, and FF = 26.5%) under an illumination intensity of 6.05 mW cm^{-2} . Despite the lower efficiencies comparing to the traditional ordered BHJ HSCs, the basic researches on these single nanowire HSCs will be definitely helpful to understand the working mechanism of organic/inorganic HSCs in nanoscale, and to accumulate knowledge about interfacial charge separation and transportation behaviors in hybrid systems. Certainly, it will enable scientists to broaden energy applications from macro-power tools to nanoscale power conversion devices.

3.1.3. Dye-Sensitized Solar Cells (DSSCs)

Since a PCE for DSSCs exceeding 7% was achieved in 1991,^[220] considerable progress has been made in this area. DSSCs can be divided into liquid-state DSSCs (ls-DSSCs) and solid-state DSSCs (ss-DSSCs) according to the state of the used electrolytes. In general, electrolytes (containing the redox couples) are sandwiched between the working electrode (often using dye-sensitized semiconductors) and the counter electrode such as platinum (Pt) to form a DSSC device, which differs from those traditional *p-n* junction solar cells.^[147] Upon light irradiation,

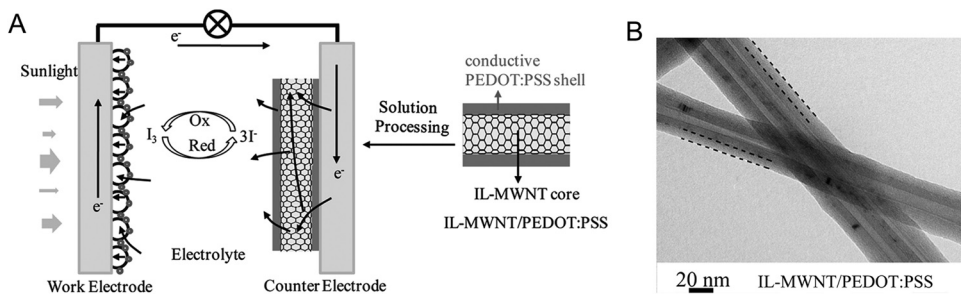


Figure 16. A) Schematic electron path of DSSCs with IL-CNT/PEDOT:PSS film as counter electrode (The conductive PEDOT:PSS molecules are active catalysts for reduction of I_3^-), and B) Representative TEM image of IL-MWCNT/PEDOT:PSS (the dotted lines have been added as a visual guide to the coating layers). Reproduced with permission.^[231] Copyright 2010, American Chemical Society.

electrons of the photosensitive dyes transit into their excited states, and then inject into conduction bands of the adjacent semiconductors, while the dye molecules themselves transit into oxidation states. The injected electrons continuously concentrate on the conducting substrate, and transport to the counter electrode through outside circuit, thus generating an electric current. The dye molecules can return from the oxidation states into the original states assisted by the electrolytes (such as I^-/I_3^-). At the same time, the electrolytes in their oxidation states recover their missing electrons by mechanically diffusing to the counter electrode, where the electrons are re-introduced after flowing through the external circuit.^[221,222] Accordingly, all the materials used for DSSCs are of critical importance for the energy conversion efficiency and the lifetime of devices.

For ls-DSSCs, the highest PCE around 12% has been reported by using liquid electrolytes consisting of liquid I^-/I_3^- redox couples.^[223,224] Unfortunately, using liquid electrolytes always encounters with the problems of the evaporation and leakage of the electrolytes, leading to the poor stability in devices. By replacing liquid electrolytes with solid electrolytes, such as conducting polymers and molecular hole conductors, the stability of DSSCs can be improved although ss-DSSCs still suffer from lower efficiencies compared to ls-DSSCs.^[222] On the other hand, conventionally used Pt electrode in both ls- and ss-DSSCs, is not only an expensive component but also a corrosive material in the presence of water containing electrolytes. Thus, there is a need to develop new DSSC systems with Pt-free counter electrodes, such as carbon, conducting PPy and PEDOT-based counter electrodes with good conductivity and durability.^[225–228]

Consequently, for the commercialization of DSSCs, it is necessary to prepare electrolyte materials, electrode materials and photosensitive dyes with high performance and low-cost. Previous reports demonstrated that conducting polymers, particularly the highly conducting PEDOT materials, were efficient electrolyte materials, and good counter electrode materials for DSSCs.^[222,229,230] More recently, 1D PEDOT nanostructures were demonstrated as promising electrode materials for the DSSC application. For example, a novel core-shell CNT/conducting polymer (PEDOT:PSS) nanostructure, using an imidazolium-salt-based ionic liquid (IL) as a linker, was developed as the counter electrode for DSSCs, which showed high photovoltaic performance (with a PCE of 4.77%, and a maximum IPCE of 64.8%) comparable to that of devices with the conventional Pt counter electrode.^[231] It was speculated that highly

conducting PEDOT:PSS shell wrapping on the IL-MWNT did not affect the carrier transfer, since the carrier could transport from IL-MWNT to PEDOT and the carrier transfer could take place on PEDOT as well (Figure 16). Furthermore, the device performance was found to be relied on the roughness of PEDOT:PSS shell. A smoother surface on the PEDOT:PSS shell would exhibit a better photovoltaic performance, owing to the difference in the charge mobility resulted from the conformational change of the PEDOT chains within this hybrid system. The use of conducting polymer as a shell to wrap CNTs, contributed to a reduced charge injection barrier and thus resulted in high device performance, which offers a novel design for high performance DSSCs. Likewise, conducting PEDOT:PSS/CNT 1D nanocomposites can also serve as the counter electrode in DSSCs, exhibiting high device performance with a PCE of 6.5%, a V_{oc} of 0.6 V, a J_{sc} of 15.5 mA cm^{-2} , and an FF of 63% under AM 1.5 illumination, which was close to that of the DSSCs with Pt as the counter electrode, and significantly better than that of the CNT/poly(styrenesulfonate acid) (PSSA) counter electrode-based DSSCs.^[232] In this case, the charge transfer process was not affected in the counter electrode of 1D CNT/PEDOT:PSS nanocomposites. However, the charge transfer process would be hindered in the CNT/PSSA electrode because CNTs were wrapped by the insulating PSSA.

Most recently, using hard-template synthesized PEDOT nanotube arrays as counter electrodes, a record high PCE of 8.3% was achieved for DSSCs.^[233] In the work, the performance of DSSCs using the nanotubular electrode was not worse than that of devices using the conventional platinized counter electrodes, and better than that of devices using their dense and flat counterparts.^[233] The reason for the improved performance was due to the increase in the effective area of the oriented PEDOT nanotubes, which caused a reduced series resistance as well as an enhanced catalytic effect with I^-/I_3^- redox. This study implies that the platinized counter electrodes are not always the optimal choice for the DSSCs using different electrolytes. More importantly, the 1D nanostructured conducting polymers are demonstrated to be one of good candidates for noble metal-free electrodes in DSSCs.

3.2. Fuel Cells

Fuel cells are also recognized as a promising green power source for mobile and portable energy applications because of their

unique features, such as the high energy density, the compact system, the fuel portability and the environment friendliness. Unlike photovoltaic energy devices, fuel cells convert chemical energy of various fuels directly into electric energy under electrochemical redox reactions, thus exhibiting high energy conversion efficiencies. Up to date, there are two general categories of fuel cells: chemical fuel cells (CFCs) and biological fuel cells (BFCs). CFCs include alkaline fuel cells (AFCs), polymer electrolyte membrane fuel cells (PEMFCs), direct methanol (or ethanol) fuel cells (DMFCs or DEFCs), solid oxide fuel cells (SOFCs), phosphoric acid fuel cells (PAFCs), and molten carbonate fuel cells (MCFCs), etc. A summary of working principles for the CFCs are shown in Figure 17A.^[234] By contrast, the latter devices, such as microbial fuel cells (MFCs), are regarded as biocatalytic systems which use micro-organisms as the catalysts to oxidize organic and inorganic matters and then generate the current (Figure 17B).^[235] All of these fuel cell technologies provide intriguing applications in the field of portable energy sources, such as power distribution and remote generation of electric energy, which have attracted increasing attention in recent years.^[236]

However, high device performance and low cost are very important for various fuel cells in real commercialization. It has been known that, a number of factors influencing the fuel cell performance and cost include electrode materials, electrolytes/substrate structures, cell components and interconnects, etc.^[237] Among them, good electrode materials are most essential for high device performance because they have great effects on the electrode kinetics, the electrochemical reactions for charge transport, and the connected resistance.^[238] Therefore, the development of novel, effective, inexpensive electrode materials including catalysts and their supports can greatly contribute to low cost and high performance fuel cells. Recent studies revealed that 1D conducting polymer nanostructures are good candidates as noble metal-free electrocatalysts, or as supports for catalysts loading due to their low-cost, large specific surface areas, good biocompatibility and environmental friendliness, superior electrical conductivity and charge transport, as well as good stability. In comparison to their bulk counterparts or conventional electrocatalysts, these 1D conducting polymer nanostructured materials can display improved electrode activities in both CFCs and BFCs.

3.2.1. Chemical Fuel Cells (CFCs)

Among the family of 1D nanostructured conducting polymers, oriented PPy nanostructures are one of representative anode materials for developing low-cost and high efficiency electrocatalysts in all kinds of CFCs. Porous AAO template-synthesized PPy nanotubes have been employed in DMFCs as Pt catalyst supports, showing an excellent electrocatalytic activity and a high stability for the oxidation of methanol.^[239] It was demonstrated that in nanotubular PPy-based anodes, as the Pt loading increased, the activity was continuously increased from 25.6 mA cm^{-2} ($\text{Pt} = 10 \mu\text{g cm}^{-2}$) to 302.5 mA cm^{-2} ($\text{Pt} = 140 \mu\text{g cm}^{-2}$), superior to that of common PPy supported Pt anodes. Nanofibrillar PPy was also synthesized as efficient supports for Pt catalyst loading.^[240] The well-dispersed Pt nanoparticles anchored well on the PPy nanofibers as characterized

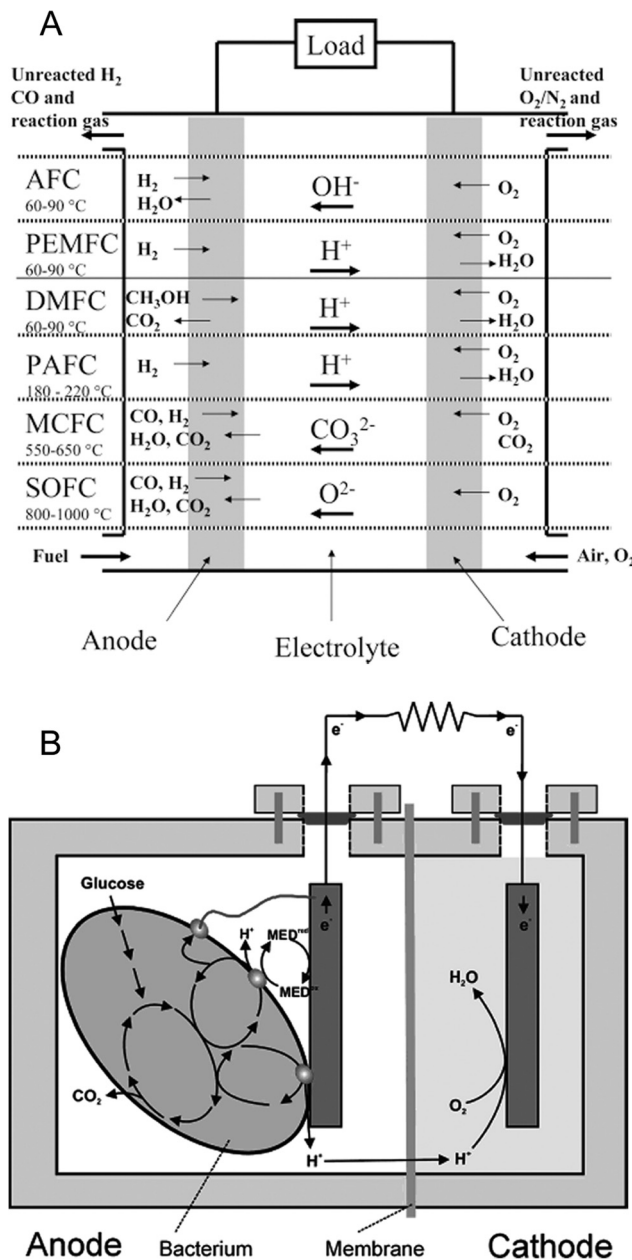


Figure 17. A) Summary of the reactions and processes that occur in the various CFCs. Reproduced with permission.^[234] Copyright 2004, American Chemical Society. B) Schematic diagram of operating principles for an MFC (among, MED means mediator). Reproduced with permission.^[235] Copyright 2006, American Chemical Society.

by TEM, and the average diameter of these particles was ca. 2.5 nm (Figure 18A). The as-fabricated Pt/PPy nanofibers catalyst exhibited a maximum stable peak current density (J_{\max}) of 14.1 mA cm^{-2} , significantly higher than that of carbon nitride (CN_x) nanofibers supports (7.0 mA cm^{-2}), and commercial carbon black powder of Vulcan XC-72 (XC-72) supports (4.6 mA cm^{-2}) (Figure 18B), which indicates a higher catalytic activity for methanol oxidation. Furthermore, the CO-poisoning tolerance of such a PPy nanofiber-based Pt catalyst was better

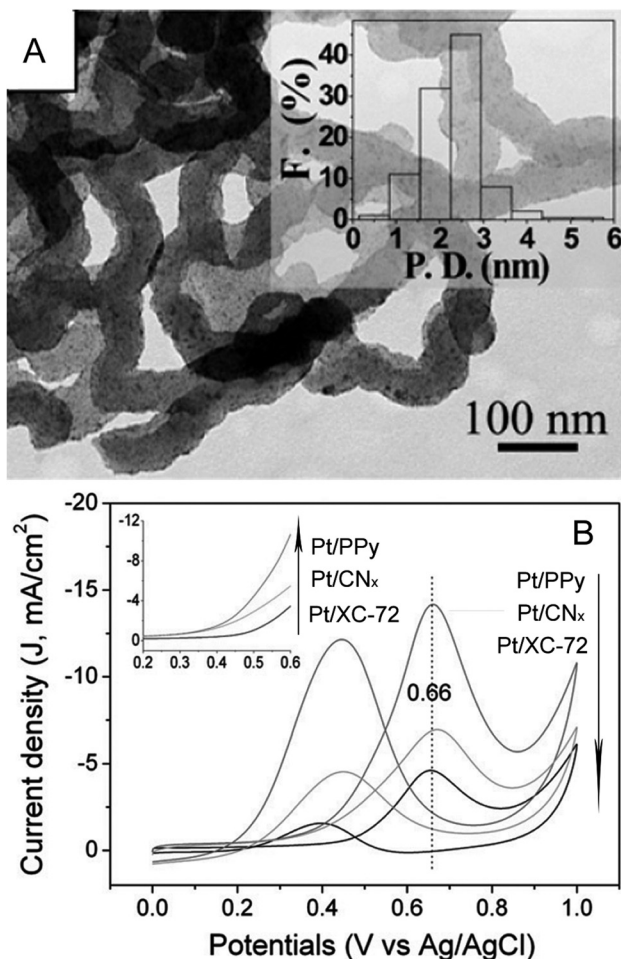


Figure 18. A) TEM image of nanofibrillar PPy/Pt catalyst (inset: the size distribution histogram of Pt nanoparticles for each catalyst based on observation of 300 particles, in which P.D. means particle diameter and F. represents frequency), and B) Cyclic voltammetry (CV) curves of nanofibrillar CN_x/Pt, nanofibrillar PPy/Pt, and XC-72/Pt catalysts in 1.0 M H₂SO₄ aqueous solution with 1.0 M CH₃OH (inset: the forward parts of the CV curves). Note: Current density = current/area of the working electrode, i.e., 0.071 cm². Reproduced with permission.^[240] Copyright 2009, The Royal Society of Chemistry.

than those of CN_x nanofiber/Pt and XC-72/Pt catalysts. Nevertheless, the chemical stability of nanofibrillar PPy/Pt catalyst was partly inferior to that of CN_x nanofiber/Pt catalyst, but it could be further improved.

To further reduce the cost and improve the performance of CFCs, several 1D nanocomposites based on PPy are thereby developed. Considering the demand for good conductivity of catalyst supports, single- or multi-wall CNTs (SWCNTs or MWCNTs) are generally employed as feasible candidates to combine and/or modify with the inexpensive PPy. The formed composites are expected to have the advantages of both components, so as to provide the catalyst supports with a high surface area and an excellent electrical conductivity for catalyst loading, such as noble Pt, and/or Pt-M (M = Ru, Pd, Co, Sn) alloy. In situ synthesized PPy-MWCNT 1D nanocomposites were investigated as Pt and Pt-Pd supports for oxidation of formic acid and

formaldehyde.^[241] The results showed that the PPy-MWCNT/Pt-Pd electrode had a higher oxidation current and a better long-term cycling stability than those of the PPy-MWCNT/Pt electrode. This enhanced performance might originate from the increase of electrochemically accessible surface areas and electronic conductivity, as well as the easier charge-transfer at PPy/CNTs interfaces, allowing a better dispersion and utilization of deposited Pt and Pt-Pd nanoparticles. A similar conclusion was also reached in the methanol oxidation by using the electrodes of PPy-MWCNT supported Pt-Ru and Pt catalysts.^[242] Additionally, bimetallic Pt-Co nanoparticles dispersed on PPy-MWCNT composites were developed as the electrode catalyst of methanol oxidation reaction in DMFCs.^[243] This catalyst showed stable methanol oxidation electroactivation and good CO-tolerance ability. Its catalytic activity was further improved by introducing an over-oxidation process, where the over-oxidation treatment could affect the arrangement and structure of the PPy matrix, thus resulted in more Pt-Co nanoparticles exposed to the surface. As a result, the Pt utilization and catalytic activity of this nanostructured catalyst were enhanced.

More significantly, PPy-directed 1D nanostructured composites offer a possibility to realize noble metal-free catalysts with electrocatalytic activity comparable to Pt and other precious metals, which is essential to develop inexpensive and efficient CFCs. Therefore, PPy-directed 1D nanostructured composites have attracted increasing attention in recent years. For example, novel cobalt porphyrin/PPy nanorod composites were synthesized and employed as the catalyst for oxygen reduction.^[244] The experimental results showed that the electrode modified with this nanocomposite has excellent electrocatalytic activity due to the dense and arrayed nanostructure of the composite.^[244] Tubular Co-PPy/MWCNT nanocomposites were also developed as effective cathode materials for oxygen reduction in PEMFCs, DMFCs, and DEFCs with temperatures ranging from 70 to 90 °C (Figure 19A–C).^[245] It was found that the power densities were improved for all of these CFC devices using Co-PPy/MWCNT composite nanotubes as the cathode electrocatalyst, and Pt-Ru/MWCNTs or Pt-Sn/MWCNTs as the anode electrocatalyst compared to other non-Pt based electrocatalysts. The performance studies showed the durability over long operating time (>50 h) for the PEMFC based on the electrode materials with MWCNT supported Co-PPy composites as the oxygen reduction catalyst (Figure 19D). These results indicated that such MWCNT supported Co-PPy nanocomposites are good electrode material candidates in various fuel cells.

Similar to PPy, conducting PANI with 1D nanostructures are another important anode materials for various CFCs devices. When used as electrocatalysts, Pt nanoparticles (with diameters of 1.5–3.0 nm) supported by PANI nanofibers (with ~60 nm diameters) were successfully developed for DMFCs.^[246] The results demonstrated that the PANI nanofiber-based anode catalyst showed a larger electrochemical active surface area and a higher methanol oxidation reaction catalytic activity than those of the Pt/C-based catalyst, suggesting its good electrocatalytic performance of high efficiency and tolerance. Moreover, PANI nanofibers were introduced into the Pt/C catalyst layer as inexpensive and durable supports, which improved the catalyst activity towards methanol oxidation, prevented the catalyst from poisoning the intermediates, and enhanced the

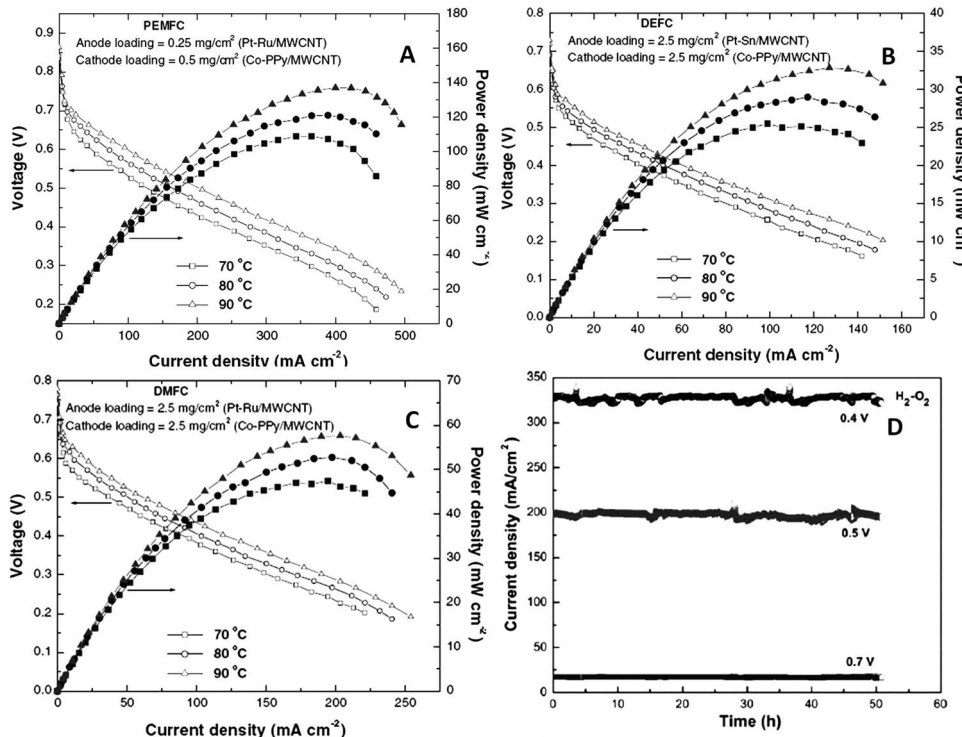


Figure 19. A–C) Polarization curves of PEMFC, DMFC and DEFC, respectively at various temperatures. D) Device performance showing the stability of PEMFC at 90 °C with cathode catalyst containing Co-PPy/MWCNT (loading: 0.5 mg cm^{-2}) and anode catalyst containing MWCNT/Pt-Ru (loading: 0.25 mg cm^{-2}) at ambient pressure. Reproduced with permission.^[245] Copyright 2008, Elsevier.

mechanical properties of the catalyst layer.^[247] 1D composite PANI/SWCNT (or PANI/MWCNT) structures were also used as support materials for Pd catalyst, which exhibited a higher electrocatalytic activity and a better long-term stability than pure PANI supported-Pd catalyst towards formaldehyde or methanol oxidation.^[248–250] Additionally, nanorod-like composites of PANI/cobalt porphyrin showed good electrocatalytic performance similar to the above mentioned cobalt porphyrin/PPY nanorods composites, suggesting another kind of good candidates as noble-free catalysts in fuel cells.^[251]

Moreover, a template route to conducting poly(*o*-phenylenediamine) (PoPD) nanotubes was developed for the DMFC application, and a greatly enhanced catalytic activity of Pt nanoparticles for oxidation of methanol was achieved.^[252] The corresponding activity of this Pt incorporated PoPD nanotube electrodes was found to be about 13 times larger than that of conventionally prepared PoPD with the same metal loading. The nanotubular morphology of PoPD contributes to the effective dispersion of Pt nanoparticles, which facilitates the easier access of methanol to the catalytic sites, thus leading to an increased activity and a higher stability.

3.2.2. Biological Fuel Cells (BFCs)

The original attempt to employ 1D nanostructured conducting polymers in BFCs, was the PANI/CNT nanocable structure, which was used as an anode material for *Escherichia coli* (*E. coli*)-catalyzed MFCs.^[253] In the study, Li et al. speculated that conducting PANI not only provided a protective effect for the micro-organisms, but also enhanced the electrocatalytic activity

of the biocatalyst. Meanwhile, the addition of CNTs could enlarge the electrode surface area and enhance the charge transfer capability, leading to an improvement of electrochemical reaction in MFCs. The improved current and power density were also observed, which are much higher than those of other similar *E. coli* based MFC systems. When using the composite anode containing 20 wt% CNT, the energy device with 2-hydroxy-1,4-naphthoquinone (HNQ) as a redox mediator showed the best discharge performance, and boosted the power output to a maximum of 42 mW m^{-2} and a cell voltage of 450 mV. However, this power density is still relatively small, and much lower than a subsequently reported value (1495 mW m^{-2}) for an *E. coli* MFC using novel mesoporous PANI/TiO₂ as an anode.^[254] Such a new porous nanostructure with high specific surface area, and excellent bio- and electro-catalytic properties, indicates that nanoporous structures will be attractive electrode materials for BFCs. To prove this point, 3D nanosized porous structures of PANI nanowire networks, were incorporated into anodes as efficient electron collectors in MFCs for an organic waste treatment.^[255] An order of magnitude increase in power density was demonstrated for the BFC systems with electrodes assembled by conductive nanowire networks, compared to those with electrodes assembled by the flat PANI structure. Thus, it is anticipated that construction of hierarchical conductive porous structures will be a promising tactic for designing advanced energy materials for BFCs and other electrochemical systems.

PPy coated CNT composites, another type of 1D conducting polymer materials, were also used as an anode material in *E. coli* catalyzed MFCs to replace the plain carbon paper anode, demonstrating that PPy could serve as a redox mediator

to facilitate the electron transfer between the *E. coli* cells and the anode.^[237,256] The power output of the MFC was found to increase along with the increased amount of PPy-CNT composite loading. By using the anode containing 5 mg cm⁻² PPy-CNTs, a power density up to 228 mW m⁻² was achieved in the absence of exogenous electron mediators. This value is much higher than other *E. coli* MFCs using efficient electron mediators, indicating the bright future of PPy-CNTs as low cost and effective electrode materials in the fuel cell application.

All the 1D conducting polymer nanostructures described above are focusing on the microbe-based BFC devices. Actually, they can also be used as novel electrode materials in enzyme-based BFCs to improve the power density and device stability (or life time). Using AAO templates, the size controlled PPy nanowires containing glucose oxidase (GOD) and 8-hydroxyquinoline-5-sulfonic acid hydrate (HQS) were synthesized and used as an anode for the glucose/O₂ enzymatic BFCs (Figure 20A).^[257] Compared to PPy film-type BFCs, the prepared

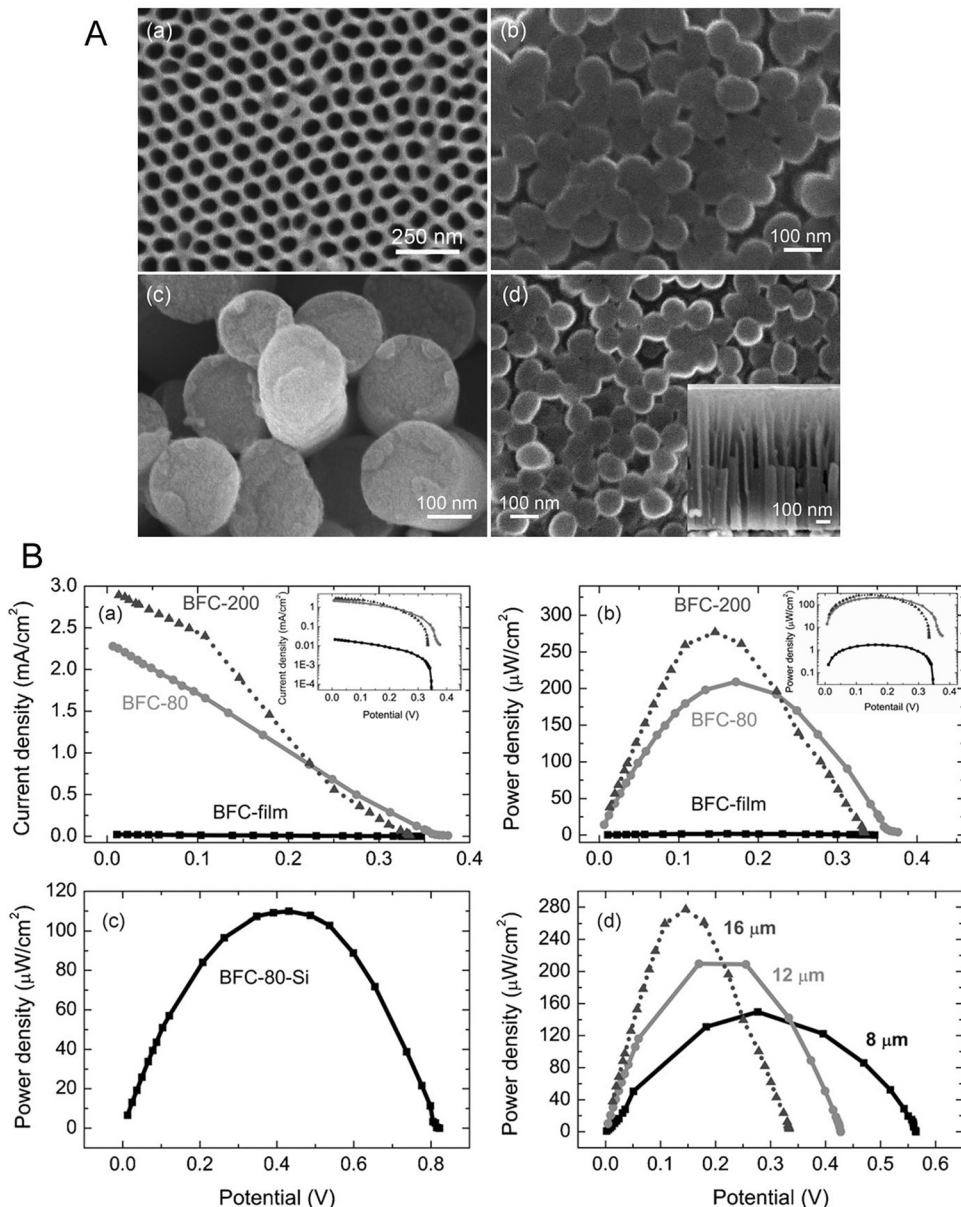


Figure 20. A) FE-SEM images of (a) the fabricated AAO template, (b) 80 nm diameter PPy-HQS-GOD nanowires, (c) 200 nm diameter PPy-HQS-GOD nanowires grown using a free-standing AAO template, and (d) 80 nm diameter PPy-HQS-GOD nanowires grown using an AAO template with Si substrate (inset: a cross-sectional view of the PPy-HQS-GOD nanowires); B) Dependence of (a) the current density and (b) the power density on the cell voltage for BFC-PPy film (BFC-PPy), BFC-PPy nanowires with 80 nm diameter and 16 μm length (BFC-80/16), and BFC-PPy nanowires with 200 nm diameter and 16 μm length (BFC-200/16), the insets show the plots in logarithm scale; (c) the power density on the cell voltage for BFC-80 with 350 nm length on Si substrate (BFC-80-Si); (d) the power density on the cell voltage for BFC-200 with different nanowire lengths of 8, 12 and 16 μm , respectively. Reproduced with permission.^[257] Copyright 2009, Elsevier.

PPy nanowire-BFCs exhibited a higher power density by about two orders of magnitude at 37 °C and pH 7.4 (Figure 20B (a) and (b)), due to the larger surface area and better enzyme loading arising from the use of PPy anisotropic nanostructures instead of PPy films. On the other hand, the device performance of PPy nanowire-based BFCs was found to be dependent on the size of the nanowires. As shown in Figure 20B (c), BFC-PPy nanowires with 80 nm diameter and 350 nm length on Si substrate (BFC-80-Si) yielded a lower power density, but a record high V_{oc} up to 0.82 V in contrast with those with 80 nm diameter and 16 μ m length (BFC-80/16). This was attributed to the short nanowire length of BFC-80-Si, since the electron transfer between the electrode and the biocatalytic active sites presumably was more efficient with a decreased distance. As the length of nanowires was reduced, the V_{oc} increased, despite the maximum power density decreased. In fact, the shorter nanowires could lead to a rapid increase in V_{oc} , but merely a slow decrease in power density (Figure 20B (d)). Nonetheless, size control of the nanowire length and diameter needs to be optimized to realize better performance BFCs.

Therefore, it can be concluded that 1D conducting polymer nanostructures are good alternatives for conventional electrode materials in various fuel cell applications, on account of their advantages and attractive properties as summarized in section 3.2. These advanced nanostructures, as one of promising energy materials, will greatly facilitate the rapid development of fuel cells, and provide the availability of low-cost, durable, and portable fuel cell devices for practical applications.

3.3. Rechargeable Lithium Batteries

Rechargeable batteries, also called as secondary batteries, belong to energy storage and release devices, which can be repeatedly charged and discharged for many times. Traditional rechargeable batteries, such as nickel-cadmium (Ni-Cd) and lead-acid batteries have been intensively studied and widely used in daily life.^[234] Nonetheless, these batteries are sometimes limited by their low capacity and poor cyclability, as well as certain toxicity. As an alternative, rechargeable lithium batteries (RLBs) are extensively investigated as new generation rechargeable cells to meet the requirements of high device performance and environmental benignity, owing to their high theoretical capacity, relatively light weight, enhanced safety, and low toxicity. Applications of RLBs are ranged from mobile phones and laptop computers to electrical vehicles and power tools.^[3] However, efforts are still required to pursue much better cell performances (e.g., lighter weight, higher energy/power density, higher rate capability, longer cycle life, and higher safety) for desired consumptions in broader fields. To address this challenge, one of the most direct and important strategies is to utilize materials that possess the expected properties and characteristics in RLBs, since the device performances can only be improved to a limited extent by optimizing the device structures.^[258] The materials used in RLBs, including anode materials, cathode materials, electrolytes, and separators are of critical importance for the devices performance such as the energy/power density, capacity, electrochemical property, cell cycle lifetime, flexibility and cost.^[259,260]

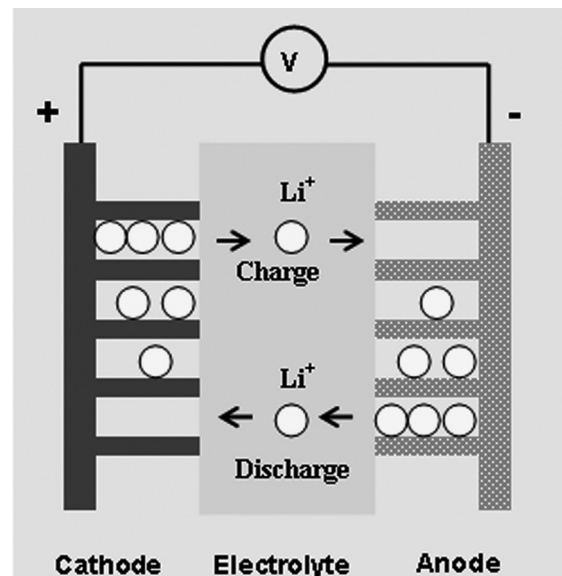


Figure 21. A schematic illustration of a rechargeable lithium battery (RLB).

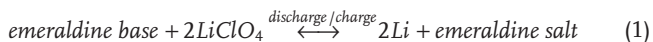
Generally, commercial RLBs use graphite as the anode materials, while classic Li ion (Li^+) intercalation compounds (i.e., $LiCoO_2$, $LiMn_2O_4$, $LiFePO_4$, etc.) are commonly employed as cathode materials. Combination of these positive/negative electrode materials with suitable electrolytes (electronic insulators but Li ions conductors) forms a rechargeable Li-ion transfer cell (Figure 21). When the RLB device is charged, Li ions are extracted from the cathode and intercalated at the anode. Upon discharge, the Li ions are released by the anode and inserted into the cathode. Based on this principle, good electrode materials must fulfill three fundamental requirements to obtain a high specific energy and energy density of RLB devices: (1) a high specific charge and discharge density; (2) a large cell voltage, which results from a high (cathode) and low (anode) standard redox potential of the respective electrode redox reaction; and (3) a good reversibility of electrochemical reactions at both negative and positive electrodes to maintain the specific charge for multiple charge-discharge cycling.^[261] Since no ideal conventional materials can satisfy all the requirements of ideal performance electrodes, a series of new functional structures and materials have so far been investigated.^[262] An available strategy of shifting from bulk materials to nanostructured materials will bring to a revolutionary progress in RBLs, particularly with respect to the cells with high performance (such as large capacity, high-rate capability, and long device cycle life).^[1,263] More significantly, a number of 1D nanostructures such as nanotubes, nanofibers etc. can provide high reactivity, short and direct diffusion paths for Li ions transfer, as well as the large contact area with electrolytes, enabling material chemists either to modify existing electrodes or to develop a new lithium reactivity concept.^[2]

1D conducting polymer nanostructures benefit from the advantages of both the functional π -conjugated polymer nature (i.e., conductivity, low-cost, light weight, and easy for molecular modification) and the low-dimensional nanostructures

(i.e., versatile growth methods, controllable morphology and size, large specific surface area, short and direct charges/ions transfer, etc.). They have been proved to be promising candidates for electrode materials in RLBs. For nanoelectrodes in RLBs, two major types of structures can be used, i.e. the nanofibers/nanotubes of pure conductive polymers,^[264] and the 1D nanocomposites of PPy, PANI, PEDOT combined with CNTs,^[265] metal oxides,^[266–269] or sulfur (S).^[270–273]

In a typical case, reported by Chen's group,^[264] template-synthesized PANI nanotubes doped with HClO_4 , were successfully obtained as the long-range hexagonal order and ca. 300 nm diameters (inset of Figure 22). These ordered PANI nanostructures revealed an effective utilization as positive electrode materials better than the commercial PANI powders in RLBs. The HClO_4 -doped-PANI tubular nanoelectrode obeyed the reaction of Li/PANI batteries^[274] as described in Equation (1), yielding a high practical discharge capacity of 75.7 mAh g⁻¹ at the 20th cycle (about 80% of the theoretical capacity and larger than

the initial value of ~ 67.5 mAh g⁻¹). Considering the weights of PANI as well as ClO_4^{-1} , the obtained capacity was much higher than that of the commercial powders (54.2 mAh g⁻¹) (Figure 22B).



After 80 cycles, the value still retained 95.5% of the highest discharge capacity, that is to say, the average capacity deterioration was less than 0.05 mAh g⁻¹ for each cycle, suggesting their superior cycling capability. At the same time, the specific discharge energy of the nanotubular electrode reached 227 Wh Kg⁻¹, exhibiting excellent storage of high specific energy for RLB devices. In addition, this electrode showed longer charge and discharge plateaus than the electrode composed of commercial powders. The improved performance for PANI nanotubular electrode materials is due to their unique 1D hollow tubular nanostructures and better electrochemical properties compared to their bulk counterparts (Figure 22A). For one thing, the ordered and relatively flexible nanotubes possess higher specific surface areas and shorter and more direct paths, thus they promote the diffusion of Li ions and support the repeated Li^+ intercalation/deintercalation during the recycling processes. For another, their higher electrical conductivity and better electrochemical property, lead to faster electronic kinetics and lower internal resistance for the electrode reactions in the corresponding RLBs. This study reveals that 1D conducting polymer nanostructures are one of promising active electrode materials in RLBs. However, the relatively lower capacity and power density limit their applications. A promising way to solve this problem is to add a more conductive phase such as CNTs to modify them so as to improve the electrode performance of RLBs.^[265,275,276] For example, RLBs based on PANI-CNTs and P3MT-CNTs, showed enhanced cell capacities of 122.8 mAh g⁻¹ and 96 mAh g⁻¹, respectively, while maintained a good cycle performance and high safety after charge/discharge time and again.^[265,276]

Apart from the role of effective electrode active materials, 1D nanostructured conducting polymers can also act as one of important electrode modification materials in RLBs, which benefits from their unique 1D nanostructures, high electrical conductivity, excellent redox electrochemical activity, and so forth. There is no doubt that, introducing conducting polymers into inorganic electrode active materials to develop 1D hybrid nanoelectrodes with enhanced properties, is a particularly significant strategy to improve the cell performances of RLBs.

Early efforts in this direction were made by Yoneyama et al.^[277] With a hard-template route, PPy-coated LiMn_2O_4 nanotubules have been developed as efficient electrode materials in RLBs. Thanks to the decrease in real current density of high specific surface area at the tubule electrodes as well as the short diffusion length for Li ions through the charging and discharging reactions, the capacity of these nanotube electrodes was found to be ca. 2.5 times larger than that of the PPy-coated LiMn_2O_4 thin-film electrodes at 0.1 mA cm⁻², which became 12 times larger with the increased current density of 1.0 mA cm⁻². After that, Torresi et al. synthesized fibril-shaped PANI/vanadium oxide (VO_x) nanocomposites which showed good electrochemical properties and can be employed as good

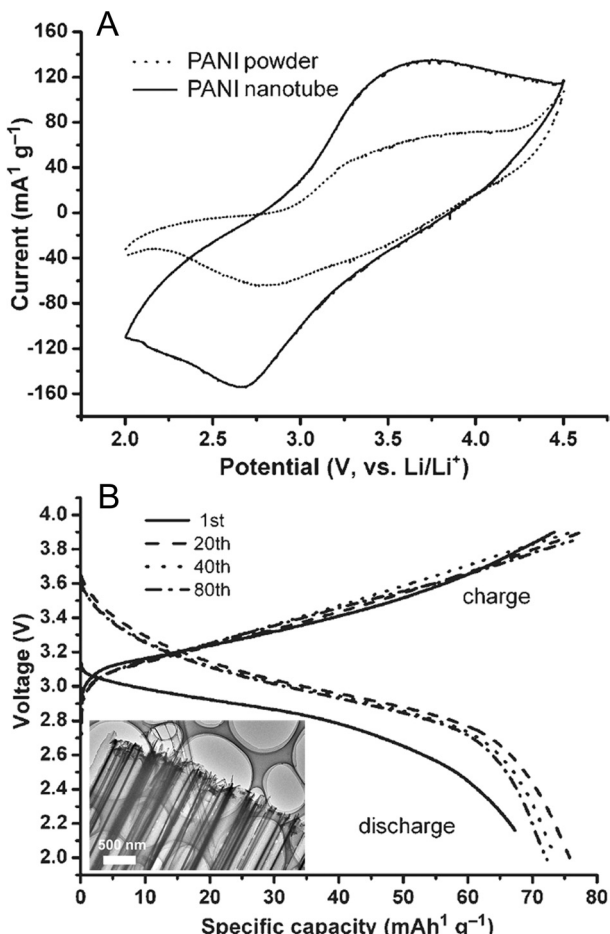


Figure 22. A) Cyclic voltammograms of the electrodes made by doped PANI nanotubes and commercial powders (temperature: 25 °C; scan rate: 1 mV s⁻¹), and B) Charge-discharge cycling performance of Li/PANI cells made with doped PANI nanotubes at the constant charge/discharge current density of 20 mA g⁻¹ and the temperature of 25 °C (Inset: TEM image of the HClO_4 -doped PANI nanotubes in ordered alignment). Reproduced with permission.^[264] Copyright 2006, Wiley VCH.

cathode materials for RLBs.^[267] The corresponding charge capacity reached $\sim 150 \text{ mAh g}^{-1}$ during the initial 10 cycles, which was higher than that of V_2O_5 nanotubular electrodes ($\sim 100 \text{ mAh g}^{-1}$). Furthermore, the cyclability of these PANI/ VO_x nanofibers was better than that of V_2O_5 nanotubes. The same group also investigated the effect of novel nanostructured PANI/ VO_x tubules on the performance of RLBs.^[268] By intercalating PANI into the intralamellar space of VO_x , the developed nanoelectrode could improve the diffusion kinetics of Li^+ intercalation due to their well-defined tubular morphology, and thus resulted in a comparable performance to other VO_x hybrid nanocomposites. Additionally, the core-shell $\text{V}_2\text{O}_5/\text{PANI}$ nanobelts were also designed and synthesized by Chen et al. for the potential application in RLBs.^[269]

Another example to demonstrate the benefits of 1D nanoelectrodes derived from conducting polymers and metal oxides is MnO_2 nanoparticles enriched PEDOT nanowires

which are efficient electrode materials in RLBs.^[266] These novel hybrid nanowires were synthesized by simply soaking template-promoted PEDOT nanowires into a KMnO_4 solution (Figure 23A–B). Namely, the oxidant (KMnO_4) was reduced to MnO_2 by oxidizing the sulfur functional group of PEDOT, and then the finely dispersed MnO_2 nanoparticles grew on the PEDOT nanowires matrix produced the 1D hybrid nanocomposite. It was observed that there was a 4-fold increase in the capacitive current after the inclusion of MnO_2 nanoparticles (Figure 23C–D). The charge storage capacity determined by the MnO_2 nanoparticles was calculated to be 300 mAh g^{-1} , close to the theoretical value of MnO_2 (308 mAh g^{-1}), which corresponded to a lithium insertion coefficient of 0.97 or $\text{Li}_{0.97}\text{MnO}_2$. Such a high capacity can be ascribed to the short diffusion path lengths and high flux of Li ions associated with the small nanosized MnO_2 particles. Meanwhile, this hybrid nanoelectrode exhibited an excellent electrochemical stability for the cycling

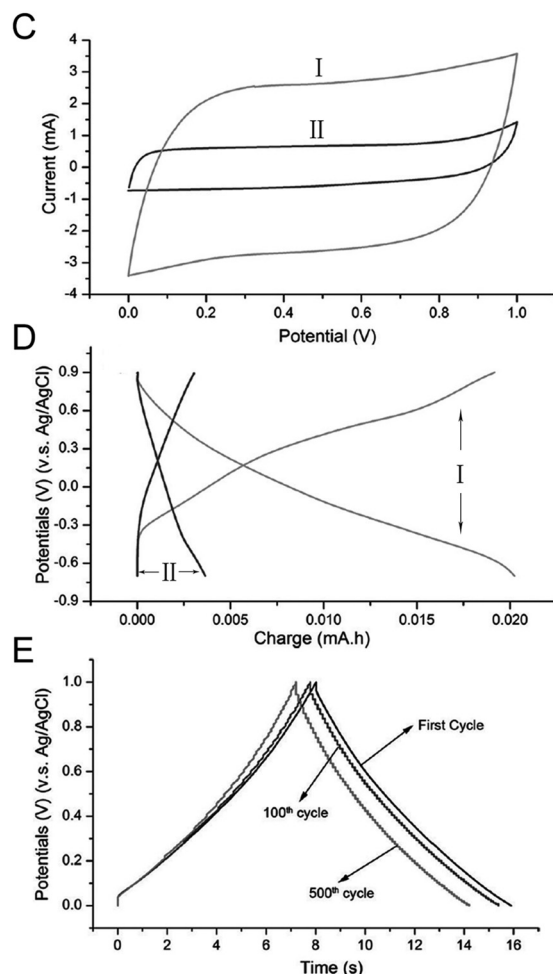
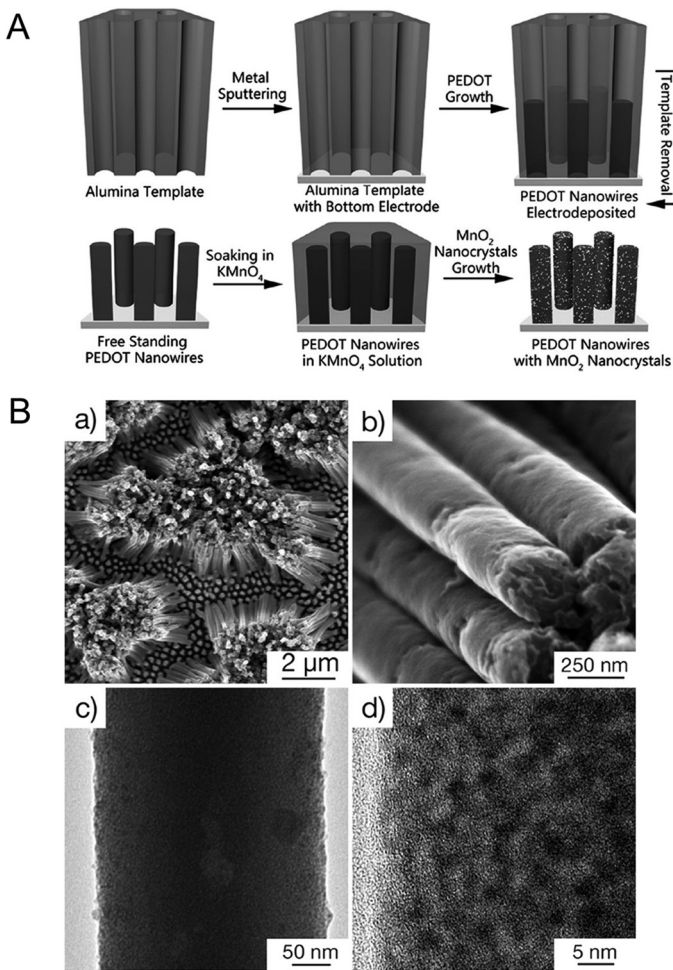


Figure 23. A) Schematic fabrication of the PEDOT/ MnO_2 hybrid nanowires. B) (a,b) SEM and (c,d) TEM images at different magnifications of PEDOT nanowires after being treated with KMnO_4 solution (10 mM) for 10 min. C) Cyclic voltammograms of PEDOT nanowires before (II) and after (I) 10 mM KMnO_4 treatment (10 min) in 1 M LiClO_4 in water, D) Galvanostatic charge-discharge curves of PEDOT nanowires (II) and hybrid PEDOT/ MnO_2 nanowires (I) at a current density of 1.25 mA cm^{-2} in 1 M LiClO_4 in propylene carbonate, and E) Electrochemical stability for the MnO_2 nanoparticles enriched PEDOT nanowires, where the galvanostatic charge-discharge tests are performed between 0 and 1 V (vs Ag/AgCl) at a current density of 30 mA cm^{-2} on the MnO_2 enriched PEDOT nanowires in 1 M LiClO_4 solution for 500 cycles. Reproduced with permission.^[266] Copyright 2010, American Chemical Society.

charge/discharge (Figure 23E). According to the charge/discharge time, the charge storage capacity loss was calculated to be 10% after 500 cycles and only 2% after 100 cycles, while the charge/discharge curve maintained its symmetrical shapes after 100 and 500 cycle tests.

More recently, a new trend toward high performance RLBs is to develop rechargeable Li/S batteries instead of conventional RLB devices. For this new type of cells, the Li-S redox couple can yield a theoretical specific capacity of 1675 mAh g^{-1} and a highly theoretical specific energy up to 2600 Wh kg^{-1} on the assumption of complete reaction of Li with S to Li_2S ($\text{S}_8 + 16\text{Li} \rightarrow 8\text{Li}_2\text{S}$), which are much larger than those of general RLBs based on Li intercalation compound or transition metal oxide electrodes.^[278] Additional merits such as low cost and abundance in nature further drive elemental S to serve as one of the most promising electrode materials for next generation RLBs. Unfortunately, this cell system suffers from the loss of the active material by forming soluble polysulfide during charge/discharge processes, and the degradation of cycle life caused by the insulating character of S.^[278,279] To solve these problems, the S electrode is thereby required to be modified and optimized. Current progresses demonstrated that 1D conducting polymer nanostructures had positive effects on the electrode performance of S in RLBs.^[270–273]

Zhang and co-workers successfully introduced PPy nanowires^[270] and poly(pyrrole-co-aniline) (PPyA) nanofibers^[272], to construct the sulfur/conducting polymers based nanocomposite electrode materials for high performance RLBs. As to the former, soft-template fabricated PPy nanowires served multiple roles in the nanocomposite cathode: a conducting additive to improve the electrical conductivity of S, a distribution agent to increase the specific surface area of S, and an absorbing agent to take up formed polysulfide during the recycling process.^[270] All of these positive effects synergically enhanced the electrochemical performance of the S-based cathode, thus boosted the initial discharge capacity to a record high value of 1222 mAh g^{-1} in rechargeable Li/S batteries, and attained a high capacity of 570 mAh g^{-1} after 20th cycles. For the latter, likewise, novel PPyA nanofibers were template-synthesized and used to fabricate the 1D nanocomposite electrode in rechargeable Li/S batteries.^[272] The developed PPyA/S electrode with 1D nanostructures, showed a larger specific surface area of $78 \text{ m}^2 \text{ g}^{-1}$, a relatively higher electronic conductivity of 58 S cm^{-1} , and a better mechanical resistance compared to the physical blending materials of S with PPyA nanofibers. These properties give beneficial effects on the electron transfer and sulfur dispersing, as well as on the prohibiting the dissolution of polysulfide, all of which lead to an improvement in cell capacity and cycling stability. Subsequently, the specific capacity

of this 1D nanocomposite electrode with the S/PPyA weight ratio of 3:1 was found to be as high as 1285 mAh g^{-1} in the first cycle, and the capacity remained at 866 mAh g^{-1} after 40 cycles.

As a further development, PPy nanotubules are also employed as highly efficient electrode components to develop high performance rechargeable Li-S batteries.^[271,273] In comparison with solid fibril structures, nanotubular conducting polymers hold larger surface area and space capacity because of the hollow morphology, so that they can provide good conductive supports for S loading and distribution in RLBs. With a co-heating route, for example, the sublimed sulfur was incorporated into the template-synthesized PPy nanotubes (Figure 24A–C).^[271] It was found that the electrical conductivity of the formed electrode was greatly enhanced by the nanotubular PPy matrix. Thus, the observed contact and charge transfer resistances for the electrode were smaller than those of the pristine S electrode during the recycling process (Figure 24D). On the other hand, the generated polysulfide was trapped in the PPy nanotubes, which hindered their diffusion to electrolytes and stabilized the cycling performance in return. Under suitable conditions, an optimized nanocomposite electrode of S/PPy nanotubes with 30 wt% S showed excellent cell performances, such as a highly

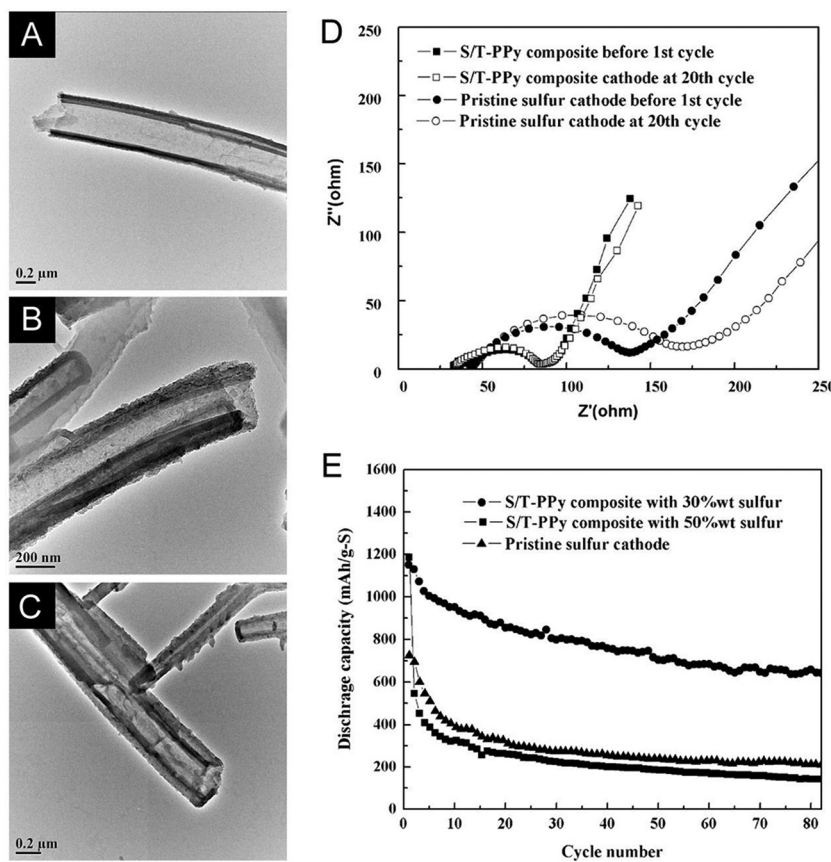


Figure 24. TEM images of (A) the PPy nanotubes (T-PPy), (B) the S/T-PPy composite with 30 wt% sulfur and (C) the S/T-PPy composite with 50 wt% sulfur. D) AC impedance spectra of the S/T-PPy composite with 30 wt% sulfur and pure sulfur electrodes and E) Cycling performance of the S/T-PPy composites and the pristine sulfur electrodes at a current density of 0.1 mA cm^{-2} . Reproduced with permission.^[271] Copyright 2011, Elsevier.

initial discharge capacity of $\sim 1152 \text{ mAh g}^{-1}$ and a reversible capacity of $\sim 650 \text{ mAh g}^{-1}$ over the 80 cycles, which were much better than those of the pristine sulfur and sulfur-rich electrodes (Figure 24E). Similarly, Wen et al. combined polypyrroles in granular (G-PPy) and tubular (T-PPy) morphology with sulfur by in situ oxidation and co-heating methods. They observed that a stable capacity close to 500 mAh g^{-1} could be maintained over 60 cycles for the S/T-PPy composite. On the contrary, the capacity of S/G-PPy composite decreased dramatically after the 30th cycle from 685 to 209 mAh g^{-1} . The reversible capacity was only 153 mAh g^{-1} at the 60th cycle. These electrochemical measurement results suggest that the S/T-PPy composite is obviously superior to the S/G-PPy composite. Consequently, the 1D nanostructured tubular PPy could be a promising electric matrix for sulfur active host in a high energy density Li-S battery application.^[273]

In brief, an improved performance of RLBs has so far been made with the aid of 1D nanostructured conducting polymers to a certain extent. As one of efficient active materials or modified matters for anodes or cathodes, they provide short, direct, and effective paths for electronic transport and Li^+ diffusion (insertion or extraction) due to their high specific surface area, good conductivity and electrochemical activity, which can lead to an improved cell capacity, long cycle life, and enhanced safety. Hence, these progresses greatly facilitate the commercialization of RLBs, especially for rechargeable Li-polymer cells and Li-S cells. Whereas, it should be noted that there are some shortcomings associated with the incorporation of 1D conducting polymer nanostructures, such as an increase in undesirable reactions on electrodes or electrolytes, and potentially more complicated processing procedures. Although, 1D nanostructured conducting polymers have provided some attractive features in the flexible and lightweight rechargeable devices, such as all-polymer batteries based on PANI/CNTs nanofibers,^[280] or PPy/cellulose nanowires,^[281] the relatively low capacity and poor cycle life are still their bottlenecks. Therefore, to achieve flexible, inexpensive, green processing energy storage and release systems with high performance is still a challenge as well as an opportunity in the area of rechargeable batteries, not only in conducting polymers-assisted RLBs, but also in other advanced energy storage devices.

3.4. Supercapacitors

Supercapacitors are also of key significance for hybrid electric automobile batteries or for home energy storage in solar panels. Compared to batteries, supercapacitors are designed for an exceptionally higher capacitance, and a longer cycle life (generally more than 100 times than that of batteries) while possess the similar device configuration (positive and negative electrodes, separator, and electrolyte) despite of the apparent limitation of lower energy density and low voltages.^[1] According to different charge storage mechanisms, these devices can be classified into electric double-layer capacitors (EDLC) and redox-based supercapacitors (also nominated as pseudocapacitors). The working principle of EDLC is based on an electrostatic process where pure physical accumulation occurs at the electrode/electrolyte interface (Figure 25A). However, the working principle of redox-based supercapacitors relies on an electrochemical process where

the reversible redox reactions take place on the electrode materials (Figure 25B).^[282–284] Their performances can be assessed by the parameters such as specific capacitance (F g^{-1}), power density (W kg^{-1}), energy density (Wh kg^{-1}), cyclic life, etc.

Generally used electrode materials in supercapacitor devices not only comprise the time-honored carbon and transition metal oxides, but also contain the fashionable conducting polymers.^[284] However, their conventional structures always suffer from poor electrode performances arising from their relatively large particle sizes and disorder structures, which are not favorable for the charge transfer and transport, thus hinder the resulting device performance. In the past decade, supercapacitor technology has benefited from the replacement of the bulk solids with the 1D nanostructured electrodes based on conducting polymers because of their low processing cost, light weight, good flexibility and high pseudocapacitance.^[38] Up

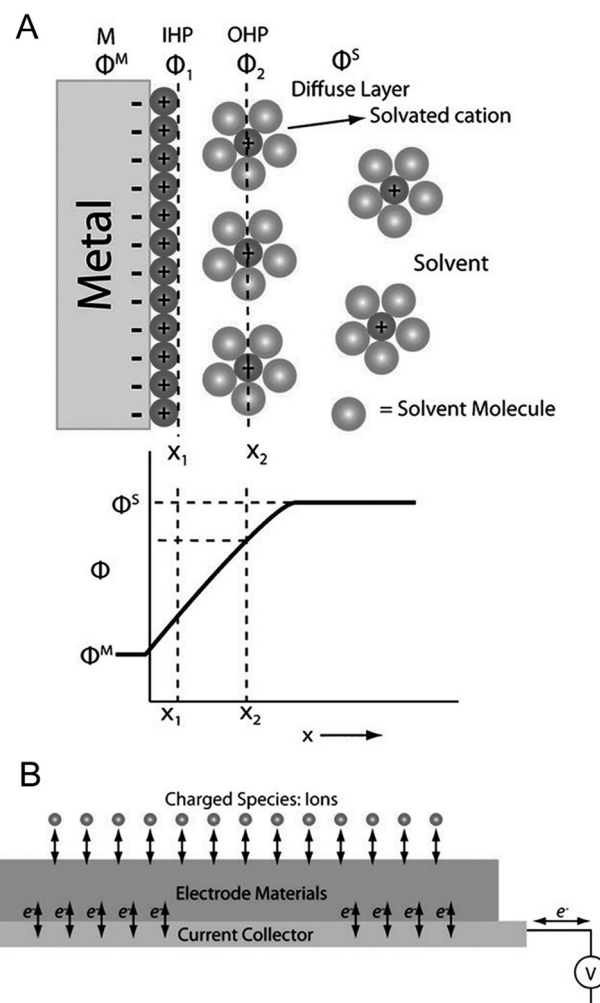


Figure 25. Schematic illustrations of working principles in supercapacitors. A) EDLC showing a traditional charge separation process. M, IHP and OHP refer to metal, inner Helmholtz plane and outer Helmholtz plane in sequence, where the graph represents the potential gradient across the double layer with Φ^S and Φ^M corresponding to the potential of the electrolyte solution and the potential of the electrode metal, respectively. B) Pseudocapacitors showing the surface charge transfer reaction. Reproduced with permission.^[283] Copyright 2011, The Royal Society of Chemistry.

to now, there are two groups of 1D electrode nanomaterials fabricated from conducting polymers: (1) pure polymeric nanostructures; and (2) binary or multiple nanocomposites. The benefits from all of them can enlarge the reactive contact area on surfaces or interfaces, improve the ion diffusion and charge transfer, thus generating a high energy density and a better device durability of supercapacitors.

Pure 1D nanostructures of conducting polymers, including nanowires,^[25,285] nanobelts,^[121] nanotubes,^[38] and their nanoarrays^[286,287] have been investigated as promising electrode materials in supercapacitor devices. Among this large family of nanostructures, vertically aligned nanowires or nanotubes of conducting polymers are particularly regarded as efficient electrodes for supercapacitors owing to their uniform oriented structures and large specific surface area which can provide an ideal pathway for the ion diffusion and charge transfer. As expected, the representative PPy nanowire arrays with controllable size (diameters: 80–100 nm, lengths: 1–4 μm) exhibited a high capacitance of 566 F g⁻¹ and maintained 70% of its initial value after hundreds of charge–discharge cycles.^[285] These PPy nanowire arrays also showed improved properties such as higher power and energy density compared to the disordered nanowire networks and the traditional PPy film, implying their great potentials in energy storage applications. Oriented nanotubular PEDOT arrays, serving as another important type electrode materials, also exhibited good electrochemical properties in spite of their low capacitance values (less than 150 F g⁻¹).^[286] But importantly, the PEDOT nanotube-directed supercapacitor can achieve a high power density of 25000 W kg⁻¹ while maintaining 80% of its energy density (ca. 5.6 Wh kg⁻¹), which is larger than those of previously illustrated supercapacitors based on PEDOT and other conducting polymer films. The high power capability could be ascribed to the fast charge/discharge occurred in thin tubule nanostructures with a short distance for the counter-ion diffusion and ion transport. Nevertheless, it should be noted that, the performance of nanotube-based supercapacitors can be further improved by optimizing the materials and device manufacture conditions.

Conducting PANI attracts much attention due to its rich electrochemical activity and high theoretical specific pseudocapacitance compared to PPy and PEDOT.^[288] Efforts in 1D nanostructured PANI ranging from nanowires to nanotubes and nanoarrays, have confirmed that the morphology has large impacts on the electrode performance of a supercapacitor, e.g. the vertically aligned structures of nanoarrays give beneficial supports for high electrode performances.^[25,289,290] Herein, taking a recent work from Wei et al. as a typical example,^[287] the fabricated arrays of PANI nanowires with 50 nm in diameter were oriented perpendicularly to the conductive substrate (**Figure 26A–B**), which exhibited excellent electrochemical properties and supercapacitor performance. As shown in Figure 26D, two distinct redox peaks in the CV curves corresponds to the transformation between the leucoemeraldine base (LB) and emeraldine salt (ES) states, and the transformation between ES and pernigraniline base (PB) states of PANI, respectively, while the peak current increases with increasing the scan rate, indicating a good rate ability of PANI nanowire arrays. To detect their capacitive properties, the galvanostatic charge-discharge tests were carried out at a series of current densities. The PANI

nanowire arrays showed typical capacitance characteristics as displayed in the charge–discharge curves shown in Figure 26E. Figure 26F presents the specific capacitance corresponding to different current densities in 1 M HClO₄ aqueous solutions calculated by the equation,^[291] $C = (I \times t)/(m \times \Delta V)$, where C is specific capacitance, I and t are charge–discharge current and time, respectively, ΔV is 0.7 V in this measurement, and m is the mass of PANI film on the substrate electrode. On this basis, a remarkable capacitance of 950 F g⁻¹ was obtained for the PANI nanowire arrays at a charge–discharge current density of 1 A g⁻¹ and retained as high as 780 F g⁻¹ at 40 A g⁻¹. This outstanding performance of relatively high capacitance at a large current density mainly benefits from their optimized ionic diffuse pathways and narrow diameters arising from 1D nanoscale morphology of the oriented arrays (Figure 26A–C), which is in favor of enhancing ion diffusion and charge transfer as well as reducing the related resistances (Figure 26C and Figure 26G). On the other hand, the PANI nanowire array based supercapacitors can approach a high energy density of ca. 100 Wh kg⁻¹ even at a high power density of 28000 W kg⁻¹, while still maintain stable in capacitance after hundreds of cycles within different ionic liquid electrolyte systems. All of these prove that they are good electrode materials for electrochemical supercapacitors though some shortcomings required to be overcome. Regardless, this study significantly suggests a useful way for the development of electrode materials for supercapacitors and other energy devices. Meanwhile, with the dramatically improved device performance, the oriented nanoarrays based on functional matters are promising for the supercapacitor application.

Compared to pure conducting polymers in 1D nanoscale, the binary or multiple composites based on 1D nanostructured PPy, PANI and PEDOT, are much more competitive electrode materials to fulfill the supercapacitor application. Incorporation of new components such as metal oxides,^[42,292–294] CNTs,^[295–301] graphene,^[302–305] and even nanodiamonds,^[306] etc. into conducting polymers to construct novel composite electrodes can obtain a series of beneficial effects, and make up the deficiencies of traditional electrode materials, finally attain to the goal of functionalized devices with improved performances.

It is known that, transition metal oxides possess the advantages of high capacitance, rich redox activity, long cycle life and good mechanical stability. Therefore, they can be introduced into pure conducting polymers to fabricate binary nanoelectrodes for supercapacitor with enhanced performance.^[307] Template-directed composite nanotubes of PEDOT/RuO₂ (**Figure 27A**) were a typical example for this kind of binary nanoarchitectures.^[292] In this case, flexible PEDOT and rigid RuO₂ provided mutual supports for each other, which simultaneously affected the redox processes determining their pseudocapacitance behavior in supercapacitors. The energy density (or specific capacitance) of PEDOT nanotubes was found to be dramatically enhanced by electrodepositing RuO₂ into their porous walls and internal surfaces, because the flexible PEDOT prevented RuO₂ from breaking and detaching from the current collector while the rigid RuO₂ kept the PEDOT nanotubes from collapsing and aggregating. As a result, a large power density up to 20000 W kg⁻¹ was achieved, and a high energy density of 28 Wh kg⁻¹ (80% of its maximum value) was maintained for the

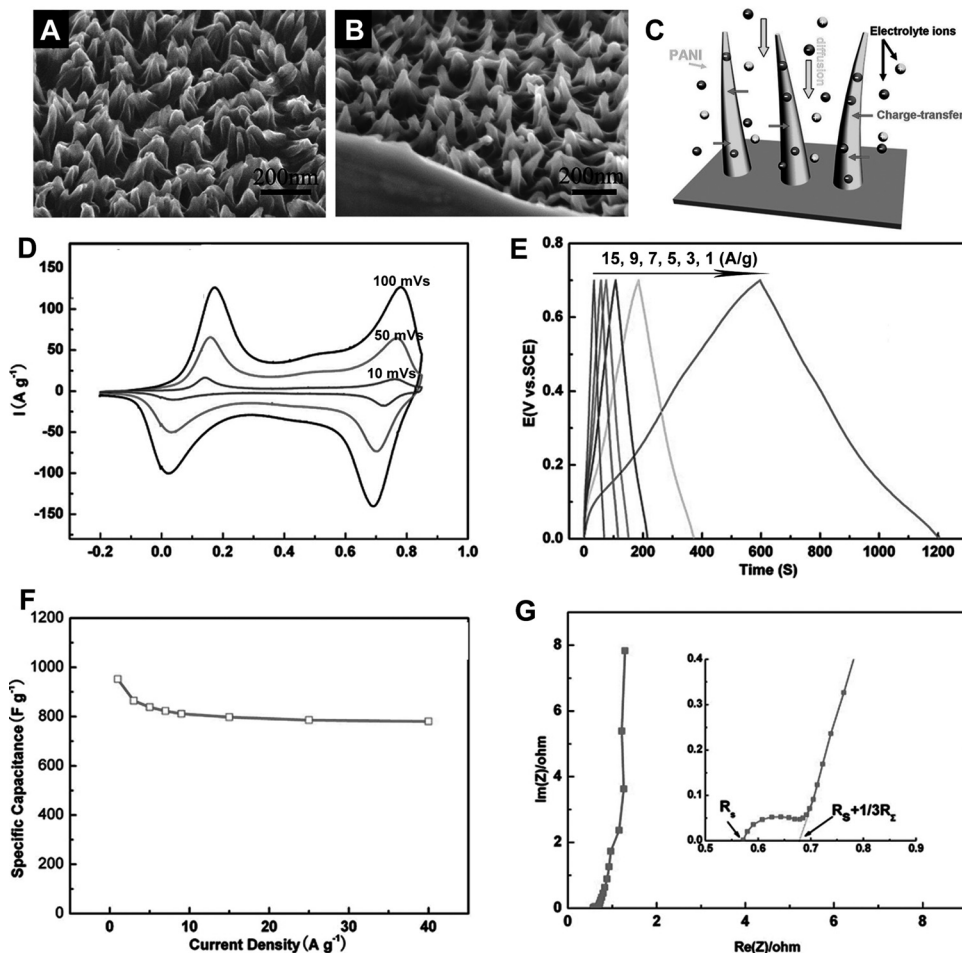


Figure 26. (A, B) SEM images of PANI nanowire arrays obtained from tilted 30° view and cross-section view of PANI nanowire arrays and separated nanowires are clearly observed avoiding aggregation using a freeze drying process, respectively; and (C) Schematic of the optimized ion diffusion path in PANI nanowire arrays. Electrochemical capacitance behavior of PANI nanowire arrays in HClO_4 aqueous solution: (D) CV at different scan rates; (E) Typical galvanostatic charge-discharge curves at several current densities; (F) Specific capacitance in different current densities; (G) Nyquist plots at a frequency range from 20 kHz to 1 Hz (inset: an enlarged curve of the high frequency region). Reproduced with permission.^[287] Copyright 2010, American Chemical Society.

supercapacitor based on such composite PEDOT/RuO₂ nanotubular electrode. Sputtering RuO₂ thin layer onto PPy nanocones to build cone-shaped nanocomposite of PPy/RuO₂ (Figure 27B) is another feasible approach to develop new hybrid electrodes with enhanced performance.^[293] As expected, a supercapacitor based on the electrode of binary products showed a three times higher capacitance, about 302 F g^{-1} , than that of pure PPy nanocones.

Although RuO₂ is an excellent capacitance material for the modification of conducting polymer electrodes, the relatively high cost of the raw material limits its commercial uses. Hence, many efforts have been made to find other metal oxides of good pseudocapacitive properties analogous to RuO₂. Considering their electrochemical nature, low-cost and environmental benignity, MnO₂ and TiO₂ are currently regarded as good candidates for the fabrication of new composite electrodes containing 1D nanostructured conducting polymers.^[284,307] A series of novel nanostructured electrodes based on them such as core-shell

MnO₂/PEDOT coaxial nanowires (Figure 27C–D),^[42,294] PEDOT nanowire supported MnO₂ nanoparticles (Figure 23B),^[266] and PANI nanowire arrays encapsulated TiO₂ nanotubes (Figure 27E)^[40] have been successfully fabricated for supercapacitor applications, which showed improved capacitive performance compared to their bulk counterparts and the monocomponent electrode because of their enhanced efficiencies for ion diffusion and charge transportation resulting from their unique nanostructures. These advancements obviously indicate the great potential of metal-oxide composites containing 1D nanostructured conducting polymers for various energy devices and microelectronic devices, which will receive increasing attention in future.

In addition to the metal oxides, carbon materials including CNTs,^[298,308] carbon fibers,^[309,310] graphene,^[311] and mesoporous carbon^[312] are also of great values in serving as functional components to develop conducting polymers containing 1D nanocomposite electrodes. Approaches to fabricate the novel

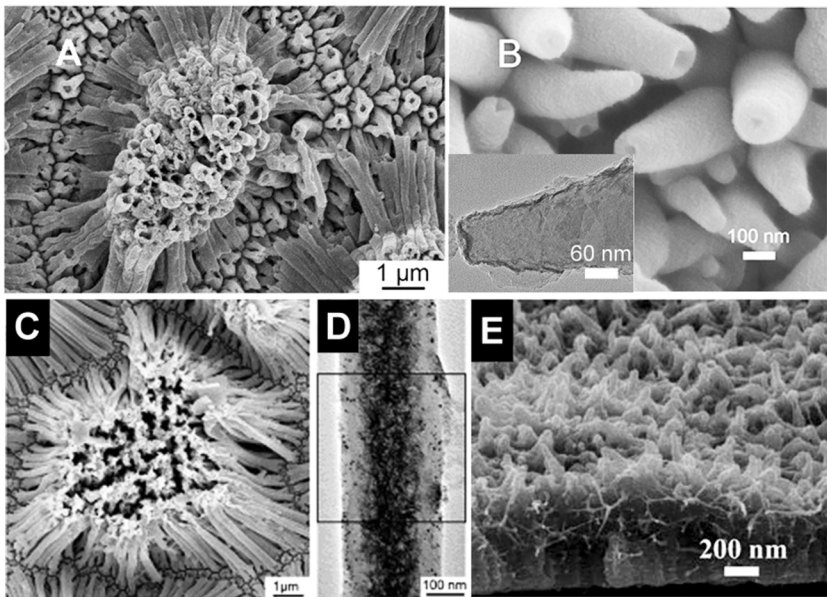


Figure 27. Morphologies of 1D conducting polymer/metal oxide nanocomposites for supercapacitors. A) SEM image of PEDOT/RuO₂ nanotubes. Reproduced with permission.^[292] Copyright 2010, The Owner Societies. B) SEM image of RuO₂ coated-PPy nanocones (inset: TEM image of a single nanocone). Reproduced with permission.^[293] Copyright 2008, American Chemical Society. C, D) SEM and TEM images of core-shell MnO₂/PEDOT coaxial nanowires, respectively. Reproduced with permission.^[42] Copyright 2008, American Chemical Society. E) SEM image of cross-sectional view of PANI nanowire array encapsulated-TiO₂ nanotubes. Reproduced with permission.^[40] Copyright 2011, The Royal Society of Chemistry.

electrodes based on conducting polymers and carbon materials (1D, 2D or 3D) can provide an efficacious solution to overcome many drawbacks of pure conducting polymers as pseudo-capacitive materials, and maintain a high capacitance at the same time.

As we know, CNTs represent one of the most used 1D carbon materials which hold good electro-conductivity, excellent mechanical stability and flexibility, as well as large specific surface area. When employed in electrodes to interact with conducting polymers, on one hand, they can provide percolating networks for enhancing the relatively poor mechanical stability of conducting polymers which allows them to be adapted to volumetric changes during charge-discharge cycles and restricts the damaging effects of swelling or shrinkage of the electrode materials.^[284] On the other hand, use of CNTs in electrodes offers the advantage of a greater control over the morphology and size of coated and/or encapsulated conducting polymers, which serves a crucial role in determining the ability of the electrolyte to access the entire composite structure and hence facilitates the ion diffusion and charge transfer process essential to the performance of redox-based supercapacitors.^[313] Consequently, several 1D nanocomposite electrodes constructed from CNTs and conducting polymers have been extensively investigated with a high specific capacitance, a superior rate capability, and an excellent cycle stability.^[314,315] Values of electrode capacitance ranging from ~200 to 350 F g⁻¹ for PPy/CNT composites,^[295,296,316] 320 to 1030 F g⁻¹ for PANI/CNT composites,^[297-300] and 60 to 160 F g⁻¹ for PEDOT/CNT composites^[301] were obtained, demonstrating their improved performance

than the electrodes based on pure conducting polymers. More interestingly, achievements of these CNT/conducting polymer composites can greatly facilitate us to design and fabricate thin, lightweight, flexible electrode materials and their energy storage devices.^[298] For example, a novel kind of highly flexible paper-like supercapacitors was designed with the device configuration of PANI-coated CNTs (shell thickness ~ 50–90 nm) as thin film electrodes and solid state H₂SO₄-PVA gel as an electrolyte (Figure 28A–E),^[308] which exhibited a high specific capacitance of 350 F g⁻¹, a well cycle stability of at least 1000 cycles, and a leakage current as small as 17.2 μA. Owing to its polymer-based structural nature, a specific capacitance as high as 31.4 F g⁻¹ for the entire supercapacitor device was further achieved, which is 6 times higher than that of current state of the art commercial products. To evaluate the practical application of this flexible supercapacitor, three device units in series were assembled as the rolled-up 15 cm long paper-scriptlike device to light a red LED (Figure 28F). The fabricated supercapacitor group had proper CV curves and galvanostatic charge/discharge curves (Figure 28G–H). After charged at 2.5 V for 15 min, it could light the LED very well up to 30 min.

As a 2D monolayer of sp²-bonded carbon, graphene can provide better networks and supports for 1D nanostructured conducting polymers compared to CNTs, because of its excellent conductivity, high flexibility, great mechanical stiffness and large specific area.^[317-319] Much attention has been given to this star material, and several binary composites of graphene or graphene oxide (GO) nanosheets and 1D conducting polymer nanostructures are extensively studied as novel promising electrode materials for energy storage devices such as supercapacitors. A highly stable and flexible nanocomposite electrode with layered structure of PANI nanofibers sandwiched between chemically converted graphene (CCG) layers have been fabricated by Shi et al. with a novel vacuum filtration method. The conductivity of this composite film (~5.5 × 10² S m⁻¹ when containing 44 wt% CCG) was enhanced about 10 times compared to pure PANI nanofiber film.^[302] The enhanced conductivity of the hybrid electrode contributes to the large capacitance of ~210 F g⁻¹, and the improved electrochemical stability, as well as the rate performances in the corresponding supercapacitor devices. Drzal et al.,^[303] on the other hand, reported that aligned monolayers of graphene nanosheets were interspersed within PPy nanofiber networks by a self-assembly process to reduce contact resistance and enhance current collectors inside the multilayer bulk electrode configuration. Therefore, the prepared nanoelectrode exhibited high ionic and electronic transport due to the combination of the fibrous PPy network and electrically conductive graphene nanosheets, yielding a high specific capacitance of ~165 F g⁻¹ with a nearly ideal rectangular cyclic voltammogram at increasing voltage scanning rates

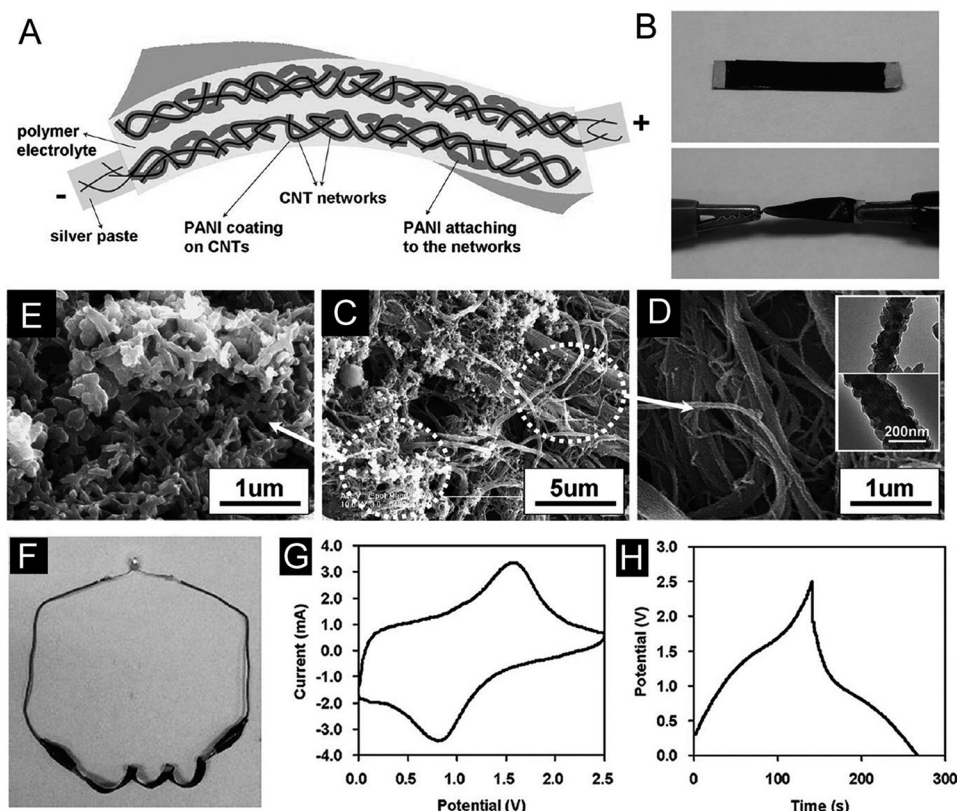


Figure 28. Configuration of the highly flexible paper-like polymer supercapacitors. (A) Schematic illustration of the PANI/CNT nanocomposite electrodes well solidified in the polymer gel electrolyte; (B) Digital graphs of the device (size $\sim 0.5\text{ cm} \times 2.0\text{ cm}$) under normal condition (top) and its highly flexible (twisting) state under electrochemical measurements (bottom). (C) Top view of the surface morphology of the PANI/CNT electrode and SEM images that show (D) PANI uniformly coating on the CNT networks (inset: TEM images of the PANI coating individual CNT and CNT bundles) and (E) the short pure PANI nanobars attaching to the networks. Demo usage of the highly flexible paper-like device: (F) A digital picture that three highly flexible supercapacitor devices in series to light a red LED; (G) CV curves at 5 mV/s and (H) One cycle of galvanostatic charge/discharge curves at 5 mA of the three in-series supercapacitor group. Reproduced with permission.^[308] Copyright 2010, American Chemical Society.

and high electrochemical cyclic stability. Recently, GO was also introduced by Zhao et al. to improve electrode performances of 1D conducting polymer nanostructures on the basis of template/template-free method.^[304,305] High electrocapacitive and rate performances, as well as a good cycling stability were realized by PANI or PPy nanofibers-based graphene nanocomposites because they have the unique properties of both graphene (or GO) and conducting polymers. As shown in Figure 29A–C, SEM and TEM results further demonstrate that the exfoliated and flexible GO nanosheets dispersed in solution have provided a large accessible surface for the attachment of conducting polymer nanofibers on both sides to form novel architectures. Such uniformed 3D nanostructure affords the abilities to improve mechanical strength of the composite electrode, and stabilize the polymers during charge-discharge cycles, and effectively reduce the dynamic resistance of electrolyte ions, finally resulting in good device performance (such as the remarkable capacitance over 500 F g⁻¹ for PPy nanofiber/GO nanocomposites).^[305] These investigations have opened up a general route to make various graphene-based and GO-based composite materials for applications beyond the electrochemical energy storage.

In addition to 1D CNTs and 2D graphene, 3D mesoporous carbon materials with ultra high specific area have also been explored as good supports for nanostructured conducting polymers in developing high performance electrode materials for supercapacitors.^[320] Attractively, ordered whiskerlike PANI nanostructures on the surface of mesoporous carbon were realized by the control of polymerization, nucleation and growth processes of PANI assisted by the well-ordered mesoporous carbon from the nanoporous template.^[312] The best discharge capacitance of the PANI/mesoporous carbon composite was nearly 900 F g⁻¹ at a current density of 0.5 A g⁻¹. When the capacitance contribution from the mesoporous carbon itself has been deducted, the capacitance increases to a value as high as 1221 F g⁻¹. Here, the loosely packed PANI nanowhiskers (10–20 nm in diameter and 80–120 nm in length) can create numerous “V-type” channels which enable the electrochemical accessibility of electrolyte ions and reduce the distance within the PANI phase (Figure 29D–F). As we know that, ions must be transferred during the charge-discharge process, which is fundamentally responsible for the electrode materials of supercapacitors displaying high specific capacitance and excellent rate charge–discharge stability. This

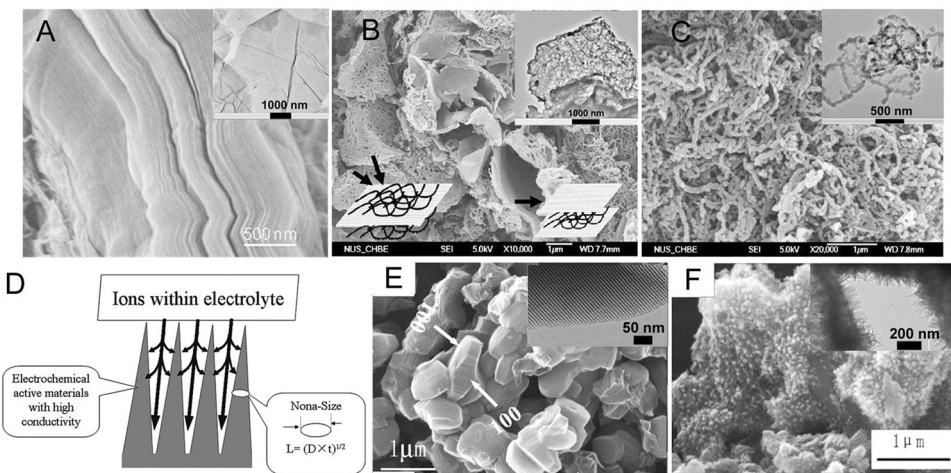


Figure 29. FE-SEM images (insets: TEM images) of (A) GO, (B) PPy nanofibers/GO, and (C) PPy nanofibers. Reproduced with permission.^[305] Copyright 2010, American Chemical Society. (D) Schematic illustration of how the required diffusion length is reduced in supercapacitors with numerous V-like channels, SEM images of (E) mesoporous carbon (inset: TEM image of mesoporous carbon seen from the [100] direction), and (F) PANI nano-whiskers/mesoporous carbon (inset: TEM image). Reproduced with permission.^[312]

study indicates a useful application of high performance composite nanomaterials derived from 1D nanostructured conducting polymers and ordered mesoporous carbon.

So far, although most of explorations have focused on the supercapacitors with mono- and binary-1D nanostructured conducting polymers, the performances of these electrode systems still have their limitations, and many devices still required to be improved and optimized. Therefore, new multivariate (ternary or more) composite systems based on conducting polymer nanomaterials, such as PPy-coated polyacrylonitrile/MWCNT,^[310] MWCNT-PSS/PEDOT/MnO₂,^[321] and MnO₂/functionalized few-walled CNTs/PEDOT-PSS^[322] are all promising electrode materials for supercapacitors.

It is particularly expected that, current investigations of conducting polymers-based 1D nanostructured electrodes will provide new opportunities for the development of affordable supercapacitors with high performance. The energy storage devices are now becoming multifunctional, and developing in the direction of being small, thin, lightweight, flexible and even roll-up devices, which can be fulfilled with the aids of both the rational designed materials and optimized device configurations.

4. Concluding Remarks and Future Perspectives

1D conducting polymer nanostructures are emerging as one of key materials for applications in energy conversion and storage systems, due to their low-cost, environmental benignity and stability, mechanical flexibility, large area processability, as well as high electrical conductivity, high charge-carrier mobility, good optical property, and unique redox electrochemical activity. This review of trends in the increasing ability to fabricate conducting polymers into well-defined 1D nanostructured materials demonstrates the emerging opportunities for discoveries and interdisciplinary research in many areas, as well as for their applications. By now, the template-based and template-free

strategies have been used as effective synthetic methodologies for the controllable synthesis of various 1D nanostructured conducting polymer materials including nanorods, nanowires, nanofibers, nanobelts, nanoribbons, coaxial nanofibers, nanotubes, core-shell nanostructures, and nanocomposites, etc. Though many synthetic progresses have been made in the past decade, more efforts still needed to be devoted to new, low cost and environmentally friendly 1D nanomaterials obtained by facile mass production processes, via which it is possible to precisely control the composition, size, and shape of the nanostuctures with good reproducibility. The diversity of these 1D nanostructures with polymer nature offers the possibility to tune and utilize their electrical, optoelectronic, mechanical properties and others according to the specific requirements for different energy device applications.

In PSC applications, most of the studies used 1D nanostructured poly(3-alkylthiophene) (P3AT) as the electron donor material, and PCBM (or its derivatives) as the electron acceptor material. These devices mostly have PCEs in the range of 1.12–4.43%. Further improvement in efficiency for PSCs based on the nanostructured P3AT/PCBM is limited by the large band-gap of P3AT, and the relatively small energy difference between the HOMO level of P3AT and LUMO level of the donor materials (e.g. PCBM). Therefore, there is a need to explore nanowires fabricated from other p-type conjugated polymer semiconductors, especially for those donor-acceptor low band-gap polymers. Novel 1D nanostructured materials derived from new low band-gap polymers with low-lying HOMO levels may boost the efficiency of PSCs to a record high level. Note that, suitable LUMO offsets between the donor and acceptor (e.g. 0.2–0.3 eV) are also desirable for the overall high efficiencies of PSCs. Besides the efficiency requirement for this application, more attention should be paid to the long term stability of PSC devices. One main challenge that has to be tackled in PSCs based on 1D nanostructured materials is to fabricate devices in large area (e.g. 100 cm²) without a decrease in efficiency. We are

aware that most reported PSCs have device areas around 0.1 cm², which should be increased for their final commercialization. It should be pointed out that so far most nanostructured materials are based on p-type polymers due to the relatively few good existing n-type polymer semiconductors. Thus there are even greater opportunities for the investigation of PSCs based on n-type nanostructured polymer semiconductors. By simply replacing n-type organic semiconductors (such as PCBM) in PSCs with n-type inorganic semiconductors (such as ZnO, TiO₂) while retaining the rest, HSCs can be fabricated. Similarly, 1D nanostructured conducting polymers play important roles as active materials for HSCs. Up to now, the record high efficiency of > 6% has been realized based on well-aligned Si/PEDOT:PSS coaxial nanowire arrays, where the increased D/A contact area and the shortened carrier diffusion distance in the highly oriented core-shell heterojunction are main reasons for the greatly enhanced efficiency. Although some progresses on the HSCs with 1D nanostructured conducting polymers incorporated have been made, the photovoltaic properties (e.g., PCE, EQE, V_{oc}, stability) of most devices are still inferior to the traditional inorganic solar cells. Therefore, more efforts should be made in order for the advancement in higher performance HSCs, especially for promoting their advantages of high durability, low cost, and versatile fabrication techniques. As another application of conducting polymers in solar cells, the substitution of the liquid electrolyte in DSSCs by solid 1D polymer nanostructured materials have led to what are called as ss-DSSCs, which has the advantages of better stability and light weight compared to ls-DSSCs since the latter one has the problems of evaporation or leakage of liquid electrolytes, thus leading to the poor stability in devices. Although, a PCE of 8.3% was recently achieved by using conducting PEDOT nanotube arrays as the counter electrode, further work should be done in order to get large area devices with an efficiency up to the commercialization level and with long term stability.

In fuel cell applications, 1D conducting polymer nanostructures are functioned either as noble metal-free electrocatalysts, or as supports for catalysts loading. They have advantages of low-cost, large specific surface areas, superior electrical conductivity and charge transport, as well as good stability, which result in the improved electrocatalytic performance of high power density and large energy density. However, the investigation on nanostructured materials applied to fuel cells is still in its early stage, therefore more studies are needed in order to understand the relationship between the structure, morphology, size, interfacial feature of nanomaterials and their electrocatalytic activities. Future design on 1D nanostructured materials should consider a balance between the electrocatalytic activity of various structures and their stability. At the same time, the development in fuel cells should also consider the scale-up feasibility and the cost of materials in order for the practical power generation applications.

In energy storage applications, the metallic conductivity and reversible convertibility between redox states of 1D conducting polymer nanostructures are useful attributes for energy storage devices such as RLBs and supercapacitors. In this review, 1D nanostructured conducting polymers are chosen as efficient active materials or modifying matters for metal oxide or sulfur electrodes, because they help to enhance the performance of

RLBs to a certain extent by providing short, direct, and effective pathways for electronic transport and Li⁺ diffusion (insertion or extraction) in metal oxide/sulfur electrodes. However, there still are some shortcomings associated with the incorporation of 1D conducting polymer nanostructures, such as low stability due to the increase in undesirable reactions on electrodes or electrolytes, and the low conductivity in the reduced form. To overcome these shortcomings, 1D conducting polymer nanostructures should be combined with novel materials/structures of better conductivity, higher capacity and safety, to form the resulting composites, which may exhibit significant improvements over conventional electrode counterparts with better mechanical and electrochemical properties. When the polymer nanostructures are used as electrode materials in the electrochemical supercapacitor application for increasing their energy density, one of major challenges is their swelling and shrinking during charge/recharge, leading to a short lifetime compared to inorganic materials. To tackle this challenge, an important approach is combining the 1D conducting polymer nanostructures with some inorganic materials (i.e., metal oxides, CNTs, graphene, and mesoporous carbons) to form composites in which the merits of the individual substances are retained. Supercapacitors and RLBs are two kinds of the most important energy storage devices widely used in our diary life, and they share similarities from device configurations to material designs. Therefore, it is possible to combine a supercapacitor and a RLB together as a "hybrid battery", which will be a storage device of choice, and would likely replace the battery as we know it today.

When employed in various energy devices, 1D nanostructured conducting polymers are demonstrated as active materials, or buffer materials, or positive and negative electrode materials, or catalyst materials, or catalyst supports. In brief, the versatility of 1D conducting polymer nanostructures has been demonstrated in this overview. With the fast development in nanotechnology as well as the availability of more rationally designed conducting polymers, the next decade will continue to see an increasing growth in energy applications of new 1D conducting polymer nanostructures which may pave a new way for meeting the world's ever-growing demand for clean and renewable energy.

Acknowledgements

This work was supported by the National Basic Research 973 Program (2011CB935904) and the 100 Talents Programme of the Chinese Academy of Sciences. We are indebted to those authors whose works have been quoted in this review. We are also grateful to many authors and publishers for the permission to reproduce their figures in this review. We thank Professors Jun Chen and Lunhui Guan for useful discussions.

Received: September 15, 2011

Published online: December 8, 2011

- [1] A. S. Aricò, P. Bruce, B. Scrosati, J.-M. Tarascon, W. van Schalkwijk, *Nat. Mater.* **2005**, 4, 366.
- [2] J. Chen, F. Cheng, *Acc. Chem. Res.* **2009**, 42, 713.
- [3] F. Cheng, J. Liang, Z. Tao, J. Chen, *Adv. Mater.* **2011**, 23, 1695.
- [4] J. Hu, T. W. Odom, C. M. Lieber, *Acc. Chem. Res.* **1999**, 32, 435.

- [5] Y. Xia, P. Yang, Y. Sun, Y. Wu, B. Mayers, B. Gates, Y. Yin, F. Kim, H. Yan, *Adv. Mater.* **2003**, *15*, 353.
- [6] H. D. Tran, D. Li, R. B. Kaner, *Adv. Mater.* **2009**, *21*, 1487.
- [7] C. Burda, X. Chen, R. Narayanan, M. A. El-Sayed, *Chem. Rev.* **2005**, *105*, 1025.
- [8] C. J. Murphy, T. K. Sau, A. M. Gole, C. J. Orendorff, J. Gao, L. Gou, S. E. Hunyadi, T. Li, *J. Phys. Chem. B* **2005**, *109*, 13857.
- [9] J.-Y. Lee, S. T. Connor, Y. Cui, P. Peumans, *Nano Lett.* **2008**, *8*, 689.
- [10] J. Liu, G. Cao, Z. Yang, D. Wang, D. Dubois, X. Zhou, G. L. Graff, L. R. Pederson, J.-G. Zhang, *ChemSusChem* **2008**, *1*, 676.
- [11] Z. Yin, B. Wang, G. Chen, M. Zhan, *J. Mater. Sci.* **2011**, *46*, 2397.
- [12] F. S. Kim, G. Ren, S. A. Jenekhe, *Chem. Mater.* **2011**, *23*, 682.
- [13] L. Jiang, X. Wang, L. Chi, *Small* **2011**, *7*, 1309.
- [14] Y. Xu, F. Zhang, X. Feng, *Small* **2011**, *7*, 1338.
- [15] M. A. Bangar, W. Chen, N. V. Myung, A. Mulchandani, *Thin Solid Films* **2010**, *519*, 964.
- [16] a) Y.-Z. Long, M.-M. Li, C. Gu, M. Wan, J.-L. Duvail, Z. Liu, Z. Fan, *Prog. Polym. Sci.* **2011**, *36*, 1415; b) H. Yoon, J. Jang, *Adv. Funct. Mater.* **2009**, *19*, 1567.
- [17] L. Xia, Z. Wei, M. Wan, *J. Colloid Interface Sci.* **2010**, *341*, 1.
- [18] H.-W. Liang, S. Liu, S.-H. Yu, *Adv. Mater.* **2010**, *22*, 3925.
- [19] R. V. Parthasarathy, C. R. Martin, *Nature* **1994**, *369*, 298.
- [20] C. R. Martin, *Acc. Chem. Res.* **1995**, *28*, 61.
- [21] C. R. Martin, *Chem. Mater.* **1996**, *8*, 1739.
- [22] J. Jang, J. H. Oh, *Chem. Commun.* **2004**, 882.
- [23] A. Rahman, M. K. Sanyal, *Adv. Mater.* **2007**, *19*, 3956.
- [24] J. I. Lee, S. H. Cho, S.-M. Park, J. K. Kim, J. K. Kim, J.-W. Yu, Y. C. Kim, T. P. Russell, *Nano Lett.* **2008**, *8*, 2315.
- [25] Y. Cao, T. E. Mallouk, *Chem. Mater.* **2008**, *20*, 5260.
- [26] M. Fu, Y. Zhu, R. Tan, G. Shi, *Adv. Mater.* **2001**, *13*, 1874.
- [27] G. Lu, W. Hong, L. Tong, H. Bai, Y. Wei, G. Shi, *ACS Nano* **2008**, *2*, 2342.
- [28] G. A. O'Brien, A. J. Quinn, D. Iacopino, N. Pauget, G. Redmond, *J. Mater. Chem.* **2006**, *16*, 3237.
- [29] K. Kim, J. W. Shin, Y. B. Lee, M. Y. Cho, S. H. Lee, D. H. Park, D. K. Jang, C. J. Lee, J. Joo, *ACS Nano* **2010**, *4*, 4197.
- [30] D. H. Park, H. S. Kim, M.-Y. Jeong, Y. B. Lee, H.-J. Kim, D.-C. Kim, J. Kim, J. Joo, *Adv. Funct. Mater.* **2008**, *18*, 2526.
- [31] M. G. Han, S. H. Foulger, *Chem. Commun.* **2005**, 3092.
- [32] Y. Z. Long, J. L. Duvail, Z. J. Chen, A. Z. Jin, C. Z. Gu, *Polym. Adv. Technol.* **2009**, *20*, 541.
- [33] J. L. Duvail, P. Rétho, V. Fernandez, G. Louarn, P. Molinié, O. Chauvet, *J. Phys. Chem. B* **2004**, *108*, 18552.
- [34] K. Kim, J.-I. Jin, *Nano Lett.* **2001**, *1*, 631.
- [35] F. Massuyseau, J. L. Duvail, H. Athalin, J. M. Lorcy, S. Lefrant, J. Wery, E. Faulques, *Nanotechnology* **2009**, *20*, 155701.
- [36] S. D. Bearden, J. P. Cannon, S. A. Gold, *Macromolecules* **2011**, *44*, 2200.
- [37] G. A. O'Brien, A. J. Quinn, D. A. Tanner, G. Redmond, *Adv. Mater.* **2006**, *18*, 2379.
- [38] S. I. Cho, S. B. Lee, *Acc. Chem. Res.* **2008**, *41*, 699.
- [39] D. Kowalski, P. Schmuki, *Chem. Commun.* **2010**, *46*, 8585.
- [40] K. Xie, J. Li, Y. Lai, Z. a. Zhang, Y. Liu, G. Zhang, H. Huang, *Nanoscale* **2011**, *3*, 2202.
- [41] D. H. Park, Y. K. Hong, E. H. Cho, M. S. Kim, D.-C. Kim, J. Bang, J. Kim, J. Joo, *ACS Nano* **2010**, *4*, 5155.
- [42] R. Liu, S. B. Lee, *J. Am. Chem. Soc.* **2008**, *130*, 2942.
- [43] D. Zhang, L. Luo, Q. Liao, H. Wang, H. Fu, J. Yao, *J. Phys. Chem. C* **2011**, *115*, 2360.
- [44] Y. Guo, H. Liu, Y. Li, G. Li, Y. Zhao, Y. Song, Y. Li, *J. Phys. Chem. C* **2009**, *113*, 12669.
- [45] M. Lahav, E. A. Weiss, Q. Xu, G. M. Whitesides, *Nano Lett.* **2006**, *6*, 2166.
- [46] J. Joo, D. H. Park, M. Y. Jeong, Y. B. Lee, H. S. Kim, W. J. Choi, Q. H. Park, H. J. Kim, D. C. Kim, J. Kim, *Adv. Mater.* **2007**, *19*, 2824.
- [47] V. Callegari, S. Demoustier-Champagne, *ACS Appl. Mater. Interfaces* **2010**, *2*, 1369.
- [48] Y. Guo, Q. Tang, H. Liu, Y. Zhang, Y. Li, W. Hu, S. Wang, D. Zhu, *J. Am. Chem. Soc.* **2008**, *130*, 9198.
- [49] R. M. Hernández, L. Richter, S. Semancik, S. Stranick, T. E. Mallouk, *Chem. Mater.* **2004**, *16*, 3431.
- [50] V. Callegari, L. Gence, S. Melinte, S. Demoustier-Champagne, *Chem. Mater.* **2009**, *21*, 4241.
- [51] C. J. Brinker, Y. Lu, A. Sellinger, H. Fan, *Adv. Mater.* **1999**, *11*, 579.
- [52] M. G. Han, S. H. Foulger, *Small* **2006**, *2*, 1164.
- [53] L. Meng, Y. Lu, X. Wang, J. Zhang, Y. Duan, C. Li, *Macromolecules* **2007**, *40*, 2981.
- [54] H. Yoon, M. Chang, J. Jang, *Adv. Funct. Mater.* **2007**, *17*, 431.
- [55] S. Samitsu, Y. Takanishi, J. Yamamoto, *Macromolecules* **2009**, *42*, 4366.
- [56] J. Han, G. Song, R. Guo, *Adv. Mater.* **2007**, *19*, 2993.
- [57] P. Anilkumar, M. Jayakannan, *Macromolecules* **2007**, *40*, 7311.
- [58] P. Anilkumar, M. Jayakannan, *Macromolecules* **2008**, *41*, 7706.
- [59] P. Anilkumar, M. Jayakannan, *J. Phys. Chem. B* **2009**, *114*, 728.
- [60] X. Zhang, J. Zhang, Z. Liu, C. Robinson, *Chem. Commun.* **2004**, 1852.
- [61] X. Zhang, J. Zhang, W. Song, Z. Liu, *J. Phys. Chem. B* **2005**, *110*, 1158.
- [62] A. B. Kaiser, *Adv. Mater.* **2001**, *13*, 927.
- [63] A. B. Kaiser, *Rep. Prog. Phys.* **2001**, *64*, 1.
- [64] X. Zhang, J. Zhang, W. Song, Z. Liu, *J. Phys. Chem. B* **2006**, *110*, 1158.
- [65] W. Zhong, J. Deng, Y. Yang, W. Yang, *Macromol. Rapid Commun.* **2005**, *26*, 395.
- [66] W. Zhong, S. Liu, X. Chen, Y. Wang, W. Yang, *Macromolecules* **2006**, *39*, 3224.
- [67] T. Hatano, M. Takeuchi, A. Ikeda, S. Shinkai, *Org. Lett.* **2003**, *5*, 1395.
- [68] G. Li, Z. Zhang, *Macromolecules* **2004**, *37*, 2683.
- [69] J. Jang, H. Yoon, *Chem. Commun.* **2003**, 720.
- [70] J. Jang, H. Yoon, *Langmuir* **2005**, *21*, 11484.
- [71] J. Jang, M. Chang, H. Yoon, *Adv. Mater.* **2005**, *17*, 1616.
- [72] X. Zhang, J.-S. Lee, G. S. Lee, D.-K. Cha, M. J. Kim, D. J. Yang, S. K. Manohar, *Macromolecules* **2005**, *39*, 470.
- [73] H. Mao, X. Liu, D. Chao, L. Cui, Y. Li, W. Zhang, C. Wang, *J. Mater. Chem.* **2010**, *20*, 10277.
- [74] X. Lu, Q. Zhao, X. Liu, D. Wang, W. Zhang, C. Wang, Y. Wei, *Macromol. Rapid Commun.* **2006**, *27*, 430.
- [75] X. F. Lu, H. Mao, W. J. Zhang, *Nanotechnology* **2007**, *18*, 025604.
- [76] J. Ota, S. K. Srivastava, *J. Phys. Chem. C* **2007**, *111*, 12260.
- [77] X. Liu, J. Ly, S. Han, D. Zhang, A. Requicha, M. E. Thompson, C. Zhou, *Adv. Mater.* **2005**, *17*, 2727.
- [78] M. Ding, Y. Tang, P. Gou, M. J. Reber, A. Star, *Adv. Mater.* **2011**, *23*, 536.
- [79] A. Ikeda, K. Nobusawa, T. Hamano, J.-i. Kikuchi, *Org. Lett.* **2006**, *8*, 5489.
- [80] L. Zhang, H. Peng, P. A. Kilmartin, C. Soeller, J. Traval-Sejdic, *Macromolecules* **2008**, *41*, 7671.
- [81] M. R. Abidian, D. H. Kim, D. C. Martin, *Adv. Mater.* **2006**, *18*, 405.
- [82] Y. Gao, S. Yao, J. Gong, L. Qu, *Macromol. Rapid Commun.* **2007**, *28*, 286.
- [83] X. Li, Y. Gao, J. Gong, L. Zhang, L. Qu, *J. Phys. Chem. C* **2009**, *113*, 69.
- [84] Y.-C. Pu, J. R. Hwu, W.-C. Su, D.-B. Shieh, Y. Tzeng, C.-S. Yeh, *J. Am. Chem. Soc.* **2006**, *128*, 11606.
- [85] X. Sun, M. Hagner, *Chem. Mater.* **2008**, *20*, 2869.
- [86] H. Tong, Y. J. Zhu, X. L. Liu, *Chem. Lett.* **2009**, *38*, 228.
- [87] T. Dai, Y. Lu, *Macromol. Rapid Commun.* **2007**, *28*, 629.
- [88] X. Yang, Z. Zhu, T. Dai, Y. Lu, *Macromol. Rapid Commun.* **2005**, *26*, 1736.

- [89] T. Y. Dai, X. M. Yang, Y. Lu, *Nanotechnology* **2006**, *17*, 3028.
- [90] H. P. Huang, X. M. Feng, J. J. Zhu, *Nanotechnology* **2008**, *19*, 145607.
- [91] X. M. Feng, Z. Z. Sun, W. H. Hou, J. J. Zhu, *Nanotechnology* **2007**, *18*, 195603.
- [92] L. J. Pan, L. Pu, Y. Shi, S. Y. Song, Z. Xu, R. Zhang, Y. D. Zheng, *Adv. Mater.* **2007**, *19*, 461.
- [93] J. Xu, X. Li, J. Liu, X. Wang, Q. Peng, Y. Li, *J. Polym. Sci., Part A: Polym. Chem.* **2005**, *43*, 2892.
- [94] X. Zhang, W. J. Goux, S. K. Manohar, *J. Am. Chem. Soc.* **2004**, *126*, 4502.
- [95] X. Zhang, S. K. Manohar, *J. Am. Chem. Soc.* **2004**, *126*, 12714.
- [96] X. Zhang, A. G. MacDiarmid, S. K. Manohar, *Chem. Commun.* **2005**, 5328.
- [97] Z. Liu, Y. Liu, S. Poyraz, X. Zhang, *Chem. Commun.* **2011**, *47*, 4421.
- [98] X. Zhang, S. K. Manohar, *J. Am. Chem. Soc.* **2005**, *127*, 14156.
- [99] Z. Niu, M. Bruckman, V. S. Kotakadi, J. He, T. Emrick, T. P. Russell, L. Yang, Q. Wang, *Chem. Commun.* **2006**, 3019.
- [100] Z. Niu, J. Liu, L. A. Lee, M. A. Bruckman, D. Zhao, G. Koley, Q. Wang, *Nano Lett.* **2007**, *7*, 3729.
- [101] Z. Niu, M. A. Bruckman, S. Li, L. A. Lee, B. Lee, S. V. Pingali, P. Thiagarajan, Q. Wang, *Langmuir* **2007**, *23*, 6719.
- [102] S. Pruneanu, S. A. F. Al-Said, L. Dong, T. A. Hollis, M. A. Galindo, N. G. Wright, A. Houlton, B. R. Horrocks, *Adv. Funct. Mater.* **2008**, *18*, 2444.
- [103] L. Dong, T. Hollis, S. Fishwick, B. A. Connolly, N. G. Wright, B. R. Horrocks, A. Houlton, *Chem. Eur. J.* **2007**, *13*, 822.
- [104] J. Ryu, C. B. Park, *Angew. Chem. Int. Ed.* **2009**, *48*, 4820.
- [105] M. Hamed, A. Herland, R. H. Karlsson, O. Inganäs, *Nano Lett.* **2008**, *8*, 1736.
- [106] M. Wan, *Adv. Mater.* **2008**, *20*, 2926.
- [107] M. Wan, *Macromol. Rapid Commun.* **2009**, *30*, 963.
- [108] M. Wan, *Conducting Polymers with Micro or Nanometer Structure*, Tsinghua University Press, Beijing and Springer, Berlin, Heidelberg **2008**.
- [109] J. Huang, S. Virji, B. H. Weiller, R. B. Kaner, *J. Am. Chem. Soc.* **2003**, *125*, 314.
- [110] J. Huang, R. B. Kaner, *J. Am. Chem. Soc.* **2004**, *126*, 851.
- [111] K. Su, N. Nuraje, L. Zhang, I. W. Chu, R. M. Peetz, H. Matsui, N. L. Yang, *Adv. Mater.* **2007**, *19*, 669.
- [112] G. Lu, C. Li, J. Shen, Z. Chen, G. Shi, *J. Phys. Chem. C* **2007**, *111*, 5926.
- [113] J. Huang, R. B. Kaner, *Angew. Chem. Int. Ed.* **2004**, *43*, 5817.
- [114] N. R. Chiou, A. J. Epstein, *Adv. Mater.* **2005**, *17*, 1679.
- [115] X. Jing, Y. Wang, D. Wu, L. She, Y. Guo, *J. Polym. Sci., Part A: Polym. Chem.* **2006**, *44*, 1014.
- [116] S. K. Pillalamarri, F. D. Blum, A. T. Tokuhiro, J. G. Story, M. F. Bertino, *Chem. Mater.* **2004**, *17*, 227.
- [117] M. R. Gizdavic-Nikolaïdis, D. R. Stanisavljev, A. J. Easteal, Z. D. Zujovic, *Macromol. Rapid Commun.* **2010**, *31*, 657.
- [118] M. R. Gizdavic-Nikolaïdis, D. R. Stanisavljev, A. J. Easteal, Z. D. Zujovic, *J. Phys. Chem. C* **2010**, *114*, 18790.
- [119] J. Zang, C. M. Li, S.-J. Bao, X. Cui, Q. Bao, C. Q. Sun, *Macromolecules* **2008**, *41*, 7053.
- [120] D. Zhang, Y. Wang, *Mater. Sci. Eng., B* **2006**, *134*, 9.
- [121] G.-R. Li, Z.-P. Feng, J.-H. Zhong, Z.-L. Wang, Y.-X. Tong, *Macromolecules* **2010**, *43*, 2178.
- [122] A. Das, C. H. Lei, M. Elliott, J. E. Macdonald, M. L. Turner, *Org. Electron.* **2006**, *7*, 181.
- [123] K. Ramanathan, M. A. Bangar, M. Yun, W. Chen, A. Mulchandani, N. V. Myung, *Nano Lett.* **2004**, *4*, 1237.
- [124] P. S. Thapa, D. J. Yu, J. P. Wicksted, J. A. Hadwiger, J. N. Barisci, R. H. Baughman, B. N. Flanders, *Appl. Phys. Lett.* **2009**, *94*, 033104.
- [125] Q. Tang, J. Wu, X. Sun, Q. Li, J. Lin, M. Huang, *Chem. Commun.* **2009**, 2166.
- [126] N. Gospodinova, D. A. Ivanov, D. V. Anokhin, I. Mihai, L. Vidal, S. Brun, J. Romanova, A. Tadjer, *Macromol. Rapid Commun.* **2009**, *30*, 29.
- [127] M. He, L. Zhao, J. Wang, W. Han, Y. Yang, F. Qiu, Z. Lin, *ACS Nano* **2010**, *4*, 3241.
- [128] X. Xiao, Z. Wang, Z. Hu, T. He, *J. Phys. Chem. B* **2010**, *114*, 7452.
- [129] G. Lu, H. Tang, Y. Qu, L. Li, X. Yang, *Macromolecules* **2007**, *40*, 6579.
- [130] S. Samitsu, T. Shimomura, S. Heike, T. Hashizume, K. Ito, *Macromolecules* **2008**, *41*, 8000.
- [131] L. Zang, Y. Che, J. S. Moore, *Acc. Chem. Res.* **2008**, *41*, 1596.
- [132] P. V. Kamat, K. Tvardy, D. R. Baker, J. G. Radich, *Chem. Rev.* **2010**, *110*, 6664.
- [133] A. Greiner, J. H. Wendorff, *Angew. Chem. Int. Ed.* **2007**, *46*, 5670.
- [134] D. Li, Y. Xia, *Adv. Mater.* **2004**, *16*, 1151.
- [135] X. Lu, C. Wang, Y. Wei, *Small* **2009**, *5*, 2349.
- [136] X. Lu, W. Zhang, C. Wang, T.-C. Wen, Y. Wei, *Prog. Polym. Sci.* **2011**, *36*, 671.
- [137] H. A. Liu, D. Zepeda, J. P. Ferraris, K. J. Balkus, *ACS Appl. Mater. Interfaces* **2009**, *1*, 1958.
- [138] D. H. Reneker, I. Chun, *Nanotechnology* **1996**, *7*, 216.
- [139] A. G. MacDiarmid, W. E. Jones, I. D. Norris, J. Gao, A. T. Johnson, N. J. Pinto, J. Hone, B. Han, F. K. Ko, H. Okuzaki, M. Llaguno, *Synth. Met.* **2001**, *119*, 27.
- [140] H. Liu, J. Kameoka, D. A. Czaplewski, H. G. Craighead, *Nano Lett.* **2004**, *4*, 671.
- [141] M. Wei, J. Lee, B. Kang, J. Mead, *Macromol. Rapid Commun.* **2005**, *26*, 1127.
- [142] J. H. Yu, S. V. Fridrikh, G. C. Rutledge, *Adv. Mater.* **2004**, *16*, 1562.
- [143] I. D. Norris, M. M. Shaker, F. K. Ko, A. G. MacDiarmid, *Synth. Met.* **2000**, *114*, 109.
- [144] I. S. Chronakis, S. Grapenon, A. Jakob, *Polymer* **2006**, *47*, 1597.
- [145] I. S. Chronakis, in *Nanostructured Conductive Polymers* (Ed.: A. Eftekhar), John Wiley & Sons, Ltd, **2010**, pp. 161.
- [146] J. Roncali, *Adv. Energy Mater.* **2011**, *1*, 147.
- [147] J. Weickert, R. B. Dunbar, H. C. Hesse, W. Wiedemann, L. Schmidt-Mende, *Adv. Mater.* **2011**, *23*, 1810.
- [148] L. J. Brennan, M. T. Byrne, M. Bari, Y. K. Gun'ko, *Adv. Energy Mater.* **2011**, *1*, 472.
- [149] W. U. Huynh, J. J. Dittmer, A. P. Alivisatos, *Science* **2002**, *295*, 2425.
- [150] K. M. Coakley, M. D. McGehee, *Chem. Mater.* **2004**, *16*, 4533.
- [151] S. Güneş, H. Neugebauer, N. S. Sariciftci, *Chem. Rev.* **2007**, *107*, 1324.
- [152] G. Li, V. Shrotriya, J. Huang, Y. Yao, T. Moriarty, K. Emery, Y. Yang, *Nat. Mater.* **2005**, *4*, 864.
- [153] C. Groves, O. G. Reid, D. S. Ginger, *Acc. Chem. Res.* **2010**, *43*, 612.
- [154] M. Helgesen, R. Sondergaard, F. C. Krebs, *J. Mater. Chem.* **2010**, *20*, 36.
- [155] P. A. Staniec, A. J. Parnell, A. D. F. Dunbar, H. Yi, A. J. Pearson, T. Wang, P. E. Hopkinson, C. Kinane, R. M. Dalgliesh, A. M. Donald, A. J. Ryan, A. Iraqi, R. A. L. Jones, D. G. Lidzey, *Adv. Energy Mater.* **2011**, *1*, 499.
- [156] M. D. Irwin, B. Buchholz, A. W. Hains, R. P. H. Chang, T. J. Marks, *Proc. Natl. Acad. Sci. U. S. A.* **2008**, *105*, 2783.
- [157] G. Zhao, Y. He, Y. Li, *Adv. Mater.* **2010**, *22*, 4355.
- [158] C. J. Brabec, S. Gowrisankar, J. J. M. Halls, D. Laird, S. Jia, S. P. Williams, *Adv. Mater.* **2010**, *22*, 3839.
- [159] L.-M. Chen, Z. Hong, G. Li, Y. Yang, *Adv. Mater.* **2009**, *21*, 1434.
- [160] J. Huang, Z. Yin, Q. Zheng, *Energy Environ. Sci.* **2011**, *4*, 3861.
- [161] H. Hoppe, N. S. Sariciftci, *J. Mater. Chem.* **2006**, *16*, 45.
- [162] G. Dennler, M. C. Scharber, C. J. Brabec, *Adv. Mater.* **2009**, *21*, 1323.

- [163] G. Li, V. Shrotriya, Y. Yao, J. Huang, Y. Yang, *J. Mater. Chem.* **2007**, *17*, 3126.
- [164] a) Y. Liang, L. Yu, *Acc. Chem. Res.* **2010**, *43*, 1227; b) R. F. Service, *Science* **2011**, *332*, 293; c) M. A. Green, K. Emery, Y. Hishikawa, W. Warta, *Prog. Photovolt: Res. Appl.* **2011**, *19*, 84; d) Z. He, C. Zhong, X. Huang, W.-Y. Wong, H. Wu, L. Chen, S. Su, Y. Cao, *Adv. Mater.* **2011**, *23*, 4636.
- [165] Q. Zheng, B. J. Jung, J. Sun, H. E. Katz, *J. Am. Chem. Soc.* **2010**, *132*, 5394.
- [166] X. Yang, J. Loos, S. C. Veenstra, W. J. H. Verhees, M. M. Wienk, J. M. Kroon, M. A. J. Michels, R. A. J. Janssen, *Nano Lett.* **2005**, *5*, 579.
- [167] S. van Bavel, E. Sourty, G. de With, K. Frolic, J. Loos, *Macromolecules* **2009**, *42*, 7396.
- [168] D. M. Stevens, Y. Qin, M. A. Hillmyer, C. D. Frisbie, *J. Phys. Chem. C* **2009**, *113*, 11408.
- [169] R. Po, M. Maggini, N. Camaiori, *J. Phys. Chem. C* **2009**, *114*, 695.
- [170] S. van Bavel, E. Sourty, G. de With, S. Veenstra, J. Loos, *J. Mater. Chem.* **2009**, *19*, 5388.
- [171] K. Maturová, S. S. van Bavel, M. M. Wienk, R. A. J. Janssen, M. Kemerink, *Adv. Funct. Mater.* **2011**, *21*, 261.
- [172] A. A. Herzing, L. J. Richter, I. M. Anderson, *J. Phys. Chem. C* **2010**, *114*, 17501.
- [173] B. Friedel, C. R. McNeill, N. C. Greenham, *Chem. Mater.* **2010**, *22*, 3389.
- [174] B.-G. Kim, M.-S. Kim, J. Kim, *ACS Nano* **2010**, *4*, 2160.
- [175] J. S. Kim, J. H. Lee, J. H. Park, C. Shim, M. Sim, K. Cho, *Adv. Funct. Mater.* **2011**, *21*, 480.
- [176] J.-H. Kim, J. H. Park, J. H. Lee, J. S. Kim, M. Sim, C. Shim, K. Cho, *J. Mater. Chem.* **2010**, *20*, 7398.
- [177] S. S. van Bavel, E. Sourty, G. de With, J. Loos, *Nano Lett.* **2009**, *9*, 507.
- [178] J. Jo, S.-S. Kim, S.-I. Na, B.-K. Yu, D.-Y. Kim, *Adv. Funct. Mater.* **2009**, *19*, 866.
- [179] J. Jo, S.-I. Na, S.-S. Kim, T.-W. Lee, Y. Chung, S.-J. Kang, D. Vak, D.-Y. Kim, *Adv. Funct. Mater.* **2009**, *19*, 2398.
- [180] S. Berson, R. De Bettignies, S. Bailly, S. Guillerez, *Adv. Funct. Mater.* **2007**, *17*, 1377.
- [181] S. Sun, T. Salim, L. H. Wong, Y. L. Foo, F. Boey, Y. M. Lam, *J. Mater. Chem.* **2011**, *21*, 377.
- [182] Y. Zhao, S. Shao, Z. Xie, Y. Geng, L. Wang, *J. Phys. Chem. C* **2009**, *113*, 17235.
- [183] J. H. Park, J. S. Kim, J. H. Lee, W. H. Lee, K. Cho, *J. Phys. Chem. C* **2009**, *113*, 17579.
- [184] T. Salim, S. Sun, L. H. Wong, L. Xi, Y. L. Foo, Y. M. Lam, *J. Phys. Chem. C* **2010**, *114*, 9459.
- [185] J. H. Lee, D. W. Kim, H. Jang, J. K. Choi, J. Geng, J. W. Jung, S. C. Yoon, H.-T. Jung, *Small* **2009**, *5*, 2139.
- [186] J. S. Kim, Y. Park, D. Y. Lee, J. H. Lee, J. H. Park, J. K. Kim, K. Cho, *Adv. Funct. Mater.* **2010**, *20*, 540.
- [187] a) H.-S. Wang, L.-H. Lin, S.-Y. Chen, Y.-L. Wang, K.-H. Wei, *Nanotechnology* **2009**, *20*, 075201; b) H.-S. Wang, S.-Y. Chen, M.-H. Su, Y.-L. Wang and K.-H. Wei, *Nanotechnology* **2010**, *21*, 145203.
- [188] X. He, F. Gao, G. Tu, D. Hasko, S. Hüttner, U. Steiner, N. C. Greenham, R. H. Friend, W. T. S. Huck, *Nano Lett.* **2010**, *10*, 1302.
- [189] H. Xin, G. Ren, F. S. Kim, S. A. Jenekhe, *Chem. Mater.* **2008**, *20*, 6199.
- [190] H. Xin, F. S. Kim, S. A. Jenekhe, *J. Am. Chem. Soc.* **2008**, *130*, 5424.
- [191] H. Xin, O. G. Reid, G. Ren, F. S. Kim, D. S. Ginger, S. A. Jenekhe, *ACS Nano* **2010**, *4*, 1861.
- [192] P.-T. Wu, H. Xin, F. S. Kim, G. Ren, S. A. Jenekhe, *Macromolecules* **2009**, *42*, 8817.
- [193] H.-C. Chen, I. C. Wu, J.-H. Hung, F.-J. Chen, I. W. P. Chen, Y.-K. Peng, C.-S. Lin, C.-H. Chen, Y.-J. Sheng, H.-K. Tsao, P.-T. Chou, *Small* **2011**, *7*, 1098.
- [194] G. Ren, P.-T. Wu, S. A. Jenekhe, *ACS Nano* **2011**, *5*, 376.
- [195] Y.-J. Cheng, C.-H. Hsieh, P.-J. Li, C.-S. Hsu, *Adv. Funct. Mater.* **2011**, *21*, 1723.
- [196] W. Ma, C. Yang, X. Gong, K. Lee, A. J. Heeger, *Adv. Funct. Mater.* **2005**, *15*, 1617.
- [197] N. D. Treat, M. A. Brady, G. Smith, M. F. Toney, E. J. Kramer, C. J. Hawker, M. L. Chabinyc, *Adv. Energy Mater.* **2011**, *1*, 82.
- [198] Z. Xu, L.-M. Chen, G. Yang, C.-H. Huang, J. Hou, Y. Wu, G. Li, C.-S. Hsu, Y. Yang, *Adv. Funct. Mater.* **2009**, *19*, 1227.
- [199] J. Y. Kim, K. Lee, N. E. Coates, D. Moses, T.-Q. Nguyen, M. Dante, A. J. Heeger, *Science* **2007**, *317*, 222.
- [200] X. Han, X. Chen, S. Holdcroft, *Chem. Mater.* **2009**, *21*, 4631.
- [201] J.-H. Huang, Z.-Y. Ho, D. Kekuda, C.-W. Chu, K.-C. Ho, *J. Phys. Chem. C* **2008**, *112*, 19125.
- [202] H. Yang, Q. Song, Z. Lu, C. Guo, C. Gong, W. Hu, C. M. Li, *Energy Environ. Sci.* **2010**, *3*, 1580.
- [203] F. Tan, S. Qu, J. Wu, Z. Wang, L. Jin, Y. Bi, J. Cao, K. Liu, J. Zhang, Z. Wang, *Solar Energy Mater. Solar Cells* **2011**, *95*, 440.
- [204] A. L. Briseno, T. W. Holcombe, A. I. Boukai, E. C. Garnett, S. W. Shelton, J. J. M. Fréchet, P. Yang, *Nano Lett.* **2010**, *10*, 334.
- [205] H.-S. Wang, S.-Y. Chen, Y.-L. Wang, K.-H. Wei, *J. Nanosci. Nanotechnol.* **2011**, *11*, 3229.
- [206] P. Ravirajan, S. A. Haque, J. R. Durrant, D. Poplavskyy, D. D. C. Bradley, J. Nelson, *J. Appl. Phys.* **2004**, *95*, 1473.
- [207] S. Tepavcevic, S. B. Darling, N. M. Dimitrijevic, T. Rajh, S. J. Sibener, *Small* **2009**, *5*, 1776.
- [208] G. K. Mor, S. Kim, M. Paulose, O. K. Varghese, K. Shankar, J. Basham, C. A. Grimes, *Nano Lett.* **2009**, *9*, 4250.
- [209] Y. Guo, Y. Zhang, H. Liu, S.-W. Lai, Y. Li, Y. Li, W. Hu, S. Wang, C.-M. Che, D. Zhu, *J. Phys. Chem. Lett.* **2010**, *1*, 327.
- [210] B. Sun, N. C. Greenham, *Phys. Chem. Chem. Phys.* **2006**, *8*, 3557.
- [211] S.-C. Shiu, J.-J. Chao, S.-C. Hung, C.-L. Yeh, C.-F. Lin, *Chem. Mater.* **2010**, *22*, 3108.
- [212] W. Lu, C. Wang, W. Yue, L. Chen, *Nanoscale* **2011**, *3*, 3631.
- [213] N. Tezuka, T. Umeyama, Y. Matano, T. Shishido, K. Yoshida, T. Ogawa, S. Isoda, K. Stranius, V. Chukharev, N. V. Tkachenko, H. Lemmetyinen, H. Imaohori, *Energy Environ. Sci.* **2011**, *4*, 741.
- [214] A. J. Mieszawska, R. Jalilian, G. U. Sumanasekera, F. P. Zamborini, *Small* **2007**, *3*, 722.
- [215] V. Callegari, S. Demoustier-Champagne, *Macromol. Rapid Commun.* **2011**, *32*, 25.
- [216] T. Xu, Q. Qiao, *Energy Environ. Sci.* **2011**, *4*, 2700.
- [217] S. S. van Bavel, J. Loos, *Adv. Funct. Mater.* **2010**, *20*, 3217.
- [218] J. Boucle, P. Ravirajan, J. Nelson, *J. Mater. Chem.* **2007**, *17*, 3141.
- [219] M. D. McGehee, *MRS Bulletin* **2009**, *34*, 95.
- [220] B. O'Regan, M. Gratzel, *Nature* **1991**, *353*, 737.
- [221] S. Yanagida, Y. Yu, K. Manseki, *Acc. Chem. Res.* **2009**, *42*, 1827.
- [222] A. Hagfeldt, G. Boschloo, L. Sun, L. Kloo, H. Pettersson, *Chem. Rev.* **2010**, *110*, 6595.
- [223] M. Grätzel, *Acc. Chem. Res.* **2009**, *42*, 1788.
- [224] N. Wang, L. Han, H. He, N.-H. Park, K. Koumoto, *Energy Environ. Sci.* **2011**, *4*, 3676.
- [225] K. Imoto, K. Takahashi, T. Yamaguchi, T. Komura, J.-i. Nakamura, K. Murata, *Solar Energy Mater. Solar Cells* **2003**, *79*, 459.
- [226] T. N. Murakami, S. Ito, Q. Wang, M. K. Nazeeruddin, T. Bessho, I. Cesar, P. Liska, R. Humphry-Baker, P. Comte, P. Pechar, M. Gratzel, *J. Electrochem. Soc.* **2006**, *153*, A2255.
- [227] Y. Saito, T. Azechi, T. Kitamura, Y. Hasegawa, Y. Wada, S. Yanagida, *Coord. Chem. Rev.* **2004**, *248*, 1469.
- [228] J. Xia, N. Masaki, K. Jiang, S. Yanagida, *J. Mater. Chem.* **2007**, *17*, 2845.
- [229] Y. Saito, T. Kitamura, Y. Wada, S. Yanagida, *Synth. Met.* **2002**, *131*, 185.
- [230] J. Xia, N. Masaki, M. Lira-Cantu, Y. Kim, K. Jiang, S. Yanagida, *J. Am. Chem. Soc.* **2008**, *130*, 1258.

- [231] L. Zhao, Y. Li, Z. Liu, H. Shimizu, *Chem. Mater.* **2010**, *22*, 5949.
- [232] B. Fan, X. Mei, K. Sun, J. Ouyang, *Appl. Phys. Lett.* **2008**, *93*, 143103.
- [233] R. Trevisan, M. Döbbelin, P. P. Boix, E. M. Barea, R. Tena-Zaera, I. Mora-Seró, J. Bisquert, *Adv. Energy Mater.* **2011**, *1*, 781.
- [234] M. Winter, R. J. Brodd, *Chem. Rev.* **2004**, *104*, 4245.
- [235] B. E. Logan, B. Hamelers, R. Rozendal, U. Schröder, J. Keller, S. Freguia, P. Aelterman, W. Verstraete, K. Rabaey, *Environ. Sci. Technol.* **2006**, *40*, 5181.
- [236] P. I. Cowin, C. T. G. Petit, R. Lan, J. T. S. Irvine, S. Tao, *Adv. Energy Mater.* **2011**, *1*, 314.
- [237] M. Zhou, M. Chi, J. Luo, H. He, T. Jin, *J. Power Sources* **2011**, *196*, 4427.
- [238] Y. Qiao, C. M. Li, *J. Mater. Chem.* **2011**, *21*, 4027.
- [239] B. Rajesh, K. Ravindranathan Thampi, J.-M. Bonard, H. Jorg Mathieu, N. Xanthopoulos, B. Viswanathan, *Chem. Commun.* **2003**, *2003*, 2022.
- [240] Y. Ma, S. Jiang, G. Jian, H. Tao, L. Yu, X. Wang, X. Wang, J. Zhu, Z. Hu, Y. Chen, *Energy Environ. Sci.* **2009**, *2*, 224.
- [241] V. Selvaraj, M. Alagar, K. S. Kumar, *Appl. Catal., B* **2007**, *75*, 129.
- [242] V. Selvaraj, M. Alagar, *Electrochem. Commun.* **2007**, *9*, 1145.
- [243] H. Zhao, J. Yang, L. Li, H. Li, J. Wang, Y. Zhang, *Int. J. Hydrogen Energy* **2009**, *34*, 3908.
- [244] Q. Zhou, C. M. Li, J. Li, X. Cui, D. Gervasio, *J. Phys. Chem. C* **2007**, *111*, 11216.
- [245] A. L. Mohana Reddy, N. Rajalakshmi, S. Ramaprabhu, *Carbon* **2008**, *46*, 2.
- [246] Z. W. Chen, L. B. Xu, W. Z. Li, M. Waje, Y. S. Yan, *Nanotechnology* **2006**, *17*, 5254.
- [247] M. Zhiani, B. Rezaei, J. Jalili, *Int. J. Hydrogen Energy* **2010**, *35*, 9298.
- [248] J. Shi, Z. Wang, H.-I. Li, *J. Mater. Sci.* **2007**, *42*, 539.
- [249] Z. Wang, Z.-Z. Zhu, J. Shi, H.-L. Li, *Appl. Surf. Sci.* **2007**, *253*, 8811.
- [250] J. Shi, D.-J. Guo, Z. Wang, H.-I. Li, *J. Solid State Electrochem.* **2005**, *9*, 634.
- [251] Q. Zhou, C. M. Li, J. Li, J. Lu, *J. Phys. Chem. C* **2008**, *112*, 18578.
- [252] T. Maiyalagan, *J. Power Sources* **2008**, *179*, 443.
- [253] Y. Qiao, C. M. Li, S.-J. Bao, Q.-L. Bao, *J. Power Sources* **2007**, *170*, 79.
- [254] Y. Qiao, S.-J. Bao, C. M. Li, X.-Q. Cui, Z.-S. Lu, J. Guo, *ACS Nano* **2008**, *2*, 113.
- [255] Y. Zhao, K. Watanabe, R. Nakamura, S. Mori, H. Liu, K. Ishii, K. Hashimoto, *Chem. Eur. J.* **2010**, *16*, 4982.
- [256] Y. Zou, C. Xiang, L. Yang, L.-X. Sun, F. Xu, Z. Cao, *Int. J. Hydrogen Energy* **2008**, *33*, 4856.
- [257] J. Kim, S. I. Kim, K.-H. Yoo, *Biosens. Bioelectron.* **2009**, *25*, 350.
- [258] H.-K. Song, K. T. Lee, M. G. Kim, L. F. Nazar, J. Cho, *Adv. Funct. Mater.* **2010**, *20*, 3818.
- [259] J. M. Tarascon, M. Armand, *Nature* **2001**, *414*, 359.
- [260] J. F. M. Oudenhoven, L. Baggetto, P. H. L. Notten, *Adv. Energy Mater.* **2011**, *1*, 10.
- [261] Y. Wang, G. Cao, *Adv. Mater.* **2008**, *20*, 2251.
- [262] D. S. Su, R. Schlogl, *ChemSusChem* **2010**, *3*, 136.
- [263] Y.-G. Guo, J.-S. Hu, L.-J. Wan, *Adv. Mater.* **2008**, *20*, 2878.
- [264] F. Cheng, W. Tang, C. Li, J. Chen, H. Liu, P. Shen, S. Dou, *Chem. Eur. J.* **2006**, *12*, 3082.
- [265] B.-L. He, B. Dong, W. Wang, H.-L. Li, *Mater. Chem. Phys.* **2009**, *114*, 371.
- [266] R. Liu, J. Duay, S. B. Lee, *ACS Nano* **2010**, *4*, 4299.
- [267] M. Malta, G. Louarn, N. Errien, R. M. Torresi, *Electrochem. Commun.* **2003**, *5*, 1011.
- [268] M. Malta, G. Louarn, N. Errien, R. M. Torresi, *J. Power Sources* **2006**, *156*, 533.
- [269] G. Li, C. Zhang, H. Peng, K. Chen, *Macromol. Rapid Commun.* **2009**, *30*, 1841.
- [270] M. Sun, S. Zhang, T. Jiang, L. Zhang, J. Yu, *Electrochim. Commun.* **2008**, *10*, 1819.
- [271] X. Liang, Y. Liu, Z. Wen, L. Huang, X. Wang, H. Zhang, *J. Power Sources* **2011**, *196*, 6951.
- [272] L. Qiu, S. Zhang, L. Zhang, M. Sun, W. Wang, *Electrochim. Acta* **2010**, *55*, 4632.
- [273] X. Liang, Z. Wen, Y. Liu, X. Wang, H. Zhang, H. M. W. Lezhi, *Solid State Ionics* **2011**, *192*, 347.
- [274] L. Yang, W. Qiu, Q. Liu, *Solid State Ionics* **1996**, *86–88*, 819.
- [275] S. R. Sivakkumar, D. R. MacFarlane, M. Forsyth, D.-W. Kim, *J. Electrochem. Soc.* **2007**, *154*, A834.
- [276] D.-W. Kim, S. R. Sivakkumar, D. R. MacFarlane, M. Forsyth, Y.-K. Sun, *J. Power Sources* **2008**, *180*, 591.
- [277] M. Nishizawa, K. Mukai, S. Kuwabata, C. R. Martin, H. Yoneyama, *J. Electrochem. Soc.* **1997**, *144*, 1923.
- [278] D. Marmorstein, T. H. Yu, K. A. Striebel, F. R. McLarnon, J. Hou, E. J. Cairns, *J. Power Sources* **2000**, *89*, 219.
- [279] X. Ji, K. T. Lee, L. F. Nazar, *Nat. Mater.* **2009**, *8*, 500.
- [280] C. Y. Wang, V. Mottaghitalab, C. O. Too, G. M. Spinks, G. G. Wallace, *J. Power Sources* **2007**, *163*, 1105.
- [281] G. Nyström, A. Razaq, M. Strømme, L. Nyholm, A. Mihranyan, *Nano Lett.* **2009**, *9*, 3635.
- [282] C. Liu, F. Li, L.-P. Ma, H.-M. Cheng, *Adv. Mater.* **2010**, *22*, E28.
- [283] R. Liu, J. Duay, S. B. Lee, *Chem. Commun.* **2011**, *47*, 1384.
- [284] X. Zhao, B. M. Sanchez, P. J. Dobson, P. S. Grant, *Nanoscale* **2011**, *3*, 839.
- [285] J. Huang, K. Wang, Z. Wei, *J. Mater. Chem.* **2010**, *20*, 1117.
- [286] R. Liu, S. Il Cho, S. B. Lee, *Nanotechnology* **2008**, *19*, 215710.
- [287] K. Wang, J. Huang, Z. Wei, *J. Phys. Chem. C* **2010**, *114*, 8062.
- [288] D. Li, J. Huang, R. B. Kaner, *Acc. Chem. Res.* **2008**, *42*, 135.
- [289] X. Zou, S. Zhang, M. Shi, J. Kong, *J. Solid State Electrochem.* **2007**, *11*, 317.
- [290] H. Zhou, H. Chen, S. Luo, G. Lu, W. Wei, Y. Kuang, *J. Solid State Electrochem.* **2005**, *9*, 574.
- [291] Y.-G. Wang, Y.-Y. Xia, *J. Electrochem. Soc.* **2006**, *153*, A450.
- [292] R. Liu, J. Duay, T. Lane, S. Bok Lee, *Phys. Chem. Chem. Phys.* **2010**, *12*, 4309.
- [293] J. Zang, S.-J. Bao, C. M. Li, H. Bian, X. Cui, Q. Bao, C. Q. Sun, J. Guo, K. Lian, *J. Phys. Chem. C* **2008**, *112*, 14843.
- [294] R. Liu, J. Duay, S. B. Lee, *ACS Nano* **2011**, *5*, 5608.
- [295] G. A. Snook, G. Z. Chen, D. J. Fray, M. Hughes, M. Shaffer, *J. Electroanal. Chem.* **2004**, *568*, 135.
- [296] C. Zhou, S. Kumar, C. D. Doyle, J. M. Tour, *Chem. Mater.* **2005**, *17*, 1997.
- [297] H. Mi, X. Zhang, S. An, X. Ye, S. Yang, *Electrochim. Commun.* **2007**, *9*, 2859.
- [298] C. Meng, C. Liu, S. Fan, *Electrochim. Commun.* **2009**, *11*, 186.
- [299] H. Zhang, G. Cao, Z. Wang, Y. Yang, Z. Shi, Z. Gu, *Electrochim. Commun.* **2008**, *10*, 1056.
- [300] H. Zhang, G. Cao, W. Wang, K. Yuan, B. Xu, W. Zhang, J. Cheng, Y. Yang, *Electrochim. Acta* **2009**, *54*, 1153.
- [301] K. Lota, V. Khomenko, E. Frackowiak, *J. Phys. Chem. Solids* **2004**, *65*, 295.
- [302] Q. Wu, Y. Xu, Z. Yao, A. Liu, G. Shi, *ACS Nano* **2010**, *4*, 1963.
- [303] S. Biswas, L. T. Drzal, *Chem. Mater.* **2010**, *22*, 5667.
- [304] K. Zhang, L. L. Zhang, X. S. Zhao, J. Wu, *Chem. Mater.* **2010**, *22*, 1392.
- [305] L. L. Zhang, S. Zhao, X. N. Tian, X. S. Zhao, *Langmuir* **2010**, *26*, 17624.
- [306] I. Kovalenko, D. G. Bucknall, G. Yushin, *Adv. Funct. Mater.* **2010**, *20*, 3979.
- [307] N. Shaigan, S. S. Djokic, in *Modern Aspects of Electrochemistry*, Vol. 48 (Eds.: R. E. White, C. G. Vayenas), Springer, New York, **2010**, pp. 117.
- [308] C. Meng, C. Liu, L. Chen, C. Hu, S. Fan, *Nano Lett.* **2010**, *10*, 4025.
- [309] J.-H. Kim, Y.-S. Lee, A. K. Sharma, C. G. Liu, *Electrochim. Acta* **2006**, *52*, 1727.

- [310] Y.-W. Ju, G.-R. Choi, H.-R. Jung, W.-J. Lee, *Electrochim. Acta* **2008**, 53, 5796.
- [311] S. Liu, X. Liu, Z. Li, S. Yang, J. Wang, *New J. Chem.* **2011**, 35, 369.
- [312] Y. G. Wang, H. Q. Li, Y. Y. Xia, *Adv. Mater.* **2006**, 18, 2619.
- [313] M. Hughes, M. S. P. Shaffer, A. C. Renouf, C. Singh, G. Z. Chen, D. J. Fray, A. H. Windle, *Adv. Mater.* **2002**, 14, 382.
- [314] E. Frackowiak, V. Khomenko, K. Jurewicz, K. Lota, F. Béguin, *J. Power Sources* **2006**, 153, 413.
- [315] C. Peng, J. Jin, G. Z. Chen, *Electrochim. Acta* **2007**, 53, 525.
- [316] K. H. An, K. K. Jeon, J. K. Heo, S. C. Lim, D. J. Bae, Y. H. Lee, *J. Electrochem. Soc.* **2002**, 149, A1058.
- [317] A. K. Geim, K. S. Novoselov, *Nat. Mater.* **2007**, 6, 183.
- [318] A. K. Geim, *Science* **2009**, 324, 1530.
- [319] M. J. Allen, V. C. Tung, R. B. Kaner, *Chem. Rev.* **2010**, 110, 132.
- [320] J. Zhang, L.-B. Kong, J.-J. Cai, Y.-C. Luo, L. Kang, *Electrochim. Acta* **2010**, 55, 8067.
- [321] R. K. Sharma, L. Zhai, *Electrochim. Acta* **2009**, 54, 7148.
- [322] Y. Hou, Y. Cheng, T. Hobson, J. Liu, *Nano Lett.* **2010**, 10, 2727.